Imperial College London

Peptide – targeted gold nanostars for the treatment of Parkinson's disease

Corinne Morfill

July 2021

A thesis submitted to Imperial College London in fulfilment of the requirements for the degree of Doctor of Philosophy (PhD)

Department of Materials

Imperial College London

Abstract

Neurodegenerative diseases are now one of the leading causes of death in the United Kingdom with cases rising. There is a heightened need for new drug therapeutics to limit or halt neurodegenerative disease progression and/or ameliorate the disease pathologies altogether. A major challenge in neurology is the lack of small brain penetrable neuroprotectants that target multiple disease mechanisms and also the Blood Brain Barrier (BBB) which severely restricts entry of neuroprotectants into the central nervous systems (CNS). There is an urgent need to develop new strategies that can target the BBB and effectively deliver drugs into the CNS. Due to their size, ease of functionalisation for maximum surface area of drug loading and ability to pass through the BBB, nanoparticles are a potential solution to deliver neurotherapeutic drugs directly to damaged neurons inside the brain to increase the efficacy of neuroprotectants.

The small peptides (H3/H6) that encompass the active motifs of the neurotrophic protein S100A4 have been shown to reduce oxidative stress and excitotoxicity *via* multiple pathways and protect neurons in animal models of neurological disorders. However, these peptides have limited brain penetration and circulation half-life. Therefore a delivery system that can improve the half – life of the peptides, shuttle the drugs across the BBB and interact directly with neurons is required. Plasmonic gold nanostars are promising candidates for delivery of standard-of-care drugs inside the brain and fluorescence-based deep tissue imaging but have not previously been trialled as carriers for neuroprotectants.

The objective of this thesis was to design, synthesise and fully characterise a new gold nanostar delivery vehicles to shuttle the H3/H6 peptides across the BBB to impaired neurons and evaluate their potential as a future treatment of Parkinson's disease. Star and spherical nanostructures were synthesised and compared, and a new protocol was devised to conjugate H3/H6 peptides onto their surface. These nanostructures were subsequently tested on *in vitro* models of neurological disorders to investigate the effects of the

nanostructure geometry on biological responses, including their potential as neuroprotectants and their interaction with neurons. Transmission electron microscopy was used to compare the interaction of the star and spherical nanostructures with cell membranes to understand the mechanisms by which the spikes of the nanostars increase their cell binding properties.

The H3/H6-nanostructures induced neuritogenesis in neurons and the star shaped nanostructures proved higher potency/efficacy than spherical AuNPs. The H3-Au nanostructures (stars and spheres) protected neurons against oxidative stress with the H3 – nanostars being more potent. Conjugation of these peptides to the surface of the nano structures did not inhibit the neurotrophic capabilities previously seen from the isolated peptides alone. ICP analysis confirmed the affinity and interaction of the nano therapeutics to the neurons, while electron microscopy demonstrated that the spikes of the nanostars were able to embed into the plasma membrane of neurons more effectively than the nanospheres, thus enhancing the internalisation rate of the nanostars, whereas the nanospheres were rarely internalised. Finally a synthesis route was devised to further functionalise these nano compounds with the small molecular L - dopa to, in future, deliver them across the BBB. This thesis shows that conjugation of custom-made dendrimers to the surface of gold nanostars may be used to activate multiple neuroprotective pathways and increase the drug potency to treat a broad spectrum of neurodegenerative disorders.

Author's Declaration

The present thesis is a record of the work carried out by me in the Department of Materials and the London Centre for Nanotechnology at Imperial College London, UK. The work described herein is my own, unless otherwise stated. Wherever contributions of others are involved, every effort is made to indicate this, with references to the literature and the acknowledgements of collaborative research. Some of the work presented in this thesis has been published in the following journal article:

Morfill, C., Pankratova, S., Machado, P., Fernando, N., Regoutz, A., Klosowski, M., Fleck, R., Xie, F., Porter, A., Kiryushko, D. Nanostars Carrying Multifunctional Neurotrophic Motifs Of S100 Proteins Protect Neurons In Models Of Neurodegenerative Disorders. **2021**. Submitted manuscript

Copyright Declaration

The copyright of this thesis rests with the author and is made available under the Creative Commons Attribution Non-Commercial No Derivatives licence. Researchers are free to copy, distribute or transmit the thesis on the condition that they attribute it, that they do not use it for commercial purposes and that they do not alter, transform or build upon it. For any reuse or redistribution, researchers must make clear to others the licence terms of this work.

Publications

Morfill, C., Pankratova, S., Machado, P., Fernando, N., Regoutz, A., Klosowski, M., Fleck, R., Xie, F., Porter, A., Kiryushko, D. Nanostars Carrying Multifunctional Neurotrophic Motifs Of S100 Proteins Protect Neurons In Models Of Neurodegenerative Disorders. **2021**. Submitted manuscript

Acknowledgements

First and foremost, I would like to thank my supervisors, Prof. Alex Porter and Dr. Fang Xie for their patient support and guidance throughout this study. Gaining from their invaluable expertise in nano technology, nano particle chemistry and electron microscopy was an opportunity I was truly blessed to have experienced.

The interdisciplinary nature of this research allowed me the opportunity to collaborate with many talented researchers across multiple disciplines. I wish to thank Prof. Roland Fleck and his team at Kings College London for allowing me to perform experiments at the Centre for Ultrastructural Imaging and to gain valuable experience in electron microscopy procedures. To Dr Michal Klosowski, Dr Mahmoud Ardakani and Dr Ecaterina Ware for your unwavering patience and support during the many long hours spent in the Harvey Flower Electron Microscopy Suite, but most importantly thank you, for the laughter that broke the stressful moments. I would also like to thank Dr Ioannis Theodorou for your continued support during my PhD, always willing to offer your expertise and support in nano synthesis, no matter where in the world you may reside.

A special thank you to Maryam Al – Ejji, Helena Dodd and Elenora Cali for the close friendships developed over the last four years. For all the emotional support and grounding with great times fuelled with coffee, chocolate and laughter. I could never have made it through this PhD without you all. Thank you to Porter group and Dunlop group members for making my time in the lab enjoyable and unforgettable.

Manjula de Silva and Kirsty Flower, to you both, I express my absolute gratitude and appreciation for allowing me to become part of the GTA team to teach and support undergraduate students in materials, engineering and medicine. This opportunity taught me so much more than I ever though it would have and made a positive impact on my own research.

Last but not least, thank you to my family for your unconditional love and support for not only my PhD but all my studies. Thank you for always being proud and encouraging me,

even if you didn’t always understand what I was talking about, I would not be here without you all.

Lastly to my Jonathan, thank you for your love, for your charisma, for sharing this journey with me through all its ups and downs, but more importantly, for being you.

Contents

Abstract ……2

Author's Declaration ……4

Copyright Declaration ……5

Publications ……6

Acknowledgements ……7

Contents ……9

List of Abbreviations ……14

List of Figures ……17

List of Tables ……28

1. Introduction ……31

2. Literature Review ……34

2.1 Parkinson's disease ……34

2.1.1 What is Parkinson's disease? ……34

2.1.2 Parkinson's disease pathology ……36

2.1.3 PD treatments and limitations ……41

2.2 S100A4 Protein ……43

2.2.1 S100A4 Derived neurotrophic motifs H3 and H6 ……45

2.2.2 Neurotrophic effects of H3 and H6 mimetics ……46

2.3 Nanotechnology ……51

2.3.1 Nanoparticles ……51

2.3.2 Neurological exposure to nanoparticles ……55

2.3.3 Nanotoxicology ……56

2.4 Blood Brain Barrier ……58

2.4.1 Crossing the BBB ……59

2.4.2 Conclusions ……61

3 Experimental Techniques ……63

3.1 Electron Microscopy ……63

3.1.1 Transmission Electron Microscopy ……66

3.1.2 Scanning Electron Microscopy ……67

3.1.3 Focused Ion Beam Scanning Microscopy ……67

4 Synthesis and Stability of Peptide – targeted gold nanoparticles for the treatment of Parkinson's disease ……70

4.1 Introduction ……70

4.2 Methods ……71

4.2.1 Gold nano particle synthesis ……72

4.2.2 Functionalising the nanostructures with the H3/H6 peptides ……73

4.2.3 Characterisation of the H3/H6 peptides on the surface of the nanostructures……79

4.2.4 Transmission Electron Microscopy (TEM) ……81

4.2.5 Statistics ……82

4.3 Results and Discussion ……82

4.3.1 Nano seed synthesis: Citrate – capped Au nano seeds ……83

4.3.2 Effect of $AgNO_3$ on optimising the nano star synthesis ……85

4.3.3 Characterisation of the 50 nm gold nano stars ……91

4.3.4 Characterisation of the 50 nm gold nano spheres ……92

4.3.5 Conjugation of H3 and H6 neuroprotective peptides onto the nanostructures' surface ……93

4.3.6 Characterisation and functionalisation of the H3/H6 Peptide - Conjugated nano compounds ……95

4.3.7 Stability of the conjugated nano structures ……102

4.4 Conclusions ……105

5. Neurotrophic Effects of H3/H6 Targeted Nanoparticles on Primary Hippocampal Neurons and Immortalized Dopaminergic Neurons (N27's) ……106

5.1 Introduction ……106

5.2 Methods ……108

5.2.1 Peptide targeted gold nano particle synthesis ……108

5.2.2 Quantifying the volume of Au per drug dose. ……110

5.2.3 Ethics statement ……111

5.2.4 Cell culturing ……111

5.2.5 Neuronal survival assay ……112

5.2.6 Neurite outgrowth ……112

5.2.7 Nanoparticle – Neuron interaction ……113

5.2.8 Statistics ……116

5.3 Results ……117

5.3.1 Volume of gold per drug dose ……117

5.3.2 Evaluating the toxicity of the peptide targeted nanoparticles ……119

5.3.3 Neurite outgrowth ……121

5.3.4 Neuronal interaction ……123

5.4 Discussion ……131

5.4.1 Biological effects of the peptide bound Nano–Neuro therapeutics ……131

5.4.2 Effect of particle geometry on drug delivery ……132

5.5 Conclusions ……134

6 Fabricating and Optimising Au Nano Stars for Blood Brain Barrier Crossing via L - dopa LAT1 Trans membrane Protein ……135

6.1 Introduction ……135

6.2 Methods ……138

6.2.1 L - dopa Functionalized nanostars ……139

6.2.2 Characterisation of the L - dopa fabricated nanostars ……144

6.2.3 Statistics ……144

6.3 Results ……145

6.3.1 L - dopa ……145

6.3.2 Nano star synthesis ……146

6.3.3 L - dopa functionalised nano Stars ……147

6.3.3.1 Substituting ascorbic acid for L - dopa functionalization ……147

6.3.3.2 L - dopa reduced nano seeds to star formation ……151

6.3.3.3 L - dopa capped nano stars ……154

6.3.3.4 EDC/NHS coupling L - dopa to PEG ……157

6.4 Conclusion ……166

7 Conclusions and Future Work ……167

8 Appendix ……173

8.1 Effect of peptide targeted nano stars on hippocampal neurons against Aβ-Induced neurotoxicity *in vitro* ……173

8.2 Toxicity study ……174

8.3 Inductively coupled plasma – optical emission spectrometry analysis ……175

8.4 XPS Confirmation of PEG – L - dopa EDC/NHS coupling ……176

9 References ……177

List of Abbreviations

AD	Alzheimer's disease
Ag	Silver
$AgNO_3$	Silver nitrate
AR	Aqua regia
ATP	Adenosine triphosphate
Au	Gold
AuNF	Gold nano flower
AuNP	Gold nano particle
AuNS	Gold nano star
BBB	Blood Brain Barrier
BSA	Bovine serum albumin
BSE	Back scattered electron
CA	Cell associated
CNS	Central nervous system
CO_2	Carbon dioxide
COMP	Catechol-O-methyltransferase
Cryo	Cryogenic
Cryo – TEM	Cryogenic transmission electron microscopy
CTL	Control
Cu	Copper
DIV	Days *in vitro*
E18	Embryonic day 18
ECs	Endothelial cells
EDC	(1-ethyl-3-(3-dimethylaminopropyl)carbodiimide)
EGF	Epidermal growth factor
EGFR	Epidermal growth factor receptor
Eo	Reduction potential
FIB	Focused ion beam
H_2O_2	Hydrogen peroxide

H3	Peptide dendrimer designed and labelled as H3
H6	Peptide dendrimer designed and labelled as H6
$HAuCL_4$	Gold (lll) chloride trihydrate
HCL	Hydrochloric acid
HEPES	M 4-(2-hydroxyethyl)-1-piperazineethanesulfonic acid
HNO_3	Nitric acid
ICP –OES	Inductively coupled plasma optical emission spectroscopy
IFN –y	Interferon – y
KDR	Kinase domain – containing receptor
LAT – 1	Large neutral amino acid transporter – 1
L - dopa	3,4-Dihydroxy-L-phenylalanine
LPS	Lipopolysaccharides
MAO-B	Monoamine oxidase B
MES	2-(N-Morpholino)ethanesulfonic acid
MPP+	1-methyl-4-phenylpyridinium
MPTP	1-methyl-4-phenyl-1,2,3,6,-tetrahydropyridine
N27	Rat immortalized mesencephalic dopaminergic neuronal cells
NB	Neurobasal medium
ND	Neurodegenerative diseases
NO	Nitric oxide
NP	Nanoparticle
NS	Nanostar
OsO_4	Osmium
PBS	Phosphate-buffered saline
PD	Parkinson’s disease
PEG	Alkyl- polyethylene glycol (PEG2000)
ROS	Reactive oxygen species
RPMI	RPMI cell growth medium
RT	Room temperature
SEM	Scanning electron microscopy
SN	Supernatant
SOD	Superoxide dismutase
SPR	Surface plasmon resonance
Sulfo-NHS	N-hydroxysulfosuccinimide

TEM	Transmission electron microscopy
THC	Thiocarbohydrazide
TNF	Tumor necrosis factor
UA	Uranyl acetate
UPS	Ubiquitin-proteasome system
UV – Vis	Ultraviolet visible spectroscopy
VEGF	Vascular endothelial growth factor
XPS	X-ray photoelectron spectroscopy
6-OHDA	6-hydroxydopamine

List of Figures

Figure 2.1 Cross section of the brain demonstrating the location of dopaminergic neurons[37]……**34**

Figure 2.2 Schematic diagram representing a normal functional neuron (left) that allows uninhibited crossing of the dopamine neurotransmitter, Vs Parkinson's disease affected neuron (right) that has a deceased synaptic crossing of dopamine leading to movement disorders[37]……**35**

Figure 2.3 Schematic diagram representing the mitochondrial transport chain. Mitochondrial dysfunction mostly occurs at complex 1, which is the start of the five step oxidative phosphorylation process thus inhibiting the cellular adenosine triphosphate (ATP) energy production[38]……**39**

Figure 2.4 S100A4 protein. Image adapted from Dmytriyeva *et al*, 2012 ……..**44**

Figure 2.5 Image showing the general structure of the 4 - branched peptide dendrimer, and the amino acid sequence of each motif; 'H3' and 'H6'. Synthetic peptides encompassing the S100A4 derived neurotrophic motifs have been generated by Schafer-N, Denmark[8] **45**

Figure 2.6 H3 and H6 mimetics can stimulate neurite outgrowth in hippocampal neurons when compared to the S100A4 parent protein positive control, (a). Identification of

the neurotrophic motifs isolated and synthesised from the S100A4 protein, (b). H3 mimetic, blue, H6 mimetic, red. Image adapted from Dmtriteva *et al,* 2012[8] ……**47**

Figure 2.7 Schematic representation of the signalling pathways activated by S100A4. Upon interacting with the cell membrane, the S100A4 protein and the two mimetics H3 and H6 trigger a cascade of proposed pathways that induces neurite outgrowth. Image adapted from Kiryusko *et al*, 2006[7]……..**48**

Figure 2.8 Neuroprotective effect of the S100A4 derived mimetics H3 and H6 in N27 dopaminergic cells against toxin induced cell death. Top – H3 and H6 protect N27's from H_2O_2 induced oxidative stress. Bottom - H3 and H6 protect N27's from OHDA-induced toxicity. Adapted from Pankratova *et al* 2018[43] ……**49**

Figure 2.9 Schematic diagram demonstrating the different shaped nanoparticles that can be synthesised by the reduction of gold. Image adapted from Piyushkumar *et al* 2020[97]**51**

Figure 2.10 Schematic diagram demonstrating the biological applications of nano particles and imaging techniques used to track them inside the body. Image adapted from Bahar et al, 2020[98] ……..**52**

Figure 2.11. Schematic diagram demonstrating the surface plasmon resonance (SPR) inducing a strong absorption of the incident light (a, c) and thus can be measured using a UV – Vis absorption spectrometer (b, d). The SPR band intensity and wavelength depends on the nano particle structure. Nano sphere (a) and nano rod (c). The wavelength peak (b) can be used to determine the size of the AuNP. Image adapted from Xavier *et al,* 2018[99] ……**54**

Figure 2.12 Schematic demonstrating the main mechanisms and factors of neurotoxicity induced by nanoparticles. Image adapted from Teleanu *et al* 2018[121] ……**57**

Figure 2.13 Schematic diagram of the blood brain barrier (BBB). Image adapted from Perkins 2011[143] ……**58**

Figure 2.14 Schematic diagram demonstrating the transport pathways to enable crossing of the blood brain barrier (BBB), image adapted from Herda *et al*, 2015[23] ……**60**

Figure 3.1 An overview of the signals generated when the electron beam interacts with a specimen. These signals may include: back - scattered electrons (BSE), secondary electrons (SE), auger electrons, electron beam induced current (EBIC) and characteristic X-ray and photons. Image adapted from John Wiley & Sons Ltd[118] ……**65**

Figure 3.2 Schematic representations of (a) scanning electron microscope (SEM), (b) transmission electron microscope (TEM). CL: condenser lens, OL: objective lens, BSE: backscatter electrons, SE: secondary electrons, EDS: energy dispersive X-rays, EELS: electron energy loss spectroscopy, ADF: annular dark field. Image adapted from John Wiley & Sons Ltd[118] ……**66**

Figure 3.3 Focussed ion beam (FIB) propels high - energy gallium ions towards the specimen surface to allow controlled material degradation. High energy gallium ions are propelled down the FIB column by electromagnets. Electromagnetic lens and an internal aperture focusses high energy gallium ions into a condensed beam, with stigmators removing beam stigmation. Image adapted from Bell *et al*[119] ……**68**

Figure 3.4 FIB can be used to remove material from the surface of a specimen through controlled degradation. A schematic representation of FIB milling to form a trench, (left)

leaving an exposed 'cliff wall' that may be characterised by SEM. SEM micrograph example of a trench formed by FIB milling. Image adapted from Bell *et al*[119] ……..**69**

Figure 4.1 EM characterisation of Au nano seeds. (a) TEM micrograph imaged at 200kV of Au nano seed synthesised with 3% sodium citrate. (b) Histogram displaying the particle size distribution and identifying the mean diameter as 12 nm ± 1 nm with a uniform size distribution. (c) TEM micrograph image at 200kV of 4% citrate reduced nano seeds. (d) Histogram displaying the particle size distribution and identifying the mean diameter as 12 nm ± 2 nm with a less size distribution. n = 200. ……..**84**

Figure 4.2 TEM characterisation of the morphological characteristics of the gold nano stars synthesised with varying concentrations of $AgNO_3$. Imaged at 200kV. 0.5 mM $AgNO_3$ (a), 1 mM $AgNO_3$ (b), 2 mM $AgNO_3$ (c) and 3 mM $AgNO_3$ (d). n = 200 ……..**86**

Figure 4.3 TEM characterisation of morphological characteristics of the gold nano stars synthesised with varying volumes of $AgNO_3$. Imaged at 200kV. 5 µL $AgNO_3$ (a), 25 µL $AgNO_3$ (b), 50 µL $AgNO_3$ (c) and 100 µL $AgNO_3$ (d). n = 200 ……**88**

Figure 4.4 TEM characterisation of the morphological characteristics of the Au nano stars synthesised with varying sized nano seeds. Imaged at 200kV, 2% sodium citrate (a), 3% sodium citrate (b) and 4% sodium citrate (d) reduced nano seeds were used to subsequently synthesise nano stars. n = 200 ……**89**

Figure 4.5 TEM Micrograph image of the 50 nm nano stars, Imaged at 200kV (a); Zeta potential demonstrating the stability of the nano stars in different media, deionized water (H_2O) pH 7.4; RPMI 1640 growth medium (RPMI) pH 7.4; Neurobasal neuronal growth medium (NB) pH 6.7; 1% bovine serum albumin (BSA) pH 6.4; measured at 37°C, three independent experiments, values are shown as means ± SEM. (b); Histogram showing the size

distribution of the nano stars, n = 200 (c) and (d) UV - Vis used to indicate if the stars are aggregated or non - aggregated and demonstrating the nano stars are uniform in size and shape ……**91**

Figure 4.6 TEM micrograph image of the 50 nm nano spheres, imaged at 200kV. (a); Zeta potential demonstrating the stability of the nano spheres in different medias, deionized water (H_2O) pH 7.4; RPMI 1640 growth medium (RPMI) pH 7.4; neurobasal neuronal growth medium (NB) pH 6.7; 1% bovine serum albumin (BSA) pH 6.4; measured at 37°C, three independent experiments, values are shown as means ± SEM. (b); Histogram showing the size distribution of the nano stars, n = 200 (c) and (d) UV - Vis used to indicate if the stars are aggregated or non - aggregated and demonstrating the nano stars are uniform in size and shape. ……..**92**

Figure 4.7 S100 A4 mother protein with the H3 and H6 peptide mimetics labelled (a). H3 and H6 peptides synthesised as tetramers for stability (b). (c) The chemical structure of PEG displaying the –SH thiol group that allows direct binding to gold and (d) is the structural representation of the cysteine amino acid used in the synthesis of the peptides that also contains the –SH thiol bond that allows direct binding to gold. ……**94**

Figure 4.8. Schematic diagram showing the steps used to produce nanospheres and nanostars and conjugate the H3/H6 (+/-PEG) onto the spherical and star shaped gold nanostructures. ……**95**

Figure 4.9 TEM micrograph image of uranyl acetate (UA) contrast staining to visualise the peptide H6 bound to the nano stars. Imaged at 200 kV……**97**

Figure 4.10 UV - Vis spectra identifying the plasmonic nano particles conjugated with the H3/H6 neuroprotective peptides +/- PEG nano spheres (a), nanostars (b). The colloidal

solutions were measured after 24hr incubation with the peptides +/- PEG, washed by centrifugation three times, and measured in deionised water at pH 7.4 ……**98**

Figure 4.11 XPS reference datasets of PEG, H3 and H6, including (a) Survey, (b) C 1*s* core level, and (c) N 1*s* core level spectra. In the survey spectra all major signals are indicated and for the core levels chemical states are labelled. Data acquired and analysed in collaboration with Anna Regoutz, UCL ……**100**

Figure 4.12 XPS data confirming peptide – particle attachment. Core level spectra including Au 4*f*, C 1*s*, and N 1*s* for (a) - (c) AuNP and (d) - (f) AuNS samples. Data acquired and analysed in collaboration with Anna Regoutz, UCL ……**101**

Figure 4.13. Zeta potentials of the conjugated nano structures in different media, deionized water (H_2O); RPMI 1640 growth medium (RPMI); Neurobasal neuronal growth medium (NB); 1% bovine serum albumin (BSA). Measured at 37°C, three independent experiments, values are shown as means ± SEM. n = 5 ……**103**

Figure 5.1 Quantification of Au administered along with the peptide doses of 2, 5, 10, 20 and 40 µg/mL as determined by ICP – OES. PEG only functionalised particles (a) AuNS + H3 vs AuNP + H3 (b), AuNS + H6 vs AuNP + H6 (c). AuNS + H3 + PEG vs AuNP + H3 + PEG, (d) and AuNS + H6 + PEG vs AuNP + H6 + PEG, (e). Significant difference found in the volume of Au administered per peptide dose between the AuNS/AuNP + H3/H6 + PEG at 40 µg/mL. *p < 0.05. Results are expressed as means ± SEM. n = 6 ……**118**

Figure 5.2 Effect of the peptide – targeted nano particles in cell survival. (A, C) Representative images of Hoechst-stained hippocampal neurons (A) or N27 cells (C) left untreated (CTL) or treated with H_2O_2/6-OHDA (A or C, respectively) in the absence or presence of H3 - AuNS (10 µg/mL). Scale bar, 20 µm. (B, D) H3-functionalized AuNP protect cultured hippocampal neurons and N27 cells against the H_2O_2 (B) and 6-OHDA- (D) induced

neurotoxicity. CTL, untreated cells; H_2O_2/6-OHDA, neurotoxin only (60 and 100 µM, respectively) - treated cells. One-way ANOVA vs H_2O_2 (C) or 6-OHDA (D), three to four independent experiments, *p < 0.05; **p < 0.01; ***p < 0.001. Data images and analysis obtained in collaboration with Darya Kiryushko (Imperial College London) ……**120**

Figure 5.3 H3 and H6 - functionalized nanoparticles promote neurite outgrowth from hippocampal neurons. AuNS Vs AuNP + H3 +/-PEG (a), stars vs spheres + H6 +/-PEG (b). (c/d) representative micrographs of hippocampal neurons treated with AuNS + H3, AuNS + H3 + PEG and AuNP + H3 (c) and AuNS + H6, AuNS + H6 + PEG and AuNP + H6 (d) conjugated nano constructs (10 µg/ml) and untreated control. Scale bar, 10 µm. One-way ANOVA vs CTL, four independent experiments. Results are expressed as means ± SEM. *p < 0.05; **p < 0.01 ...**122**

Figure 5.4 Cell association studies. Evaluating the N27 cell membrane binding/insertion properties of the two different drug delivery geometries, NS vs NP. In each graph, the ratio (%) of total gold content is shown detected in the cell - associated (CA) fraction or in the supernatant (SN) for the two nanostructure geometries. PEG only constructs (a). H3 only conjugated NS/NPs (b). H6 only conjugated NS/NPs (c). H3 + PEG conjugated NS/NPs (d). H6 + PEG conjugated NS/NPs (e). One-way ANOVA vs four independent experiments. Results are expressed as means ± SEM. *p < 0.05; **p < 0.01; ***p < 0.001. n = 3 ……**124**

Figure 5.5 Cell binding activity of all peptide bound constructs, graphing both cell associated (CA) nano compounds and the nano structures found in the supernatant (SN) after 24 hr cell treatment. Experiment formed in triplicate with the mean +/- SEM reported …..**125**

Figure 5.6 Immortalized dopaminergic neuron (N27), treated with H3 - AuNSs for 24 hrs at concentration 20 µg/mL. The cells were plunged into liquid nitrogen for fixation, then freeze dried for 24 hrs. Imaged using TEM operated at 200 kV. Image obtained in collaboration with Professor Roland Fleck, KCL ……**126**

Figure 5.7 FIB – SEM images acquired at 10 kV *via* Auriga showing H3 - AuNSs interacting with the hippocampal neuronal network. Image (a) demonstrates nanostars embedded in the dendrite membrane of the neuron. Image (b) shows the nanostars are membrane bound……..**128**

Figure 5.8 TEM micrograph images showing the interactions between the H3 and H6 NS/NPs and cultured hippocampal neurons (20 µg/mL) (A). (B) Quantification of AuNP/AuNS distribution across cell compartments. Total number of NSs and NPs analysed: H6 NPs, n = 1291; H6 NSs, n = 1260; H3 NPs, n = 1041. AuNP/AuNS counts in each compartment are normalized to the total AuNP/AuNS count for each particle type (set to 100%). One - way ANOVA Star + H6 vs Sphere + H6 particles found internalised and extracellular *p < 0.05. Images obtained in collaboration with Dr Pedro Machado, Centre for Ultrastructural Imaging, Kings College London ……**130**

Figure 5.9 Summary of the best performing nano structure for drug delivery. (a) Demonstrates the AuNPs + H3/H6 were the better performing structure in the cell association studies *via* ICP analysis. (b) AuNS + H3/H6 were the best performing delivery system for neurite outgrowth. (c) Demonstrates the NSs as the better performing structure in the neuronal interaction studies via TEM analysis ……**132**

Figure 6.1 TEM micrograph image of successful synthesis of L - dopa nano flower (AuNF) by the Porter group[59, 60]. Use of 4 mL of 15 mM L - dopa and varying the volume of 0.1 M $HAuCL_4$ (12.5 µL (a), 50 µL (b), 100 µL (c)) allowed chemical control of the particle size. (d) TEM images confirming transport of L- dopa gold nano flowers (AuNF) across BBB endothelial *via* LAT 1 transporter protein using *in vitro* primary brain endothelial cells. Images adapted from Zhan Yuin Ong *et al*[59] ……**136**

Figure 6.2 Transcytosis of AuNS by diameter for PEGylated (left) and Transferrin (Tf) coated nanostructures (right). Results showed that D3 cell crossing increases linearly with spike length. Image adapted from Rodrigues *et al*[67] ……**137**

Figure 6.3 Schematic displaying the chemical structure of L - dopa ……..**145**

Figure 6.4 Schematic diagram demonstrating the synthesis procedure used to produce 12 nm seeds. 3% sodium citrate was used to reduce the oxidised $HAuCL_4$ to form bulk gold particles with a mean diameter of 12 nm ……**146**

Figure 6.5 Schematic diagram demonstrating the chemical synthesis procedure used to produce the 50 nm stars. 12 nm nano seeds were grown into stars *via* seed mediated growth by the addition of 100 mM L - ascorbic acid and 3 mM silver nitrate, stabilized with 1 mM PEG ……**147**

Figure 6.6 Schematic Diagram displaying the substitution of reducing agents - 100 mM L-Ascorbic acid for 15 mM L - dopa - to form the 50 nm nano stars. The molarity of silver nitrate (3 mM) was kept the same to enable the formation of the branch like structures. The stars were stabilised with 1 mM PEG ……**148**

Figure 6.7 TEM micrograph images of L - dopa reduced nano stars. 100 µL 3 mM $AgNO_3$ remained constant throughout the trials, with the following chemical modifications: (a) 200 µL NP seeds, 100 µL $HAuCL_4$ and 200 µL 15mM L - dopa (b) 200 µL NP seeds, 100 µL $HAuCL_4$ and 300 µL 15mM L - dopa (c) 200 µL NP seeds, 100 µL $HAuCL_4$ and 150 µL 15mM L - dopa (d) 200 µL NP seeds, 200 µL $HAuCL_4$ and 150 µL 15mM L - dopa (e) 100 µL NP seeds, 100 µL $HAuCL_4$ and 150 µL 15mM L - dopa (f) 100 µL NP seeds, 200 µL $HAuCL_4$ and 150 µL 15mM L - dopa. Imaged using Joel 2100f operated at 200 kV ……**150**

Figure 6.8 Schematic diagram demonstrating the chemical synthesis procedure used to produce L - dopa reduced Au nano seeds ……**152**

Figure 6.9 L - dopa functionalised nano particles produced *via* reducing 10 mM $HAuCl_4$ with 15 mM L - dopa (a) particles then gown into stars via the seed mediated growth method of reducing acidified $HAuCl_4$ bound to the NPs with ascorbic acid while forming branches with the addition of $AgNO_3$ (b). (c) Graph displaying the size variation of the L - dopa reduced NPs formed when changing the L - dopa concentration parameters, n = 200 ……**153**

Figure 6.10 Schematic diagram demonstrating the chemical synthesis procedure used in attempt to produce L - dopa capped Au nano stars……**155**

Figure 6.11 Schematic diagram providing a visual overview of the EDC/NHS coupling method used to couple L - dopa to PEG onto the surface of the nano stars ……**158**

Figure 6.12 TEM images representing a visual analysis of the EDC/NHS L - dopa coupled PEG functionalised AuNSs. The individual results are as follows: Experiment 1 (a), Experiment 2 (b), Experiment 3 (c), Experiment 4 (d), Experiment 5 (e), Experiment 6 (f). Joel 2100f operated at 200kV ……**160**

Figure 6.13 Reference XPS demonstrating the binding energy peaks to enable differentiation between L - dopa and PEG ……**161**

Figure 6.14 XPS data demonstrating the attachment potential for organic material binding. (Au 4f/Ag 3d) Data normalised to carbon, the strength of the peak determines bound material ……**161**

Figure 7.1 TEM image of the successful L - dopa functionalised AuNS *via* EDC/HHS coupling. The particles produced were ca. 50 nm. The AuNS demonstrated a very high yield of PEG – L - dopa binding to the NS surface. This will enable further functionalisation with the H3/H6 peptides ……**170**

Figure 8.1 S100A4 mimetic peptides and peptide - conjugated AuNP/NS protect hippocampal neurons against Aβ – induced neurotoxicity *in vitro*. (A) Representative images of Hoechst - stained hippocampal neurons left untreated (CTL) or challenged with oligomeric $A\beta_{1-42}$ (Aβ) in the absence or presence of H3/H6 peptides, H3 - AuNP (nano spheres), or H3 - AuNS (nano stars, all 10 µg/ml). Scale bar, 10 µm. (B, C) H3/ and H6 peptides (B) and (+/- PEG) - H3 - functionalized AuNP/NS (C) protect cultured hippocampal neurons against Aβ - induced death. CTL, untreated cells; Aβ (8 µM) – neurotoxin only-treated cells. H3 - PEG, H3 and PEG - functionalized AuNP/NS. PEG, PEG - only conjugated AuNP/NS. One - way ANOVA vs Aβ, three to four independent experiments, *p < 0.05; **p < 0.01 ……**173**

Figure 8.2. ICP standards used to quantify the gold content in the gold samples analysed in this study ……**175**

Figure 8.3 Full XPS spectra of the elemental peaks for all 6 EDC/NHS coupling L - dopa to PEG experiments under different conditions ……**176**

List of Tables

Table 4.1 Table to show the dependence of the concentration of sodium citrate on the diameter of the spherical gold seed ……**72**

Table 4.2 Peptide: PEG ratios for gold nanostars (left panel) and nanospheres (right panel) ……**79**

Table 4.3 Table summarising the effect that changing the concentration of $AgNO_3$ had on the length of spikes formed during synthesis. The spike length was measured from the core of the star to the tip of the spike using ImageJ. n = 200 ……**86**

Table 4.4 Table summarising the effect of changing the volume of $AgNO_3$ had on the quantity of spikes formed during synthesis. The quantity of spikes were measured by recording how many spikes were visible per star using ImageJ. n = 200……**88**

Table 4.5 Table summarising the effect of changing the nano seed size on the overall formation and geometry of the nano stars. The nano stars were measured by visual representation measured by using ImageJ. n = 200……**89**

Table 4.6 Summary of the effects of different chemical parameters on the morphological characteristics of the gold nanostars ……**90**

Table 4.7 Table summarising the physical properties of the Au nanostars and nanospheres. Au nanostar (middle panel) and Au nanosphere (right panel) physical properties including core size, particle diameter (measured tip to tip), quantity of spikes per star and the length of the spikes measured by Image J. These calculations gave the surface available for drug binding. n = >200 ……**94**

Table 4.8. Peptide : PEG ratios for full surface coverage of gold nanostars (left panel) and nanospheres (right panel). To achieve 100% AuNS/AuNP peptide only full surface coverage, 50 µL/100 µL of 2 mg/mL H3/H6 peptide was required. To achieve 100% AuNS + peptide + PEG full surface coverage, 37.5 µL of 2 mg/mL H3/H6 peptide and 31.2 µL of 1 mM PEG was required. 75 µL of 2 mg/mL H3/H6 peptide and 62 µL of 1 mM PEG was required for AuNP + peptide + PEG 100 % surface coverage ……**97**

Table 4.9 pH values of the media containing the peptide targeted nano structures measured for zeta potential analysis **104**

Table 6.1 Table showing the varying volumes of the synthesis components to produce L - dopa functionalised nanostars ……**140**

Table 6.2 Table showing the volume of L - dopa trialled to stabilise the nanostars per synthesis……**141**

Table 6.3 Table showing the different modifications trialled during the six different variations used to couple the L - dopa to PEG *via* EDC/NHS chemistry ……**143**

Table 6.4 The different volumes of 15 mM L - dopa used to bind to the nanostar surface in an attempt to form L - dopa capped functionalised nano stars ……**155**

Table 6.5 Table showing the different pH values of the solutions. Middle panel, showing which medium in which the EDC was dissolved and pH. Right panel, at the point in the protocol shown in Figure 6.11 after the Sulfo – NHS was added to form the amine ester, the particles were re - suspended in MES buffer with different pH. ……**159**

Table 6.6 Table providing an overview of how efficient the binding of either the PEG or L - dopa was on the particle surface (a), the confirmation that the PEG molecules were still bound to the AuNS at the end of the experiment (b). (c) Confirms the presence of L - dopa in the particle solution and (d) confirms the yield of L - dopa molecules detected cross linked with the PEG in the presence of EDC/Sulfo – NHS to form a stable amide bond ……**163**

1 Introduction

Currently 1.2 million patients per year are affected by Parkinson's disease (PD) in Europe[1]. Data from the WHO have suggested that brain disorders account for 35% of the burden of all diseases in Europe[2]. Moreover, the incidence of PD is forecast to double by 2050 primarily as a result of the ageing population. Even at their current incidence rate, neurodegenerative diseases place a very large economic cost on states and majorly impact patient quality of life. The economic cost of PD in Europe is estimated at €140 Billion per year, where the costs are divided between direct healthcare costs (40%), direct non-medical costs (20%) and also costs associated with patient's production losses (40%)[1, 2]

At this present time, PD still remains incurable due to the unknown exact aetiology of the disease. How the onset of the disease is triggered also still remains elusive. Much research has gone into further understanding the pathogenesis of PD and many treatments have since been made available. However, these current therapeutics are short acting and only target the disease symptoms, having no impact on preventing or slowing the disease progression. The quest to develop effective therapeutics is majorly hindered by the Blood Brain Barrier (BBB), preventing drugs from entering the brain parenchyma and targeting the neurons. Nano-neurotherapeutics are fast developing as they are sufficiently small to cross the BBB, but more importantly have unique intrinsic properties and can be engineered with a high surface area to perform multiple functions such as cargo drug delivery, cell targeting and bioimaging[3, 4, 5].

Current treatments for PD only treat the symptoms and fail to protect or regenerate the damaged neurons. Previously identified S100A4 protein, that emits multifunctional trophic factors in the nervous system has shown to be markedly overexpressed in human brains after injury and during neuropathologies[6, 7, 8]. Previous research has confirmed that the S100A4 protein is neuroprotective, both *in vitro* and *in vivo* against many of the detrimental effects seen in PD pathology. More importantly, these beneficial effects of the S100A4 protein

can be reproduced by its two peptide mimetics, H3 and H6, that Porter group have designed, that encompasses the neuroactive motifs of the S100A4 protein[6, 7, 8].

There are many advantages for using small peptides over protein/growth factor-based therapeutics, as they are low cost and readily producible. They can easily be chemically modified, but most importantly they specifically encompass the neuroactive attributes of the parent protein thus minimizing potential side effects. This platform technology can activate multiple neuroprotective pathways and potentially treat several neurological conditions.

The purpose of this thesis is to design and develop a novel nano – platform consisting of nano particles of differing morphologies that will act as a delivery vehicle that can be functionalised with the H3 and H6 peptide mimetics as cargo that will enable BBB crossing, neuronal protection and growth of damaged neurons inside the brain. The nano particle morphologies; nanostars and nanospheres, will be compared to determine the most effective structure for delivery of the peptides.

Chapter 2 of this thesis introduces current scientific literature, addressing Parkinson's disease, with an in depth discussion on the disease pathology and how it is treated so far to date. The literature will emphasise the use of nanotechnology used in medicine, focusing on how nano particles can be used as a drug delivery system. This review introduces novel neuro - protectant therapeutics previously designed by Porter group that have demonstrated to alleviate many of the PD pathological hallmarks. Enabling nano particles to cross the BBB is also discussed in depth to provide an understanding of the challenges faced when designing a drug therapeutic to treat any neurological disorder.

Chapter 3 provides an overview of the principle experimental techniques employed to obtain the data throughout this thesis.

The first results section, **Chapter 4**, focuses on the optimisation of gold nano particles of differing morphologies as intended drug delivery systems that were then subsequently conjugated with the two novel neuroprotective drugs.

The second results section, **Chapter 5**, demonstrates the application of these new novel nano therapeutics on hippocampal neurons and dopaminergic cells. This chapter examines the most effective drug alongside the most effective drug carrier on combating the disease pathologies seen in PD patients. Through an array of biological assays, the new nano

compounds were investigated for their neuroprotective abilities against oxidative stress and toxicity. An important part of PD pathology is the loss or damage of dopaminergic neurons, therefore, this chapter investigates the effects these nano compounds have on stimulating new neurite extensions in hippocampal neurons. They were further explored by electron microscopy imaging to understand how the particles and neurons interact and if the morphological structure of the nano particle acting as the delivery system impacts the neuronal interaction and drug delivery.

In the third results section, **Chapter 6**, a synthesis protocol is developed and refined to functionalise the nanostars and particles with L - dopa to target the LAT 1 transmembrane protein that would allow the particles to be shuttled across the BBB and target the dopaminergic neurons in the brain. The particles are designed so that they have multiple target functionalities: 1. They can cross the BBB; 2. They can be used for bioimaging using fluorescence enhancement, and 3. They can be conjugated, in future, with H6/H3 peptides to protect neurons.

The final conclusions found from this study are summarized in **Chapter 7**, along with suggestions to further this study. **Chapter 8** presents the appendices of this thesis.

2 Literature Review

2.1 Parkinson's disease

2.1.1 What is Parkinson's disease?

Parkinson's disease is part of a group of conditions called motor system disorders[9]. It is the second most common neurodegenerative disease, following Alzheimer's disease[6]. Parkinson's disease (PD) was first described by James Parkinson in 1817[11]. PD is potentially one of the most perplexing and mystifying neurological disorders. The most common form of Parkinsonism is said to be Idiopathic PD[9]. Other forms of Parkinsonism's include, but not limited to, vascular PD, drug – induced PD, genetically inherited PD and juvenile PD[10]. The pathological hallmark of the disease is characterised by the loss or impairment of dopaminergic neurons that lie within the Pars compacta region of the substantia nigra[12] (Figure 2.1).

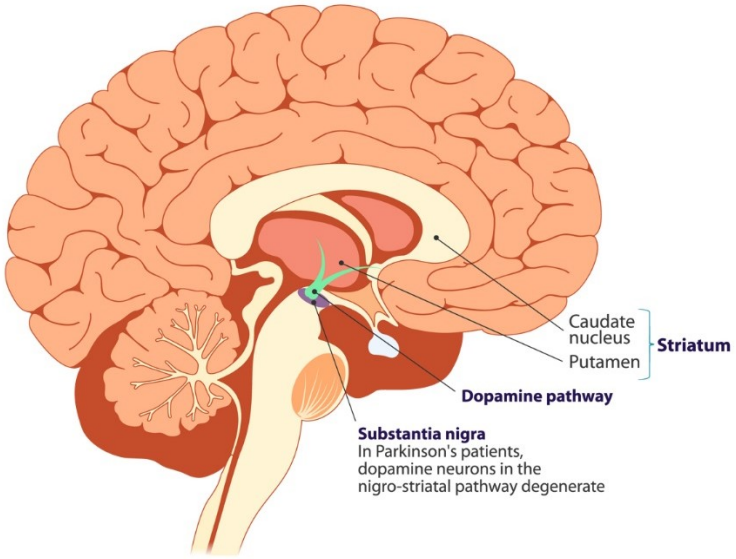


Figure 2.1 Cross section of the brain demonstrating the location of dopaminergic neurons[37].

The accumulation of the protein; alpha-synuclein, allowing the formation of lewy bodies within surviving neurones has also been of interest as this falls under the category of dementia with lewy bodies, but patients demonstrate parkinsonism features[6]. Under natural circumstances, dopamine; a chemical neurotransmitter is released in the striatum, to allow smooth, purposeful motor control[13,37].

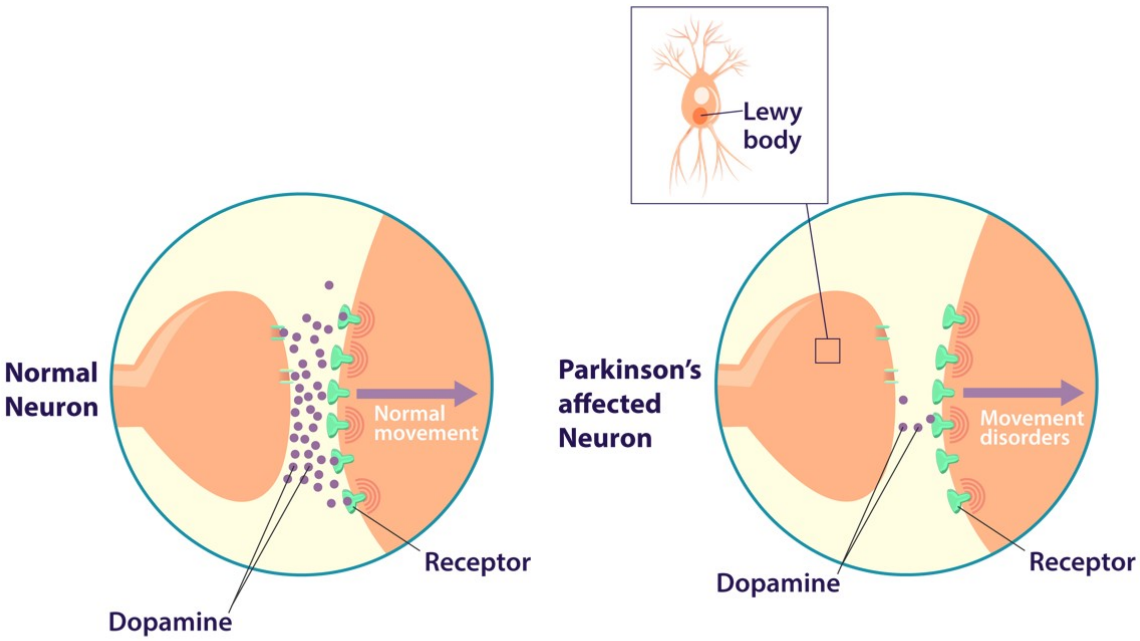


Figure 2.2 Schematic diagram representing a normal functional neuron (left) that allows uninhibited crossing of the dopamine neurotransmitter, Vs Parkinson's disease affected neuron (right) that has a deceased synaptic crossing of dopamine leading to movement disorders[37].

Dopamine is vital to facilitate movement, therefore, deficits in dopaminergic neurons can render individuals unable to direct or control their movements in a conventional manner[10, 13]. Physically, the motor deficits are primarily shown in the form of a resting tremor, which is apparent in the hands, arms, legs and face of an individual, particularly in the jaw[10]. A depreciated level of dopamine can present in the form of decreased or slowness of movement, also known as bradykinesia and also akinesia, demonstrating muscle rigidity or stiffness in an individual's limbs and trunk movement[10]. As the disease advances, additional motor deficits may develop, particularly in postural reflexes, displaying instability or impaired

balance and co – ordination[12]. Furthermore, alongside the fore mentioned physical impairments, patients may potentially develop non-motor symptoms[13]. These non-motor symptoms can have equal detrimental effects to an individual's everyday life causing cognitive impairments that lead to dysfunction in areas such as: memory, thought, language and behaviour as well as sleep disorders and depression[13].

Other forms of Parkinsonism, for example, familial Parkinson's disease, the cause is either known or at least suspected, or the possibility that the disorder occurs as a secondary effect of another, primary neurological disorder[10]. The cause of idiopathic Parkinson's remains undetermined.

There have been considerable advances to date in defining the aetiology and the pathogenesis of PD including environmental factors, neuroinflammation, genetic mutations, mitochondrial dysfunction and oxidative stress with a view to identify abnormalities, that can then provide targets to enable the development of novel disease modifying therapeutics to prevent or delay the progression of PD.

2.1.2 Parkinson's disease pathology

Aetiology

So far to date the characterisation of idiopathic Parkinson's disease is known to be the loss of dopamine producing neurons. The reasoning behind what causes the neuronal death still remains undefined, therefore, no protective measures against cell death have been 100% effective. Through extensive research, there are many factors that can cause cellular mutations such as environmental factors and genetic mutations that potentially lead to Parkinson's disease, in the form of toxin-induced and Familial PD. It is possible that Parkinson's disease may occur through the inflammation of neurons or that an external or an internal toxin selectively destroys dopaminergic neurons[11, 14, 15, 18, 31, 34]

Environmental Factors

Epidemiological studies have identified neurotoxins, such as; 1-methyl-4-phenyl-1,2,3,6,-tetrahydropyridine (MPTP) and Rotenone, as being of particular interest in research, due to their ability to inhibit the complex 1 function in the electron transport chain, within the mitochondria[14]. Prolonged exposure to these toxins has shown a heightened risk for Parkinsonism[11, 14, 15].

The link of MPTP and the death of neurons producing dopamine has been confirmed through rodent and post-mortem studies[15]. MPTP has the ability to cross the blood brain barrier (BBB), where, in the presence of enzyme monoamine oxidase B (MAO-B) converts MPTP to its active metabolite MPP+ (1-methyl-4-phenylpyridinium)[15]. The active metabolite, MPP+ is a substrate for the dopamine transporters (DAT) therefore, via these dopamine transporters, MPP+ transported into dopamine producing neurons[15]. Once imported, it can then bind, exert its toxicity and thus, inhibit complex 1 function within the electron transport chain[16]. This then leads to a disruption in the oxidative phosphorylation function, resulting in the excessive production of reactive oxygen species (ROS) leading to oxidative stress and cell death[14].

There are many common pesticides, herbicides and chemicals such as; Rotenone, permethrin, beta – hexachlorocyclohexane (beta – HCH), paraquat and 2, 4 – dichlorophenoxyacetic acid (2,4-D, weed killer) that have the same ability as neurotoxin MPTP to cross the blood brain barrier, access dopamine neurons and inhibit the complex 1 function of the electron transport chain[11]. Rotenone has one exception in the fact that it can activate microglia following exposure[14]. Studies have shown high and low amounts of rotenone signify neurodegeneration with the presence of microglia, due to phagocytosis of dying cells[11].

Inflammation

Neuroinflammation plays a key role in the pathogenesis of PD. Naturally, inflammatory mechanisms prove positive in healing and limit injury. However, high levels of neuroinflammation can cause tissue damage[14]. In post-mortem PD studies, glial cells such as; microglia, astrocytes and oligodendrocytes in the substantia nigra and striatum, are activated[13]. During the resting state, microglia display enlarged morphological characteristics that allow them to monitor their microenvironment[18]. These characteristics include branching structures that can extend and retract to allow detection for cells that have been damaged and also identify invading pathogens and toxins, such as Rotenone and MPTP[14, 18]. The activation of glial cells, results in morphological changes in phenotype and gene expression in which they then secrete pro-inflammatory mediators[14]. These mediators, including, but not limited to, lipopolysaccharides (LPS), tumor necrosis factor (TNF), interferon – y (IFN-y), Interleukin-1β (IL-1β) and Interleukin-6 (IL-6), have neurotoxic effects by catalysing the production of nitric oxide (NO), thus enhancing oxidative stress[11, 35]. As well as neurotoxins, alpha-synuclein aggregation has also shown to enhance microglial activation, which then leads to the release of cytotoxic factors[13]. Research past and present have been investigating the role of anti-inflammatory mechanisms with the potential of having a neuroprotective effect[13, 17].

Mitochondrial Dysfunction and Oxidative Stress

It has been widely recognised that mitochondrial dysfunction and oxidative stress can trigger apoptosis of dopaminergic neurons, thus presenting Parkinsonism features. Mitochondrial dysfunction mostly occurs at complex 1 of the mitochondrial transport chain, however, there has been no conclusive explanation yet to date to fully explain the complex 1 deficit[19, 22].

In vitro studies have found that through the isolation of mitochondria within PD patients, there exhibits the inhibition of NADH - Ubiquinone, resulting in decreased levels of adenosine triphosphate (ATP) [19]. As well as decreased levels of ATP, there is a reduction of oxidative phosphorylation and an escalated development of reactive oxygen species (ROS) [19]. Anti – oxidant defence systems provide a homeostatic balance against reactive oxygen species under normal physiological conditions[22]. Excessive production of ROS and limited antioxidant defence imbalance, results in oxidative stress. Through the imbalance, free radicals are produced, such as super oxide anions (o_2^-)[19]. These free radicals are unstable and liable to cause damage to cells.

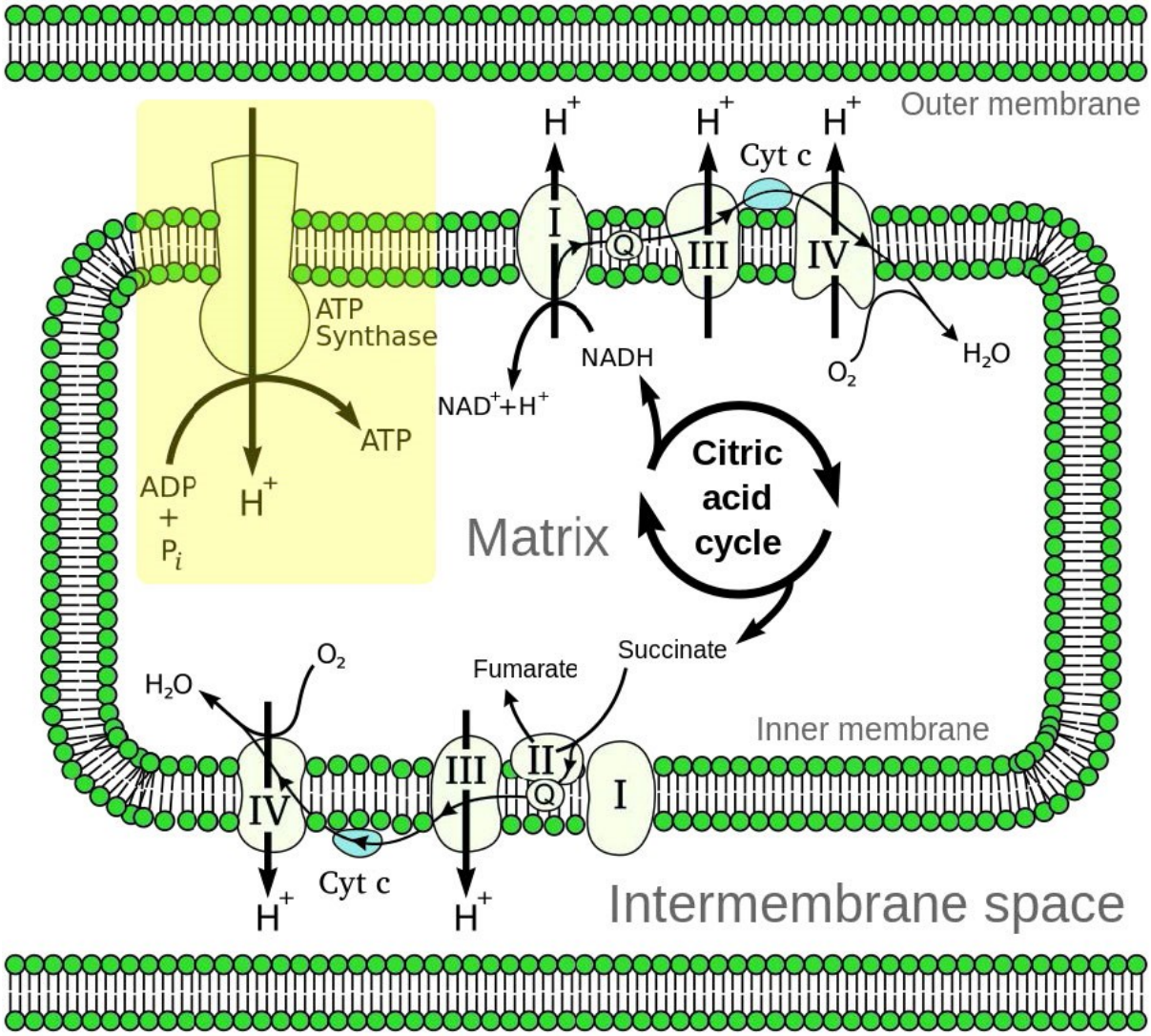


Figure 2.3 schematic diagram representing the mitochondrial transport chain. Mitochondrial dysfunction mostly occurs at complex 1, which is the start of the five step oxidative phosphorylation process thus inhibiting the cellular adenosine triphosphate (ATP) energy production[38].

Normally, free radical damage is kept under control by the body's endogenous antioxidant defences such as superoxide dismutase (SOD) [20]. It is shown that superoxide dismutase (SOD) found within the cells cytoplasm and mitochondria as well as extracellularly, can potentially decrease the risk of PD due to the antioxidant and anti-inflammatory properties that allow free radical super oxide anions (o_2^-) to be dismutased into a less toxic hydrogen peroxide (H_2O_2) and molecular oxygen (O_2) which then reduces oxidative stress by keeping the levels of excess ROS balanced[17]. Severe oxidative stress and limited anti – oxidant defences can activate apoptosis. Reactive oxygen species that is generated by the mitochondria as a by-product of oxidative phosphorylation and can lead to oxidative damage of proteins, DNA and lipids[9, 22].

Genetic Findings

Several genes have been identified as being associated with Parkinson's disease. Five of which are definitively associated with Familial Parkinson's disease (PD). These are the SNCA gene, PARK2 gene, PARK1 gene, PARK7 gene and LRRK2 gene[9, 21, 23, 24].

The Synuclein, alpha non A4 component of amyloid precursor (SNCA) gene, is responsible for generating the small protein α – synuclein which aids in regulating the transmission of dopamine[9, 23]. So far to date, at least 18 mutations in the SNCA gene have been recorded[24]. A defect or mutation in the 'SNCA' gene, that encodes protein α – synuclein not only impairs the neurotransmission of dopamine, but also induces the misfolding or excess production of α – synuclein, which can then form protein aggregates, which is seen in the pathology of lewy body Parkinson's[9, 23]. Defects in the SNCA gene has also been associated with early onset PD and autosomal dominant PD[9].

The PARK2 gene encodes for the protein Parkin, which acts as an ubiquitin E3 ligase, predominantly involved in the degradation of organelles[9, 23]. Parkin tags damaged organelles with ubiquitin molecules which then stimulates ubiquitination as part of the ubiquitin-proteasome system (UPS) that then degrades and disposes of damaged organelles through autophagy[21]. A defect in the PARK2 gene can cause a loss-of-function in the Parkin protein

that inhibits the ubiquitin-proteasome system resulting in a build - up of damaged organelles, seen in autosomal recessive juvenile 2 PD[9, 24].

PINK1 gene (PTEN-induced putative kinase 1) is responsible for mitochondrial kinase[9]. PINK1 works in collaboration with Parkin (PARK2) to mediate the mitochondrial quality control system[21]. A defect or mutation of this gene can inactivate the genes function and results in neuronal death through oxidative stress or by the build - up of damaged mitochondria[9, 25].

PARK7 (PD autosomal recessive early onset 7) encodes for the protein DJ - 1, which is a H_2O_2 responsive protein[9]. The proteins function is to act as a mitochondrial antioxidant through as well as a redox sensor. It also aids in the folding of newly produced proteins into their 3 – dimensional shape[9, 25]. As with PINK1 a defect or mutation in the mitochondrial antioxidant function, can lead to neuronal death through oxidative stress, resulting in PD and also a mutation in the protein folding function of DJ – 1 will lead to misfolding of proteins, thus, parkinsonism features[9, 31].

Gene 'LRRK2' (Leucine-rich repeat kinase 2) has multifunctional kinase properties, in which mutations or defects in the kinase activity can lead to autosomal dominant late onset PD[9]. LRRK2 gene encodes for protein, dardarin. This protein is not well understood, but is thought to play a part in protein – protein interaction. Its kinase activity plays an important role in assisting the transfer of phosphate groups which is vital in switching cellular activity on and off[9, 23]. How the mutations/defects in this gene leads to PD is not well characterised even though over 100 mutations in this gene have been identified[9, 23, 25, 31].

2.1.3 PD treatments and limitations

The key issue in treating PD (aside from establishing an exact root cause) is the ability for molecules to cross the blood brain barrier (BBB). Unless they are small, non – polar or a gas, they are unable to cross without associated transport[27, 28]. Two main therapeutics for PD at present are L- dihydroxyphenylalanine (L - dopa) and Monoamine oxidase (MAO) B inhibitors selegiline and rasagiline.

Although there is no cure for PD, there are many treatment options available to alleviate parkinsonism features, but not all therapies are effective in all patients. The primary treatment available is levodopa which aids the production of dopamine[31]. L - dopa is used in PD patients to enhance dopaminergic transmission by stimulating the D1 receptor in the striatum to improve PD motor functions[26].

Levodopa shows to have the desired effects initially, but as the disease progresses and the continual loss of dopaminergic neurons occur, ultimately, results in the deficiency in the metabolism of the drug and hence the storage and release of dopamine, thus causing difficulty in performing voluntary muscle movements[31]. Dopamine is unable to cross the BBB as it is polar in nature, therefore unable to diffuse across the BBB membrane[28]. L - dopa is also polar, but as it is produced from the amino acid L-tyrosine, it is able to attach to the transmembrane transporter; L-type amino acid transporter (LAT - 1). LAT - 1 then enables L - dopa to cross the BBB via facilitated diffusion[28]. L - dopa is then decarboxylated to form dopamine and is focused in the pre – synaptic nerve terminal. L - dopa is not without its side effects, which have proven to include increased toxicity and inflammation after prolonged use[26].

The effects of the simulated dopamine released from the levodopa treatment only lasts between 1-3 hours[36]. This can be enhanced by the administration of catechol-O-methyltransferase (COMT) inhibitors like tolcapone or entacapone, as these inhibitors will increase the absorption of levodopa, thus prolong the half- life effects of levodopa alone[36]. As well as COMT inhibitors, dopamine agonists such as monotherapy can be co-administered with levodopa to improve symptoms, although some dopamine agonists are just as effective, especially in the management of dyskinesia's when used alone due to their dopaminergic stimulation properties, nevertheless, due to the continual loss of dopaminergic neurons, dopamine agonists will only suffice as a lone treatment for a limited period[31, 32, 33].

Monoamine oxidase (MAO) B inhibitors, such as selegiline and rasagiline are of particular interest due to the substantial amount of data confirming their neuroprotective mechanisms. MAO-B enzymes catalyse the breakdown of neurotransmitters including dopamine[29, 30]. As previously stated, a lack of dopamine is one of the pathological characteristics of PD. MAOs are located on the outer mitochondrial membrane in both neurons and glial cells. MAO-B inhibitors are designed to slow the metabolic breakdown of

dopamine, thus, allowing prolonged dopamine action[29, 30]. Selegiline is also used as an anti-depressant as dopamine is not the only neurotransmitter to be affected, but serotonin, epinephrine and norepinephrine are also targeted to breakdown by MAOs. Selegiline dosing is important as too much or too little MAO – B inhibitor can cause further neurological disorders. As MAO-B are primarily found in blood platelets, there is not the issue of the inhibitors crossing the BBB, there is however, an issue with selegiline producing a toxic metabolite; amphetamine[29, 30].

Monoamine oxidase (MAO) B inhibitors are of particular interest at present due to their neuroprotective mechanisms[36]. MAO-B inhibitors presently available are selegiline and rasagiline[32, 33], with rasagiline being of most interest, due to rodent studies confirming clear neuroprotective effects against neurotoxin MPTP and its metabolite MPP+ and the toxic damage caused by 6-hydroxydopamine. It has also shown to have a positive effect to mitochondrial dysfunction, thus, reducing the rate of apoptosis[31]. Rasagiline is under current investigation to determine the possibility that this drug could potentially have a disease modifying effect[36].

Although there are a number of viable treatment options for PD, they still remain unsatisfactory. There is a need for further development of disease modification therapeutics and novel treatments to prevent or delay the progression of PD.

2.2 S100A4 protein

The S100A4 protein (Figure 2.4) belongs to the S100 family of calcium – binding proteins. They can be found in the cytoplasm or nucleus of many different cells and the S100A4 protein is primarily associated in cancer biology due to its metastasis – promoting properties. An increase in the S100A4 protein has shown significant increase in tumor growth. It is also reported that extracellular S100A4 enhances cell proliferation and so regulates tumor progression through the interaction of the epidermal growth factor (EGF) receptor (EGFR) ligands, and the associated enhancement of EGFR/ErbB2 receptor signalling[38, 39, 40].



Figure 2.4 S100A4 protein. Image adapted from Dmytriyeva *et al*, 2012.

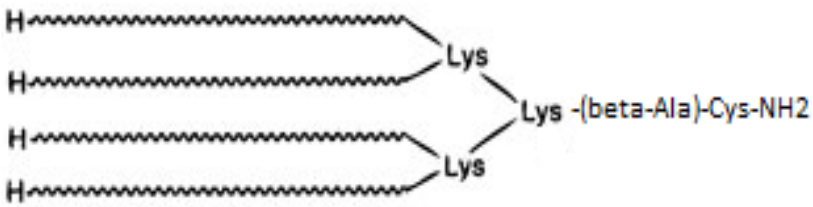
As S100 proteins in general have no enzymatic activity, they interact with other proteins to enable them to exert their effects[40]. The S100A4 protein stimulates tumor cell migration through being upregulated by heterotetrameric β-catenin/T-cell factor complex. Blocking or inhibiting the β-catenin protein, then has the opposite effect where S100A4 expression is down regulated, thus reducing tumor cell migration[38, 39, 40]. S100A4 has the ability to induce tube formation in endothelial cells via a RAGE-independent pathway that may have an effect on angiogenesis. S100A4 promotes the expression of vascular endothelial growth and cell migration through modulating the vascular endothelial growth factor (VEGF), which increases the kinase domain – containing receptor (KDR) expression and Matrix metallopeptidase 9 (MMP-9) activity via the RAGE receptor[38, 39, 40]. In terms of cancer biology, the inhibition of the S100A4 protein is a desired therapeutic approach for the treatment of cancer.

However, the growth promoting properties of the S100A4 protein are of desirable quality in respect of brain injury and neurodegeneration. S100A4 protein expression has been

detected at sites of trauma (lesions) and neurogenesis, thus suggesting that S100A4 plays a role in neuronal plasticity. Oligomeric S100A4 have been shown to promote the growth and survival of cultured neurons, and demonstrate neuroprotective effects after brain injury via the activation of the ERK1/2 pathway and many other pathways and channels shown in Figure 2.6[6, 7]. The effects of the S100A4 protein in neurobiology is not as well characterised as that in cancer biology. However, it has shown promising attributes to justify further investigation, especially focusing on Porter groups successful synthesis of S100A4 derived peptides that mimic the neurotrophic effects of the S100A4 parent protein[6, 8, 43].

2.2.1 S100A4 derived neurotrophic motifs H3 and H6

The H3/H6 peptide mimetics are synthesized as tetramers composed of four monomers coupled to a lysine backbone. In the peptides a beta-alanine spacer has been inserted at the root of the dendrimer and functionalized with a cysteine amino acid incorporating a thiol (-SH) bond. The amine group ($-NH_2$) on the cysteine denotes that the cysteine is a c-terminal amide (uncharged) rather than a c-terminal carboxylic acid (negative charge). This is important for neurite growth[8].



H3 H-KELLTRELPSFLGKRT(>K)(>K)(beta-Ala)C-NH_2

H6 H-NEFFEGFPDKQPRKK(>K)(>K)(beta-Ala)C-NH_2

Figure 2.5 Image showing the general structure of the 4 - branched peptide dendrimer, and the amino acid sequence of each motif; 'H3' and 'H6'. Synthetic peptides encompassing the S100A4 derived neurotrophic motifs have been generated by Schafer-N, Denmark[8].

The peptide was synthesized starting with the root i.e. first cysteine, then beta-alanine and then the lysines. The lysines each have two amino groups onto which two more lysines can be coupled which enabled the branching. When all 3 lysines have been coupled, there are four amino groups and the four identical peptides in the branches are synthesized on these amino groups. The H3-peptide is highly homologous within the S100 family, while the H6-peptide (C-terminal of S100A4) shares little homology with other S100 members ('unique' motif). Figure 2.5 represents a schematic image of synthesized peptides. The jagged lines are a representation of the individual H3 and H6 peptide sequences. Dmytriyeva *et al*, had previously found that Tetramerization was found to be necessary to mimic the neuritogenic activity of the S100A4 protein[6, 7, 8, 43].

2.2.2 Neurotrophic effects of H3 and H6 mimetics

These biologically active motifs (H3/H6) of the S100A4 protein, have the potential to become a novel therapeutic for Parkinson's disease, as they have proven to stimulate neurite outgrowth, protect neurons from *in vitro* toxin induced death and can cross the blood brain barrier. They are easily synthesised, modified and administered and given the fact they are isolated short sequences of the 'parent' protein, they exhibit limited side effects[6, 7, 8, 43].

<u>Neurite outgrowth</u>

The full characteristics of these novel peptides are still to be determined, as at present, very little is known still. Studies shown so far to date, confirm that both the H3 and H6 peptides mimic the neuritogenic abilities of the 'parent' S100A4 protein shown in Figure 2.6[8]. The proposed pathways/mechanisms utilised to stimulate the neuritogenic abilities is shown in Figure 2.7.

As previously mentioned, one of the pathological hallmarks of PD is the loss or damage of dopaminergic neurons. Therefore, the ability of these peptides to mimic the growth promoting properties of the S100A4 parent protein, that have proven positive to stimulate the growth of new neuronal neurites (Figure 2.6) if of great interest when designing a drug therapeutic to treat PD[6, 7, 8, 43].

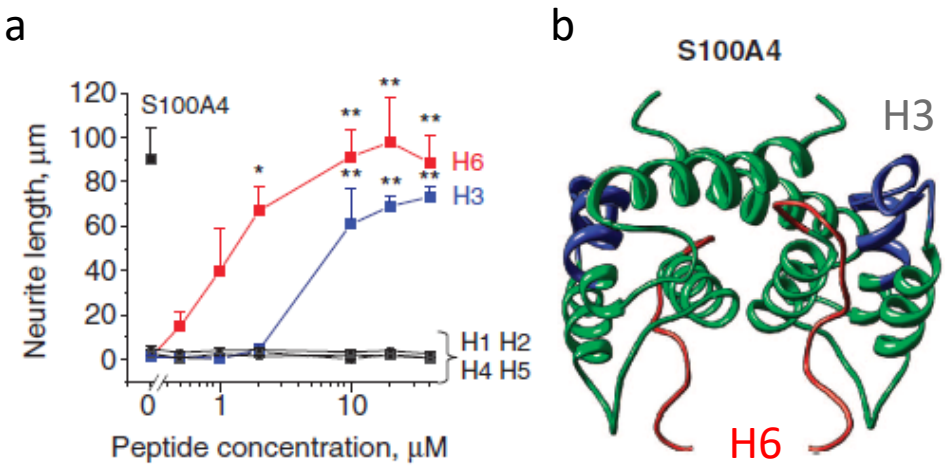


Figure 2.6 H3 and H6 mimetics can stimulate neurite outgrowth in hippocampal neurons when compared to the S100A4 parent protein positive control, (a). Identification of the neurotrophic motifs isolated and synthesised from the S100A4 protein, (b). H3 mimetic, blue, H6 mimetic, red. Image adapted from Dmtriteva *et al,* 2012[8].

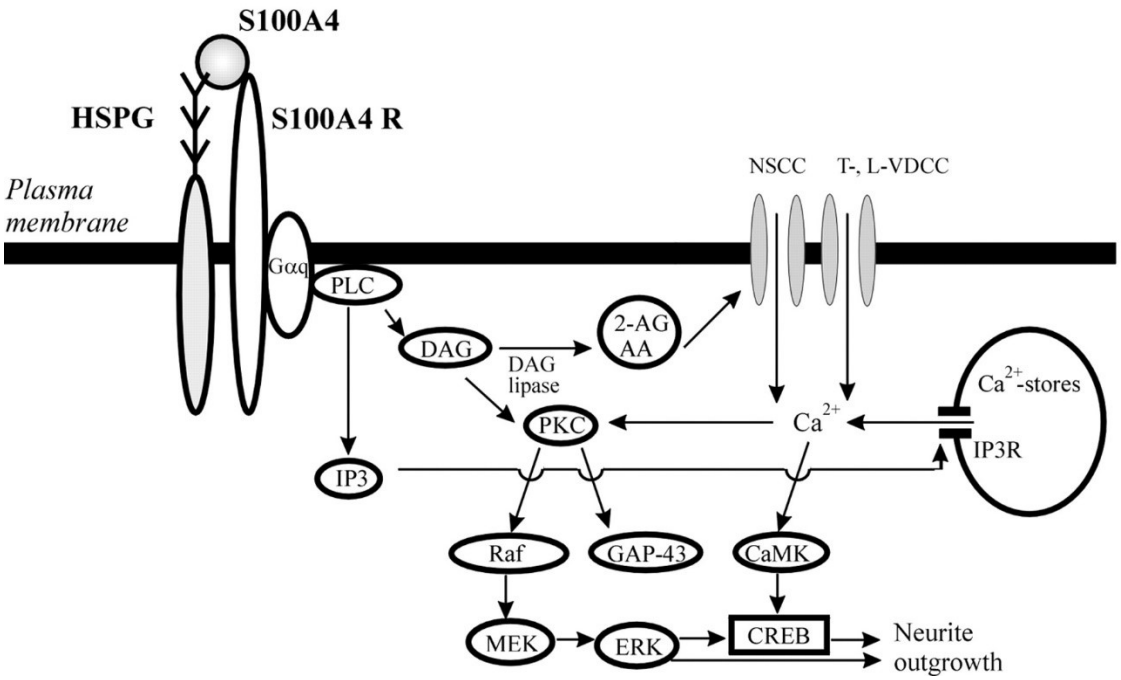


Figure 2.7 Schematic representation of the signalling pathways activated by S100A4. Upon interacting with the cell membrane, the S100A4 protein and the two mimetics H3 and H6 trigger a cascade of proposed pathways that induces neurite outgrowth. Image adapted from Kiryusko *et al*, 2006[7].

Neuroprotection

An important find was that both H3 and H6 motifs were able to activate and increase phosphorylation of Akt, ERK 1/2 and CREB messengers that are involved in S100A4 induced signalling, thus proving neuroprotective against oxidative stress; another important pathological hallmark seen in PD pathology in *in vitro* models. The survival rate of the dopaminergic neurons when subjected to neurotoxins H_2O_2 and OHDA can be seen in Figure 2.8[43]. These results make the H3 and H6 peptide mimetics contenders for further investigation as oxidative stress is one of the leading factors causing neurodegeneration in PD. Both the motifs demonstrated a significant reduction or complete lack of neuroprotection when ERK1/2 pathway and Akt were pharmacologically inhibited[6].

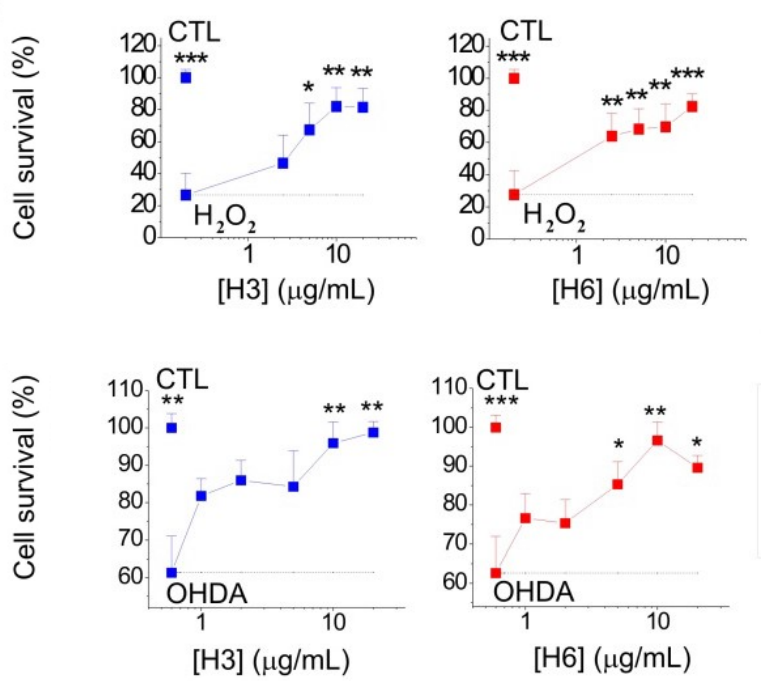


Figure 2.8 Neuroprotective effect of the S100A4 derived mimetics H3 and H6 in N27 dopaminergic cells against toxin induced cell death. Top – H3 and H6 protect N27's from H_2O_2 induced oxidative stress. Bottom - H3 and H6 protect N27's from OHDA-induced toxicity. Adapted from Pankratova *et al* 2018[43].

Dmytriyeva *et al*, further explored the S100A4 mimicking motifs H3 and H6 in brain injury models. The results were also conclusive for neuroprotection demonstrating a 50% reduction in neuronal death by the H3 peptide and 70% reduction by the H6 peptide at the site of injury and also provided protection against oxidative stress. After the positive effects from the two motifs, they were then tested to see if they could substitute the functions of the S100A4 protein in S100A4-deficient animals. Their findings demonstrated that the S100A4 knockout mice were more susceptible to brain trauma than the wild type mice[6]. The results, once again proved positive for neuronal survival, as both the motifs were able to decrease neuronal loss in the knock out mice to the same level as the wild type mice[6]. To further determine if the two peptides may have merit in a clinical setting, traumatic brain injury was induced in mice, they were then treated with either the H3 or the H6 peptide. After two hours of treatment it was determined that both the peptides were able to delay neuronal death by nearly two-fold[6].

Role of ErbBs

Little is known about the role of ErbBs in Parkinson's disease (PD) and Alzheimer's disease (AD) however, ErbB activation improves neuronal survival and synaptic function in AD models and ErbB4 is highly phosphorylated in the neurons of AD human brain and of APP/PS1 mice, a model of AD. Furthermore, oligomeric amyloid beta (Aβ) - a major inducer of neurotoxicity in AD - binds to ErbB4 presumably increasing Aβ insertion into neuronal membranes[6, 7, 8, 43].

Recent studies, demonstrated Aβ disrupted membrane structures in cell lines and hippocampal neurons, and this deleterious effect was counteracted by the H3 - peptide representing another important aspect of neuroprotection. Thus, the S100 - derived peptides target multiple neuroprotective mechanisms and may be effective for a range of neurological disorders [43].

H3 and H6 and the Blood Brain Barrier

A very important finding was that H3 and H6 peptides are able to cross the blood brain barrier. It is not clear exactly how the peptides cross the blood brain barrier, however, this does leave the opportunity open to explore further. H3 and H6 were detected in blood plasma and cerebrospinal fluid after systemic administration[6, 7, 8, 43], however, the peptides (H3/H6) proved to have limited circulation half-life therefore, would require an effective delivery system to enhance the half - life and stability of the peptides to enable them to be transported across the BBB and into the neurons whereby they can exert their therapeutic effects.

2.3 Nanotechnology

2.3.1 Nanoparticles

Gold Nanoparticles (AuNPs) are widely used in many scientific disciplines and therefore, synthesised in different ways. Physical and mechanical methods involve ball milling, Laser ablation, thermal evaporation or lithography to name a few[69]. For biological synthesis, it is possible to generate nanoparticles by using bacteria, fungi or by using plant extracts as a reducing agent added to aqueous $HAuCl_4$[69, 51, 55]. However, it is the chemical synthesis that is of interest to this review and piece of research, which similarly uses a reduction method; more specifically the focus will be on the reduction of $HAuCl_4$ by trisodium citrate dihydrate[69]. The addition of citrate also acts as a stabilising agent and is a commonly employed method to generate nanoparticles of smaller size, i.e. 10-20nm[53]. Particle size and shape can be controlled through manipulating experimental parameters. So far to date, particle sizes range between 5nm to 100nm with different shape structures such as rods, clusters, stars, spheres, cubes and shells having been characterised[69, 52] (Figure 2.9).

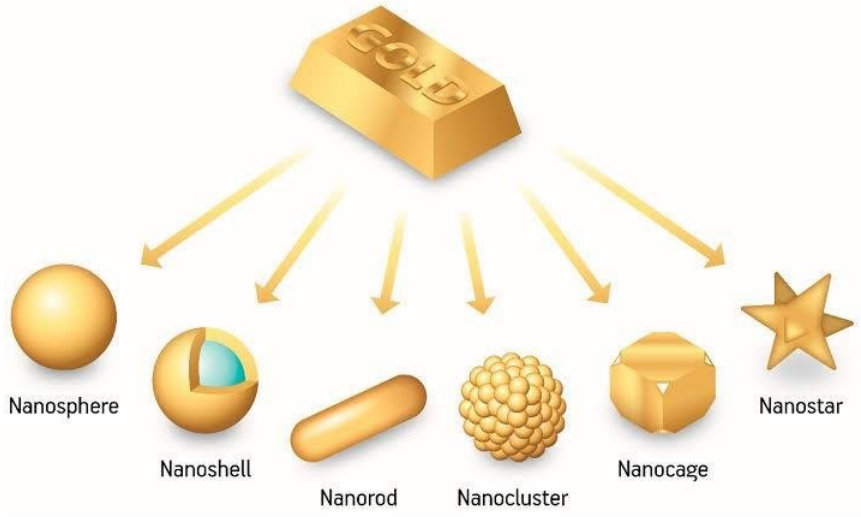


Figure 2.9 Schematic diagram demonstrating the different shaped nanoparticles that can be synthesised by the reduction of gold. Image adapted from Piyushkumar *et al* 2020[97].

Spherical AuNPs have proven extensively popular due to their ease of manipulation. Not only can the size and shape be altered to allow for large surface – to – volume ratio, but so can the surface chemistry and aggregation state, thus allowing high biocompatibility and low toxicity making them an attractive tool in nanomedicine[53].

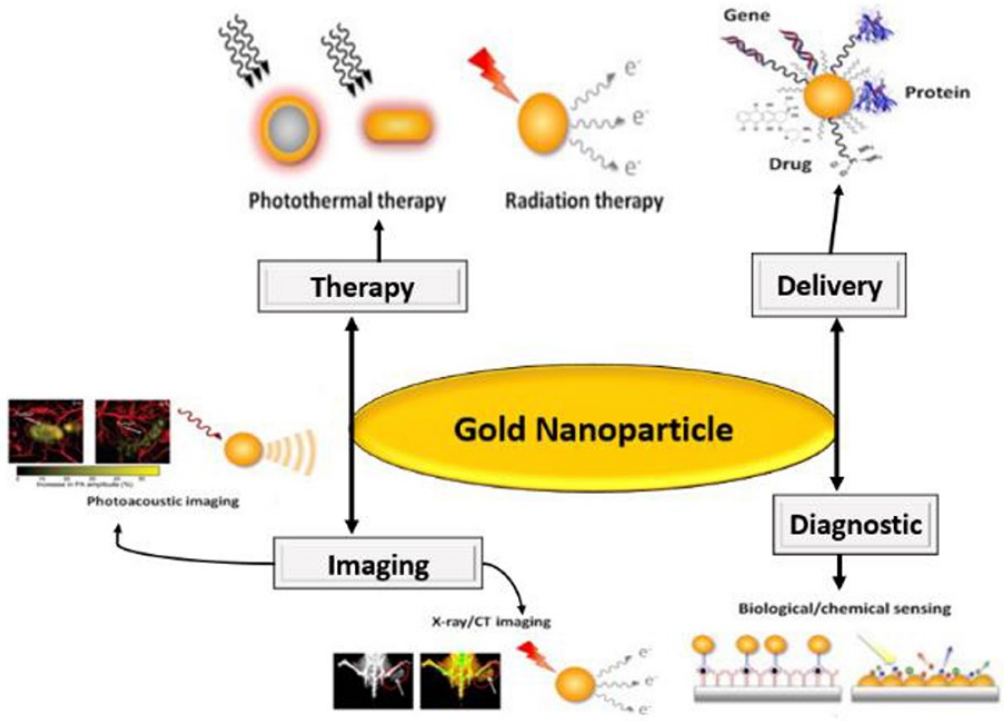


Figure 2.10 Schematic diagram demonstrating the biological applications of nano particles and imaging techniques used to track them inside the body. Image adapted from Bahar et al, 2020[98].

The reason gold nanoparticles have sparked a lot of interest is due to the fact they are very useful in many different ways in both biological and chemical disciplines (Figure 2.10). They have many favourable advantages, to include the capacity for them to be synthesised to different sizes and shapes and also their unique optical properties. They generate large surface areas that provide strong binding affinities towards thiol, disulphide and amine groups. This then allows various peptides/proteins, antibodies and many other biomolecules to be conjugated onto the nanoparticle surface. Another attribute of gold nanoparticles that has proven beneficial in studies is that as Au has a high atomic number, therefore, can be

traced non - invasively by CT imaging in vivo (Figure 2.10). They can also be quantitatively detected by atomic absorption methods ex vivo[54].

As AuNPs have a high electron density, Transmission electron microscopy (TEM) is predominantly used to detect colloidal gold particle interactions and associated biological and chemical agents. Scanning electron microscopy is also commonly used to aid in the characterisation of AuNPs[58].

Gold nanoparticles display an intense colour that comes from the basic photo - physical response that is non – existent in non – metallic particles[56].

Huang and El –Sayed (2010, p14) state that "When a metal particle is exposed to light, the oscillating electromagnetic field of the light induces a collective coherent oscillation of the free electrons (conduction band electrons) of the metal. This electron oscillation around the particle surface causes a charge separation with respect to the ionic lattice, forming a dipole oscillation along the direction of the electric field of the light. The amplitude of the oscillation reaches maximum at a specific frequency, called surface plasmon resonance (SPR) The SPR induces a strong absorption of the incident light and thus can be measured using a UV–Vis absorption spectrometer. The SPR band intensity and wavelength depends on the factors affecting the electron charge density on the particle surface such as the metal type, particle size, shape, structure, composition and the dielectric constant of the surrounding medium (Figure 2.11), as theoretically described by Mie theory"

Plasmon nanoparticles, notably gold and silver, produce a much stronger SPR band compared to other metals. Typically for gold nanoparticles of 10-30nm the SPR band is around 520 nm in the visible region[56, 57].

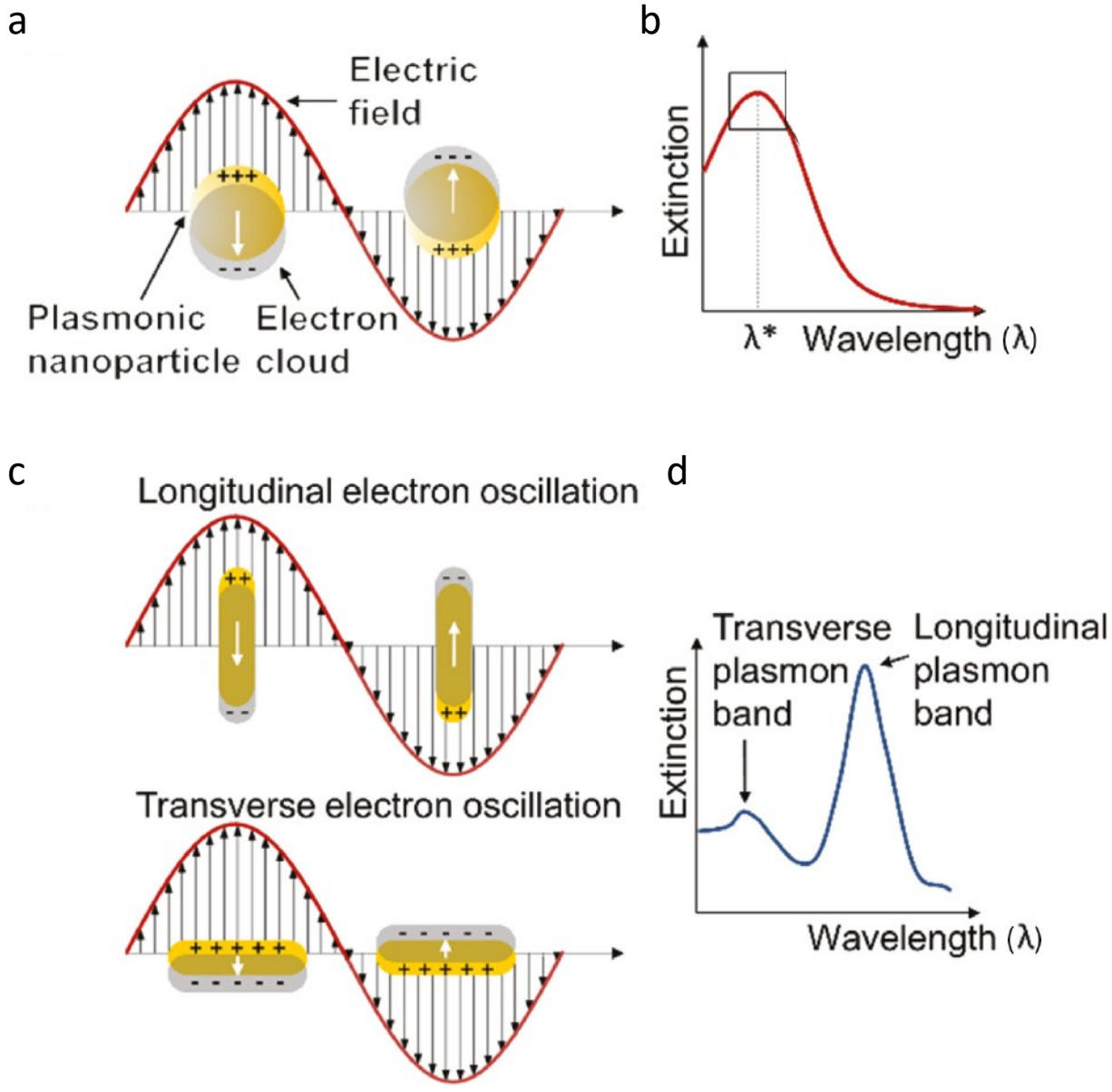


Figure 2.11. Schematic diagram demonstrating the surface plasmon resonance (SPR) inducing a strong absorption of the incident light (a, c) and thus can be measured using a UV – Vis absorption spectrometer (b, d). The SPR band intensity and wavelength depends on the nano particle structure. Nano sphere (a) and nano rod (c). The wavelength peak (b) can be used to determine the size of the AuNP. Image adapted from Xavier *et al,* 2018[99].

The use of gold nano particles used today in medical studies is very broad. Genomic studies, immune - analysis, clinical chemistry, bio - sensors', cancer cell detection all utilise gold nanoparticles. AuNPs are highly sought after in cancer therapy, for many reasons including; tumor detection, drug/DNA and antigen delivery, monitoring and imaging of cancer

cells. As AuNPs can be easily manipulated to function as required, it could be argued that they can be used and become a very important tool in all medical applications, not just limited to diagnostics, drug delivery and hygiene[58]. Many antitumor agents, such as; paclitaxel, sulphonamide, 5-fluorouracil, doxorubicin and Herceptin to name a few, have been successfully conjugated onto gold nanoparticles by either physical absorption, or through thiol linkers[58].

2.3.2 Neurological exposure to nanoparticles

Nanoparticles are proving more popular to functionalise as delivery vehicles for neurological drug therapeutics due to their ability to target and cross the BBB. There are many successful treatments to date that incorporate nanoparticle technology to treat neurological disorders such as PD, ALZ and stroke[121].

In Alzheimer's disease, biodegradable polymeric nanoparticles have successfully been fabricated with polyethylene glycol and/or poly(lactic-co-glycolic acid) and functionalized with specific antibodies[122, 123] or oligopeptide drugs[124] that have shown to eliminate and prevent the formation of amyloid fibrils, that mark the main pathological feature of ALZ disease.

For the treatment of Parkinson's disease, many different types of nanoparticles to date have been studied. Some of these studies have reported ex vivo of chitosan nanoparticles for the delivery of selegiline, a well-known anti - Parkinson agent[125], and pramipexole[126], a new form of dopamine agonist that has shown to effectively counter the progression of Parkinson's disease[127]. Additionally, the use of cerium oxide nanoparticles that can protect neurons against reactive oxygen species (ROS) - induced damage, has proven beneficial in improving motor dysfunctions as well as decreasing neuronal apoptosis[128]. The final nano particle based treatment for PD worth mentioning is the use of polymeric nanoparticles. It has been found that polymeric nanoparticles can efficiently deliver

microRNA, which potentially induces the migration of neurons into the lesioned site and ameliorate motor symptoms[129].

2.3.3 Nanotoxicology

Albeit, great advances have been made to date using nanoparticles of different size and morphologies, sadly, there is still an element of nano - toxicity that needs to be addressed. Nanotoxicology is rapidly growing especially due to the increase in application of nanomaterials in biomedicine, biotechnology, and environmental industry and the development of standardized nano - toxicological studies is crucial[130, 131, 132]. Nanotoxicology is also necessary since the interactions of nanoparticles with living cells and tissues are often unpredictable due to their unique physicochemical properties[133, 134].

Through any exposure route; ingestion, inhalation, through skin contact or intravenously, once crossed the BBB, nanoparticles have a tendency to accumulate in specific brain regions, where they can access the neural cells, including neurons, astrocytes, and microglia[138]. This in turn is what causes neurotoxicity. Figure 2.12 demonstrates the main mechanisms and factors of neurotoxicity induced by nanoparticles defined as any adverse effect on the structure, function, or chemistry of the central nervous system as a consequence of biological, chemical, or physical influences[121].

The neurotoxic effect can either result in the direct alteration of the structure or activity of the neural system or it can lead to subsequent effects due to glial activations and glial - neuronal interactions[139]. Furthermore, neurotoxicity can manifest through various mechanisms, including oxidative stress, resulting in cell apoptosis and autophagy, immune responses and neuroinflammation, which will affect the blood brain barrier function[140].

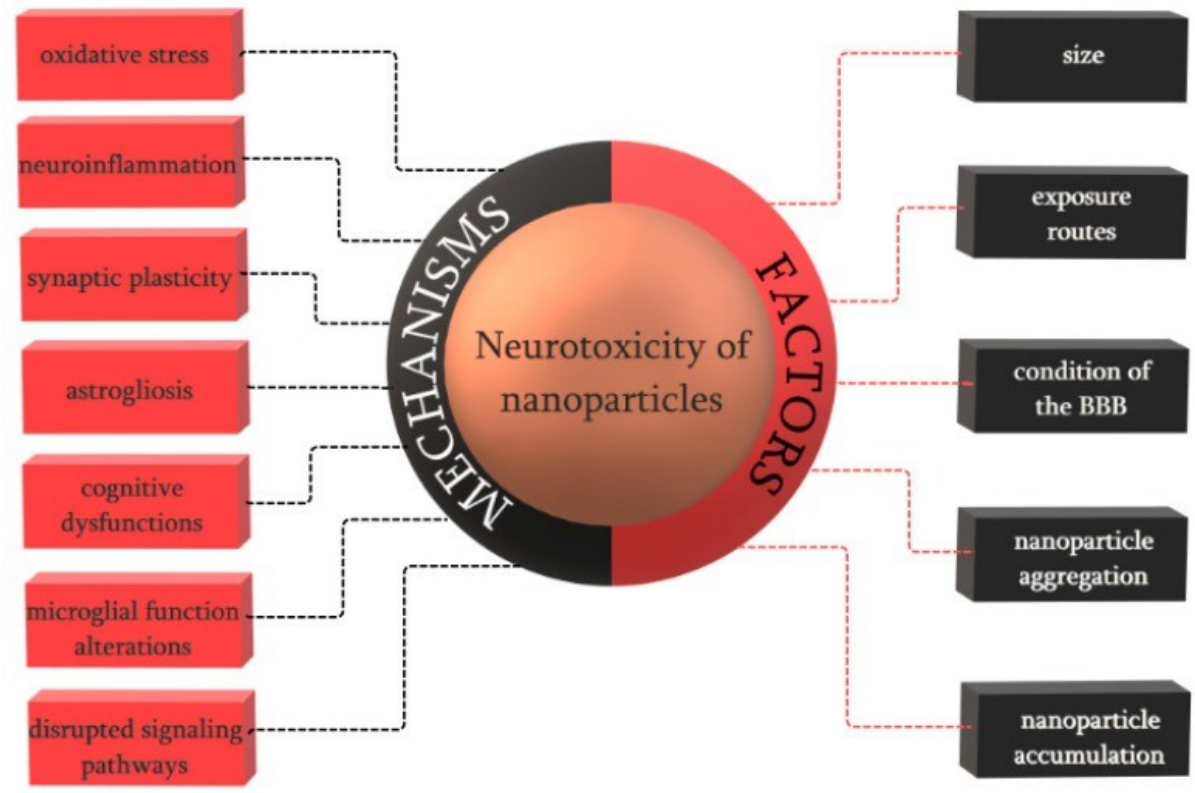


Figure 2.12 Schematic demonstrating the main mechanisms and factors of neurotoxicity induced by nanoparticles. Image adapted from Teleanu *et al* 2018[121].

The neurotoxicity of nanoparticles is most often caused by the enhanced production of reactive oxygen species (ROS) that ultimately leads to oxidative stress[141]. This then subsequently leads to the release of cytokines that then proceeds to cause neuroinflammation, and finally, through apoptotic mechanisms, neuronal death[141]. Many of the commonly used nanoparticles, including titanium dioxide nanoparticles, iron oxide nanoparticles, silver nanoparticles, gold nanoparticles, silica nanoparticles, and carbon-based nanoparticles, have been reported as potentially neurotoxic materials[142].

Unfortunately, the unique properties of nanoparticles that account for their beneficial effects in medical applications are those same physicochemical characteristics that are responsible for the nano – toxicity that results in human and environmental health concerns

[133, 135]. Moreover, the nanoparticle induced toxic effects may be considerably different than those of the bulk materials[136]. As such, understanding these health concerns is fundamentally necessary for the successful application of nanoparticles in biomedicine[137].

2.4 Blood Brain Barrier

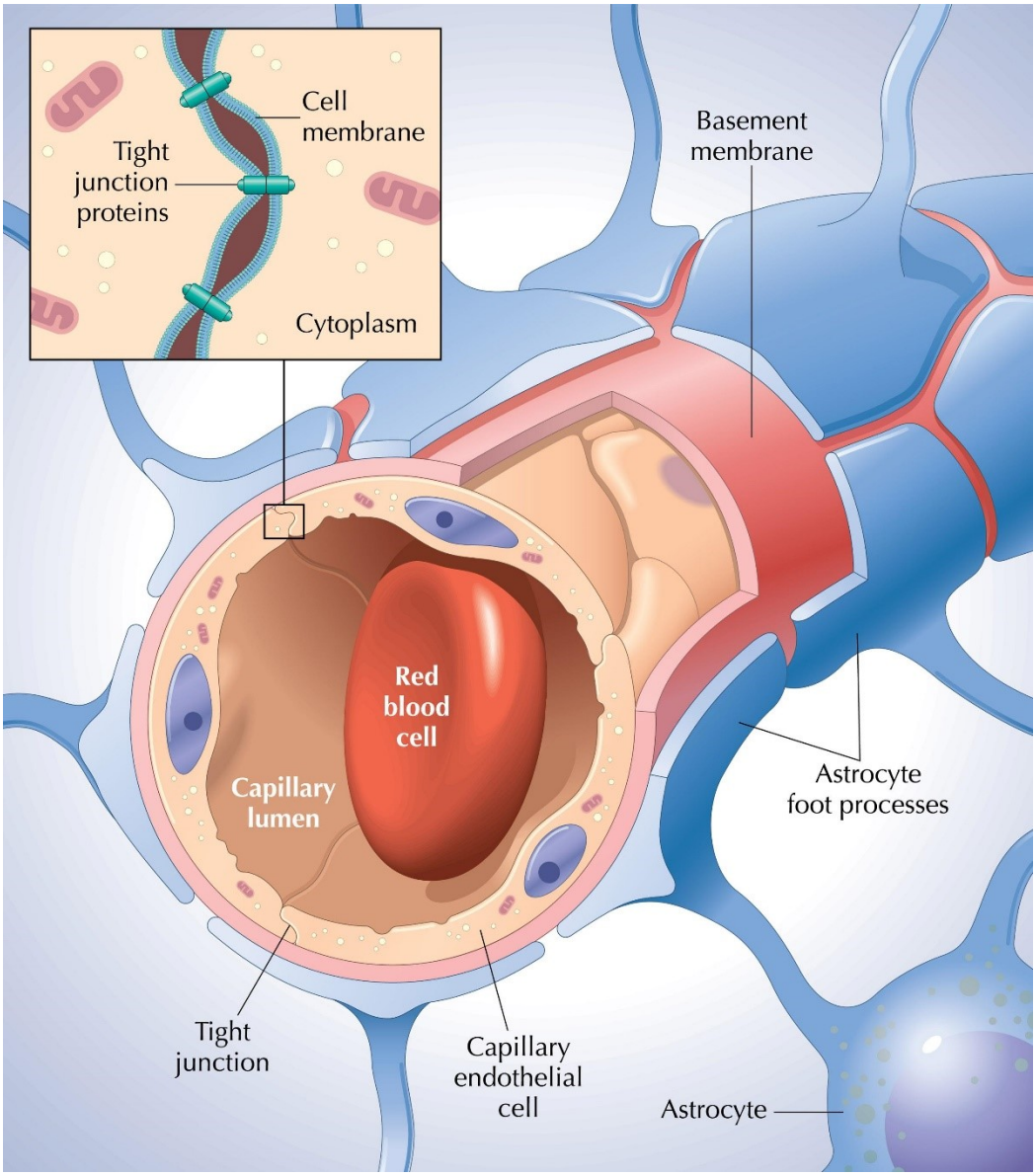


Figure 2.13 Schematic diagram of the Blood Brain Barrier (BBB). Image adapted from Perkins 2011[143].

The blood–brain barrier (BBB) is a term used to describe the unique properties of the microvasculature of the central nervous system (CNS) as shown in Figure 2.13. CNS vessels are continuous non - fenestrated vessels, but also contain a series of additional properties that allow them to tightly regulate the movement of molecules, ions, and cells between the blood and the CNS shown in Figure 2.14[144, 145]. This highly restrictive barrier allows BBB endothelial cells (ECs) to tightly regulate CNS homeostasis, which is critical for normal neuronal function, but more importantly the ECs regulatory capabilities protect the CNS from toxins, pathogens, inflammation, injury, and disease[144, 145].

However, it is this tight regulation of molecules being restricted from crossing the BBB that in turn, the nature of the BBB provides an obstacle for drug delivery to the CNS, and methods to target, modulate or bypass the BBB for delivery of therapeutics are of high importance[146].

2.4.1 Crossing the BBB

Peptide conjugated nanoparticles are a very popular method for targeted drug delivery in nanomedicine. There are different reasoning's as to why you might conjugate peptides to nanoparticles. For instance; site specification, for imaging purposes or to limit peptides bio - degrading. There has been numerous data confirming gold nanoparticles crossing the blood brain barrier (BBB), but limited results for peptide conjugated nanoparticle crossing the BBB. This is a large issue to overcome when trying to establish therapeutics for neurological disorders.

It has been estimated that approximately 98% of drugs with small molecular weights are not able to cross the BBB and practically all drugs of a large molecular weight, which is why there is such a need to develop delivery mechanisms that can penetrate the BBB to provide new neurological therapeutics[54]. Nanoparticles are gaining more and more attention as drug delivery systems as they have the ability to cross the BBB therefore, can increase the uptake of specific drugs. Gold nano particles are of low toxicity to the BBB and in the blood, so they can be present in the blood longer to allow specific drug molecule interactions on the luminal side of the BBB that will then allow the nanoparticle to cross[54]. Gold nanoparticles

can be easily manipulated to target BBB crossing, for example, linkers to the particle surface can be changed for specificity as can the size of the particles. Specific peptides with high affinity to BBB receptors can also be attached to the particles as the particle surface and coating is of high importance during the intracellular uptake process[54].

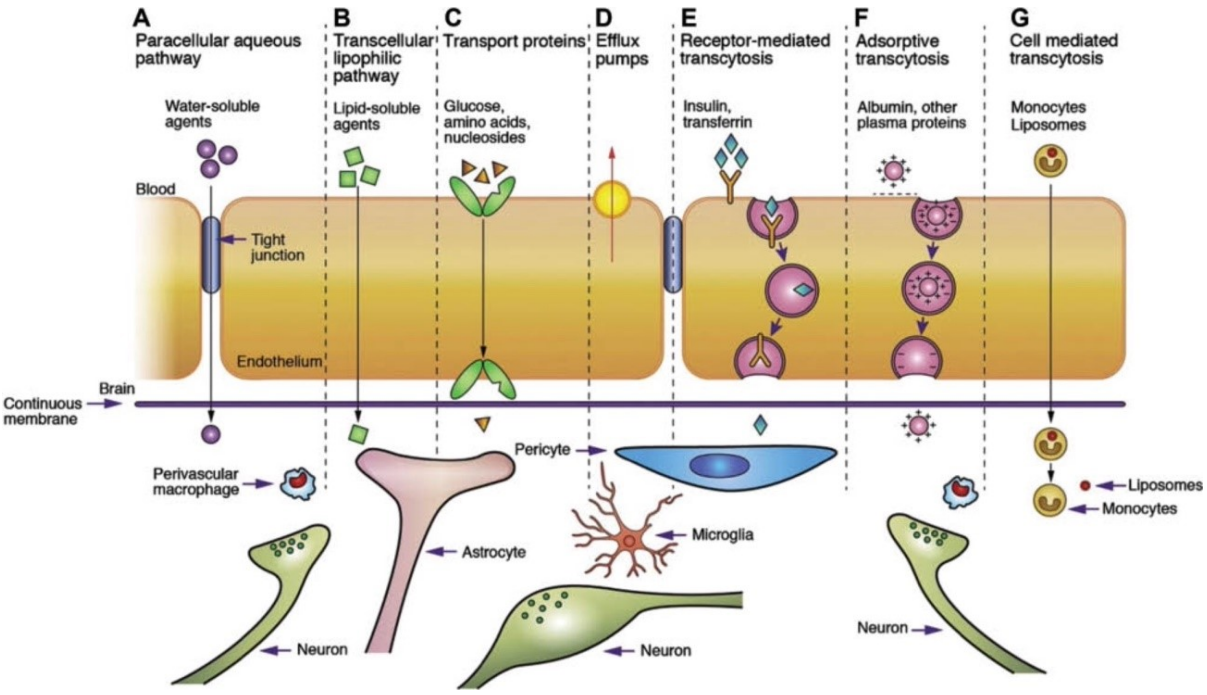


Figure 2.14 Schematic diagram demonstrating the transport pathways to enable crossing of the blood brain barrier (BBB), image adapted from Herda *et al*, 2015[23].

Shilo *et al*, developed insulin-targeted 20 nm gold nanoparticles (INS-GNPs) to investigate 1) if they can successfully cross the BBB and 2) to quantify the amount of particles crossing the BBB. It was concluded that the particles were able to cross via the receptor – mediated endocytosis (Figure 2.14, E) process and that two hours after mice were injected with the INS-GNPs, they found over five times more INS-GNPs in the mouse brains compared to the control[54].

Clark and Davis have demonstrated gold nanoparticle BBB crossing via receptor mediated transcytosis (Figure 2.14, E). They engineered 80nm gold nanoparticles containing transferrin with an acid-cleavable linkage between the transferrin and the nanoparticle core, designed to facilitate crossing via receptor mediated transcytosis. The nanoparticles could then bind to the BBB transferrin receptors and then separate during transcytosis allowing the nanoparticle to be released into the brain. These transferrin targeted nanoparticles demonstrated a heightened ability to cross the BBB and after systemic administration into mice, they found high quantities in the brain parenchyma, when they compared to similar nanoparticles that did not contain the acid-cleavable linkage[147].

Pradesa et al, produced an earlier finding of conjugated nanoparticles crossing the BBB, where they conjugated a neuroprotective peptide (CLPFFD) that has the ability to breakdown toxic aggregates of β-amyloid, a main cause of Alzheimer's disease. For them to get their particle across the BBB they added a short peptide sequence (THRPPMWSPVWP) to the nanoparticles that has proven to interact with the transferrin receptor. Having this peptide attached to the nanoparticle allowed transport of their endocytic vesicle through the endothelial cells of the BBB, thus, the neuroprotective peptide then recognised and bound to the toxic aggregates of β-amyloid in the central nervous system[148].

2.4.2 Conclusions

There are a lot of drugs that could potentially treat PD but are not able to across the BBB. Hence, these neuroprotective drugs need to penetrate the BBB with the help of a nanoparticle to act as the drug carrier. When it comes to crossing the BBB it would be optimal to take advantage of the brain's surface receptors as nanoparticles can be specifically coated with ligands, such as antibodies or proteins that can selectively interact with the BBB receptors and thus aid in crossing. The nanoparticle's morphology is recognised as being a key factor influencing cellular uptake and distribution. A number of studies have now shown how a nanoparticle's shape strongly influences the particle's internalization and functional behaviour.

Whilst the interaction of cells with spherical nanoparticles has been widely investigated, there is much focus now being placed on elongated and anisotropic morphological structures due to their versatility and very attractive properties such as cell specific uptake and enhanced circulation times. Therefore, establishing the link between the nanoparticles' geometry and their penetrating and uptake efficiency directly on BBB models is of upmost importance, so that nano - carriers can be efficiently engineered for BBB interactions.

Furthermore, as shape influences the nanomaterials' preferential accumulation in particular cell types, thus increasing selectivity, nano structures with star like morphology could be the next contender in shuttling neurotherapeutics across the BBB.

3 Experimental techniques

3.1 Electron Microscopy

Electron microscopy (EM) allows high resolution imagery of both biological and non - biological specimens down to the nano scale that are unable to be reached by standard light microscopy. EM employs a beam of energetic electrons, which are controlled and focused by electrostatic and electromagnetic lenses, which act as the source of specimen illumination[118]. These Energetic electrons are generated from tungsten or LaB6 filaments (i.e. thermionic sources) or from field emission sources, with electromagnets propelling negative electrons down a high-vacuum column, onto a specimen.

The maximum resolution (*d*) that may be achieved is proportional to the wavelength (λ) of the incident electron beam:

Equation 3.1

$$\boldsymbol{d = \frac{\lambda}{2nsin\alpha}}$$

Where *n* is the refractive index of the medium and *α* is the half - angle of the maximum electron cone that can enter or exit the lens. According to de Broglie's principle of wave particle duality, the wavelength (λ) of an electron within an incident electron beam is inversely proportional to the momentum (*p*):

Equation 3.2

$$\lambda = \frac{h}{p}$$

Where *h* is Planck's constant and p represents the momentum that is related to the kinetic energy of the particle by:

Equation 3.3

$$p = \sqrt{2m_{\circ}E}$$

Where m_o represents the mass of the electron. *E=eV*, where *e* is the electron charge and *V* is the potential whereby the electrons are accelerated:

Equation 3.4

$$\lambda = \frac{h}{\sqrt{2m_{\circ}eV}}$$

Based on the relativistic effects of particles travelling close to the speed of light within vacuum (c), the electron wavelength can be described by:

Equation 3.5

$$\lambda = \frac{h}{\sqrt{2m_{\circ}eV\left(1+\frac{eV}{2m_{\circ}c^2}\right)}}$$

Therefore, demonstrating the wavelength of electrons within the incident beam is related to the acceleration potential.

A primary electron beam that interacts with a specimen can generate several different signals (Figure 3.1). These signals include characteristic X-rays, photons, back-scattered electrons (BSE), Auger electrons and secondary electrons (SE)[118]. These signals can be collected and amplified. Thus allowing electron microscopes to provide morphological, compositional and crystallographic information about specimens down to the nano scale.

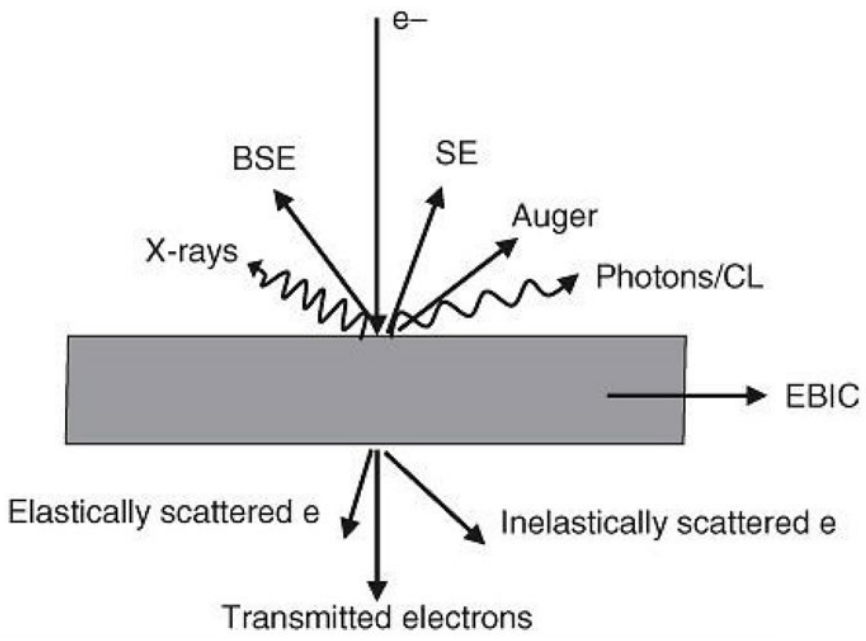


Figure 3.1 An overview of the signals generated when the electron bean interacts with a specimen. These signals may include: back - scattered electrons (BSE), secondary electrons (SE), Auger electrons, electron beam induced current (EBIC) and characteristic X-ray and photons. Image adapted from John Wiley & Sons Ltd[118].

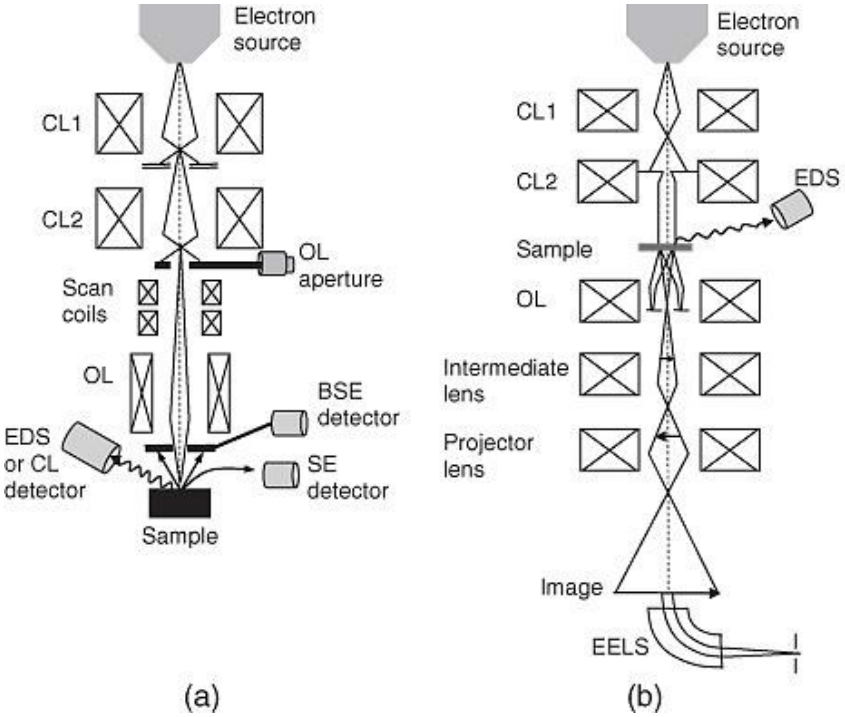


Figure 3.2 Schematic representations of (a) scanning electron microscope (SEM), (b) transmission electron microscope (TEM) CL: condenser lens, OL: objective lens, BSE: backscatter electrons, SE: secondary electrons, EDS: energy dispersive X-rays, EELS: electron energy loss spectroscopy, ADF: annular dark field. Image adapted from John Wiley & Sons Ltd[118].

3.1.1 Transmission Electron Microscopy

For effective Transmission electron microscopy (TEM) imagery, specimens with a thickness less than 100 nm are required. TEM (Figure 3.2, b) provides high resolution information by passing a primary electron beam through a specimen thus, allowing information about its internal structure to be observed[118]. An energetic electron beam is focused by an initial electromagnetic condenser lens (CL1), whilst the condenser aperture works to control the beam intensity and CL2 functions to direct the probe onto the specimen. Scattered electrons emerging from the sample are collected by the objective lens which then collates them at the back focal plane, to which the objective apertures facilitate the selective passage of scattered electrons that gives rise to tuneable image contrast. A series of projector lenses are able to magnify the electrons that pass through the objective aperture and so those

electrons that pass though the specimen are collected by bright field (BF), dark field (DF) and high angle annular dark field (HAADF) detectors that enable images to be electronically captured.

3.1.2 Scanning Electron Microscopy

Scanning electron microscopy (SEM) operates by raster scanning of an electron probe over the surface of a conductive sample (Figure 3.2, a). SEM is generally used to examine specimens of bulk material as appose to thin specimens. The diameter of the electron probes determine the spatial resolution, in which scanning coils, located below the electromagnetic condenser lenses (CL), are utilised to move the probe over the specimen (Figure 3.2, a). SEM instruments can collect backscattered (BSE), secondary (SE) and transmitted electron signals. BSE and SE detectors capture the electrons after they are accelerated towards the positively charged grid of a scintillator. This collision results in the formation of photons, amplified by a photomultiplier that allows the BSE detector to give topographical information of the specimen[118]. For specimens that do not conduct electricity, samples are required to be coated with thin metal films (chromium, carbon or gold) at approximately 2-10 nm to reduce a build-up of surface electron charge and thus reduce specimen damage.

3.1.3 Focused Ion Beam Scanning Electron Microscopy

Focussed ion beam (FIB) milling involves the controlled degradation of material at the surface of a specimen that in turn provides tomographic information of a specimen through simultaneous SEM imaging and elemental analysis. A high - energy gallium beam is formed through the extraction of gallium from a liquid metal ion source (LMIS) located at the top of the FIB gun (Figure 3.3). The electromagnetic lens and internal apertures focus the high energy gallium ions into a condensed beam that is then directed to the specimen surface. The FIB probe is then raster-scanned over the sample surface to remove material in a controlled manor, with the current of the FIB beam defining the degree of material removed per second.

This removes surface material of the specimen that is of no interest to leave a trapezoidal trench region which exposes the internal structure of the specimen material for analysis (Figure 3.4), via SEM characterisation.

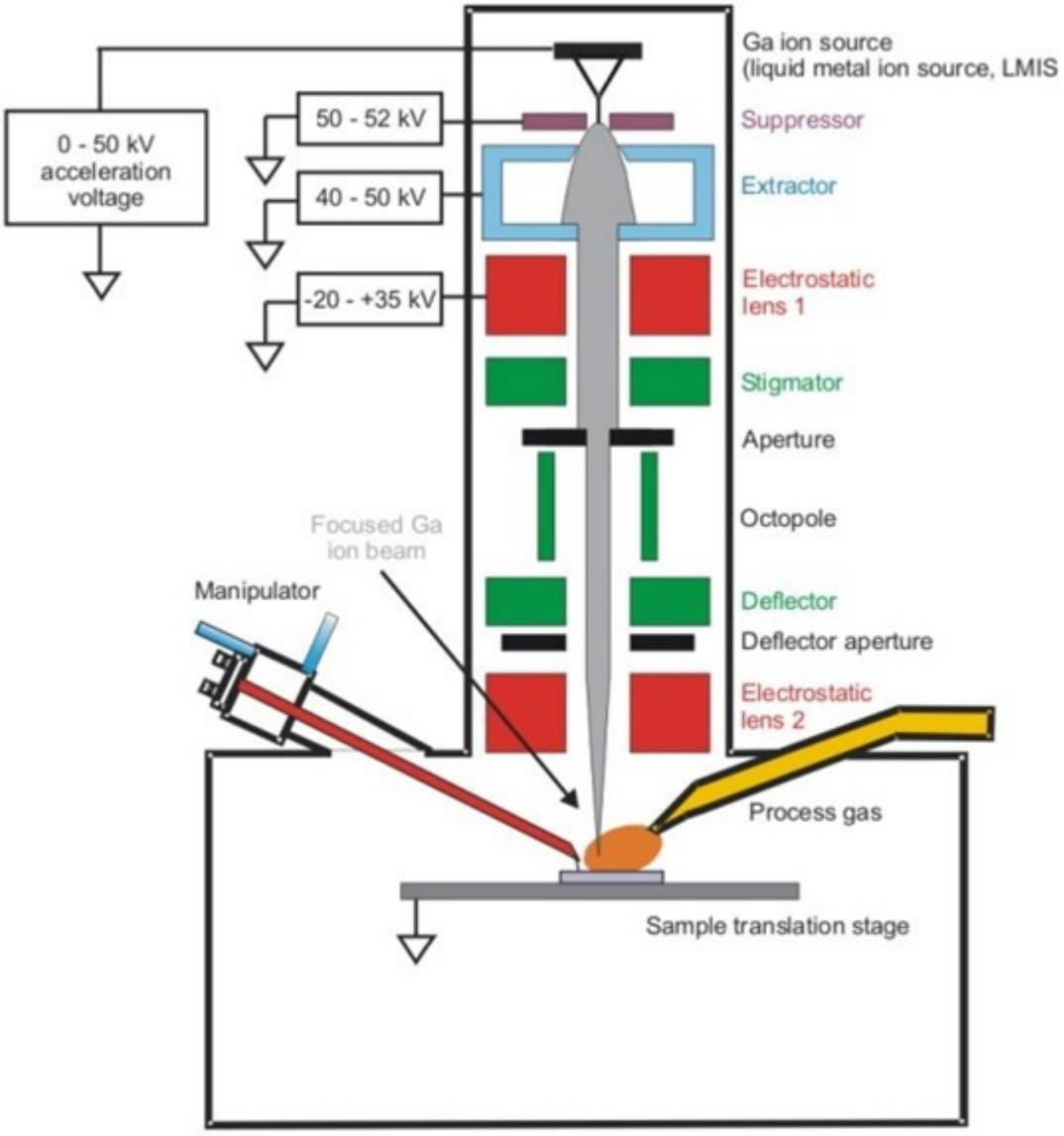


Figure 3.3 Focussed ion beam (FIB) propels high - energy gallium ions towards the specimen surface to allow controlled material degradation. High energy gallium ions are propelled down the FIB column by electromagnets. Electromagnetic lens and an internal aperture focusses high energy gallium ions into a condensed beam, with stigmators removing beam stigmation. Image adapted from Bell *et al*[119].

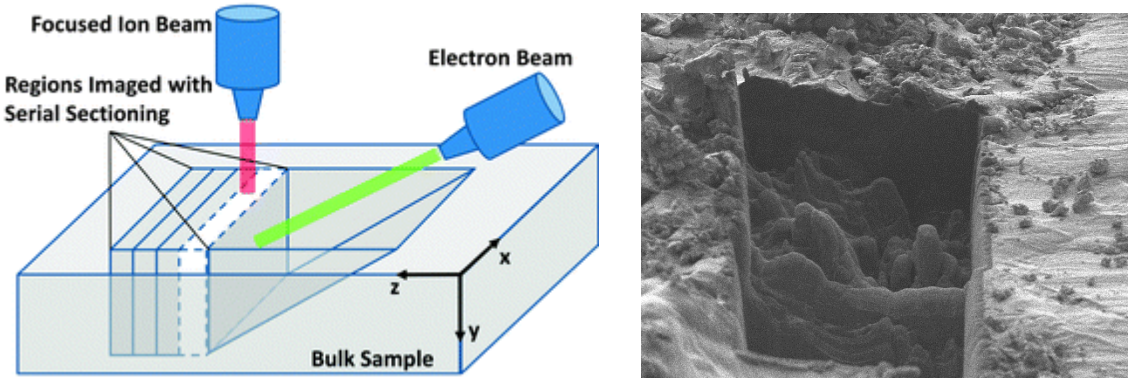


Figure 3.4 FIB can be used to remove material from the surface of a specimen through controlled degradation. A schematic representation of FIB milling to form a trench, (left) leaving an exposed 'cliff wall' that may be characterised by SEM. SEM micrograph example of a trench formed by FIB milling. Image adapted from Bell *et al*[119].

4 Synthesis and Stability of Peptide – targeted gold nanoparticles for the treatment of Parkinson's disease

4.1 Introduction

A challenge in neurology is the lack of small neuroprotectants targeting multiple disease mechanisms. Previously, Porter group have designed small peptide dendrimers (H3/H6) encompassing the neuroactive motifs of the protein S100A4. These motifs have been synthesised and tested for their neuroprotective effects. The group found the peptides induce neurite outgrowth from hippocampal, dopaminergic, and motor neurons[6, 8, 43]. These peptides also protect neurons in cell and animal models of brain trauma by diminishing oxidative stress and excitotoxicity, *via* multiple pathways. They also protected neurons against Parkinson's disease associated neurotoxicity *in vitro* and in animal models of neurodegeneration and genetically induced peripheral nerve degeneration *in vivo* [6, 8, 43].

The advantages of utilizing these small peptides over protein/growth factor-based therapeutics, is that they specifically encompass the neuroactive motifs of the parent protein and thus minimize the potential side effects. They are low cost and readily producible, and can easily be chemically modified.

In spite of their advantageous properties, however, these peptides can only penetrate inside the brain in small quantities and their blood circulation half-life is low, rendering them unviable as a clinical treatment. Our group have shown that nanoflower shaped structures functionalised with L - dopa cross brain endothelial cells in culture in significant quantities (~40%)[59, 60] and could be used as a vector to transport the S100A4 peptides inside the brain to the damaged neurons.

Nano-neuro therapeutics are small but can be engineered with a high surface area for drug loading, delivery and brain targeting. The purpose of this chapter was to develop a synthesis route to controllably tune the morphology and colloidal stability of the star-shaped and spherical gold nanoparticles and to conjugate H3 and H6 as a 'cargo' onto their surface. The overall goal was to design highly controlled nano-neuroprotectants with future potential to interact with neurons and cross the BBB to treat a spectrum of neurodegenerative disorders *in vivo*.

Transmission electron microscopy (TEM) techniques were used to characterise the morphology and diameter of the gold nanostar and nanosphere nano-vectors. This technique enabled a direct visualisation of the modification process these particles underwent to achieve the best functional properties. Inductively Coupled Plasma – Optical Emission Spectroscopy (ICP – OES) and electron microscopy were used to determine the amount of gold and surface area of the particles to calculate the drug loading onto each of the structures.

This chapter shows successful fabrication and optimisation of gold nanostars (NSs) and nanospheres (NPs) conjugating to novel S100A4 peptides; H3 and H6 neurotrophic motifs. These new nano-neuro therapeutics were further examined to determine the efficacy of the binding and the stability of the particles. As both the nanostructures are plasmonic they can be detected by Ultraviolet–visible spectroscopy (UV – Vis), which confirmed the agglomeration state of the particles in the colloidal solutions, their uniformity of size and shape and successful binding of the H3 and H6 peptides. X-ray Photoelectron Spectroscopy (XPS) confirmed the presence of the peptides on the surface of the nano structures. The binding of the peptides to the Au nano structures by XPS was determined in collaboration with Dr Anna Regoutz at the Department of Chemistry, University College London.

4.2 Methods

All equipment used for the analytical chemistry experiments were first thoroughly cleaned with concentrated aqua regia (HCL: HNO3 3:1 v/v) prior to use to remove all organic contaminants from the glassware.

4.2.1 Gold nano particle Synthesis

Spherical nano particle synthesis

Spherical citrate-stabilized gold (Au) nanoparticles were synthesised using a Turkevich method of citrate reduction[61]. Following and modifying the protocol described by Yuan *et al*, 2012[5], solutions of sodium citrate were prepared by dissolving either 0.1 g (1% (w/v)), 0.2 g (2% (w/v)), or 0.3 g (3% (w/v)) tri - sodium citrate in 10 mL of deionised water by bath sonication. 10 mM $HAuCl_4 \cdot 3H_2O$ was prepared by dissolving 0.394 g of Gold(lll) chloride trihydrate in 100 mL deionised water, then stored light protected at 4^0C. In an AR cleaned 250 mL Erlenmeyer flask with a 1-inch stir bar, 48.75 mL of deionised water and 1.25 mL of the 10 mM $HAuCL_4$ solution was added and bought to the boil. At boiling point, 1 mL of either 1%, 3% or 4% (w/v) sodium citrate solution was added whilst under vigorous stirring until the solution had changed colour to red. At this point, the colloidal solution was quickly cooled, washed by centrifugation three times then stored at 4^0C light protected. The volume of sodium citrate added was dependent on the desired size of the nano spheres, see table 4.1 below.

Sodium citrate % (w/v)	*Nano particle size (nm)*
1%	50
2%	12
3%	12

Table 4.1 Table to show the dependence of the concentration of sodium citrate on the diameter of the spherical gold seed.

Star nano particle synthesis

Yuan *et al*, 2012[62] protocol was followed for the subsequent synthesis of the gold nanostars. A 10 mL acidified 0.1 mM $HAuCl_4 \cdot 3H_2O$ solution was prepared by adding 100 µL of 10 mM $HAuCl_4$, 10 µL of 1 M HCL and 9890 µL of deionised water into a vial, placed under moderate stirring at room temperature (RT). 200 µL of the 12 nm (3% (w/v)) Au seeds were then added, then quickly followed with 100 µL of 3 mM $AgNO_3$ and 50 µL of 100 mM ascorbic acid. The color of the solution changed from faint red to blue as soon as the ascorbic acid was added, which indicated the nano stars had formed and the synthesis was complete. Whilst still stirring, 125 µL of 1 mM of Polyethylene glycol (PEG) was added after completion of synthesis to stabilise the nanostars. They were then washed 3 times by centrifugation, and stored at 4^{o}C light protected.

4.2.2 Functionalising the nanostructures with the H3/H6 peptides

The nano spheres and nano stars were fabricated as transport vehicles to deliver the neuroprotective peptides; H3 and H6 to the brain. The peptides were reconstituted to the concentration of 2 mg/mL and left for 24 hours at 4°C and light protected before use.

S100A4 peptide mimetic synthesis

Peptides (sequences H3: KELLTRELPSFLGKRT, H6: NEFFEGFPDKQPRKK) were synthesized as tetramers composed of four monomers coupled to a lysine backbone (purchased from Schafer-N, Denmark). Tetramerization was previously found to be necessary for the neuritogenic activity of S100A4[36].

Inductively Coupled Plasma Optical Emission Spectroscopy (ICP-OES)

ICP – OES was used to detect and quantify Au atoms in a 10 mL sample to determine the amount of peptide required to cover the surface area of both the nano spheres and nano stars. A 10 mL nano star synthesis was performed *via* the method stated above. Simultaneously a 10 mL sample of nano spheres was generated by taking 4 mL of the 1% (w/v) nano sphere solution, as per the 1% (w/v) citrate synthesis method described above, and diluting in 4 mL deionised water. The nano sphere and nano star samples were then centrifuged down in 15 mL Falcon tubes until all gold had been pelleted, and the supernatant removed. 500 µL of concentrated aqua regia (AR) (HCL: HNO3 3:1 v/v) was added to the samples and left to digest overnight. 10 mL deionised water was then added to dilute the aqua regia concentration and the samples were then run on a ThermoScientific iCAPTM 7400 ICP-OES instrument against a set of standards of known varying concentrations of gold. The absorbance was measured and recorded to enable the characterisation of the Au by presence and quantification.

Determining the quantity of peptide per particle (equation)

The below equation was used as a starting point to estimate the volume of peptide molecules required to cover the surface of both the 50 nm nano spheres and nano stars. All values are estimations/starting points and were later optimised as shown in the results section. The results from the ICP-OES showed an equal concentration of gold for both the nano star 10 mL synthesis and the nano sphere 10 mL synthesis, therefore, as they both had the same concentration of gold for peptide binding. The following calculations were based on the 50 nm spheres. The first calculation was used to determine the actual surface area of a 50 nm nano sphere, which may be represented as follows:

Equation 4.1 $$A2 = 4\pi r^2$$

Where A2 is equal to the surface area of a 50 nm nano sphere and *r* is equal to the radius of the nano sphere particle (*r* = 25 nm), Therefore, the estimated surface area of a 50 nm sphere is **7854 nm².**

With the surface area of one particle calculated, the quantity of nano particles in a 10mL synthesis was to be calculated and thus, the overall surface area in a 10 mL synthesis needed to be determined. Firstly, the volume of one nano sphere was determined and may be represented as follows:

Equation 4.2 $$V = \frac{4}{3}\pi r^3$$

Where $\boldsymbol{V}$ is equal to the volume of a 50 nm nano sphere and *r* is equal to the radius of the nano sphere particle (*r* = 25 nm), Therefore the estimated volume is **6.5×10⁴ nm**³ per particle. Secondly, the mass of one particle was determined and may be represented as follows:

Equation 4.3 $$W = V \text{ x } \rho$$

Where $\boldsymbol{W}$ equals the weight of one particle, $\boldsymbol{V}$ equals the volume of one nano particle (6.5×10^4 nm^3) and **ρ** equals the gold nano particle density (19.32 g/cm^3). Converted into level units, the weight of one particle is estimated to be **$1.25\text{x}10^{-15}$ g**. Thirdly, the quantity of nano particles in a 10 mL synthesis needed to be identified, and may be represented as follows:

Equation 4.4 $$W^a/W^b = Qty$$

Where W^a equals the physical weight of gold from a 10 ml synthesis and W^b equals the weight of one particle ($1.25\text{x}10^{-15}$ g). The estimated quantity of particles in a 10 mL solution equals **$4.98\text{x}10^{16}$**. Then finally, the total surface area of all particles in a 10 mL synthesis was calculated and may be represented as follows:

Equation 4.5 $A = A2\ x\ Qty$

Where A = Total surface area, $A2$ = Surface area of one particle (7853.98 nm²) and Qty is the estimated quantity of particles in a 10 mL synthesis ($4.98x10^{16}$). Therefore, the overall surface area in a 10 mL nano particle synthesis is **$3.91x10^{20}$ nm²**.

As the surface area in a 10 mL synthesis was calculated, the estimated amount of peptide required to cover surface area of nanoparticles in the solution was calculated. As it was not entirely possible to gain a visual of how the peptides were structurally formed on the particle surface, it couldn't be determined if the peptide coiled itself around the particle or attached in a linear formation. A simple area of a circle calculation was performed as an indication of surface coverage to allow the experiment to go ahead. This calculation is based on the maximal 'footprint' of the peptides. As the peptides were synthesized as tetramers composed of four monomers, made up of amino acids, their size was calculated in angstroms, estimated at 120 Å per peptide molecule. This translates to 12 nm in "diameter". The area of a circle may be represented as follows:

Equation 4.6 $A3 = \pi r^2$

Where $A3$ = area, and *r* is equal to the radius of the peptide "diameter" (*r* = 6). Therefore, the estimated area of a peptide molecule was valued at **113.1 nm²**

Having estimated the peptide area, calculating the total amount of peptide molecules required to cover the surface area of all nano particles in a 10 mL synthesis may be represented as follows:

Equation 4.7 A / $A3$ = Qty

Where A is equal to the total surface area (3.91×10^{20} nm^2), $A3$ is equal to the peptide area (113.1 nm^2). Therefore the total number of peptide molecules required to cover the surface area of the nano particles in a 10 mL synthesis is **3.46×10^{18}**. This value was then converted into moles which may be represented as follows:

Equation 4.8 molecules / Avogadro's number = moles

Where molecules equals the total number of peptide molecules (3.46×10^{18}) and Avogadro's number equals 6.02×10^{23}. The approximate amount of peptide moles required to cover the surface area of all nano particles in a 10 mL synthesis equals **5.75×10^{-6}** mol. This is an underestimation and likely the nano structures could accommodate more peptide molecules per particle, however, this calculation was an estimation to enable the peptide – particle functionalisation process to begin.

The peptides were made up to the concentration of 2 mg/mL, so the final calculation was to determine what volume of 2 mg/mL peptide would give provide the 5.75×10^{-6} mol required.

By first converting the concentration into moles, using equation 8 above, equalling **2.5×10^{-4} mol**. The estimated volume may be represented as follows:

Equation 4.9 V = mol *(a)*/mol *(b)*

Where mol *(a)* equals moles required (5.75×10^{-6}) and mol *(b)* equals moles available (2.5×10^{-4}), the volume of 2 mg/mL peptide required equals **23 µL** per 10 mL nano particles synthesis.

Nanostar - Peptide conjugation synthesis

To fabricate the nano Stars with the H3 or H6 peptides, the nano stars were synthesised as stated above (4.2.1) with the peptides replacing the PEG to stabilise the structures. The nano particles were also synthesised in the presence as well as absence of PEG. PEGylation of polypeptide drugs is widely used in pharmaceuticals, due to its ability to protect them from degradation by proteolytic enzymes, to increase compound half-life and prevent the generation of neutralizing antibodies[65].

The peptide nanostar hybrids were prepared by following the afore-mentioned nanostar synthesis. After the colour change from clear to blue, 50 µL of either the 2 mg/mL H3 or the 2 mg/mL H6 was added and left to stir for 24 hrs at room temperature.

The peptides plus PEG (at 75:25 peptide: PEG molar ratio) functionalized nanostars were synthesized as mentioned above. 37.5 µL of either H3 or H6 was added to the stirring nano stars and incubated for 24 hr, then 31.2 µL of PEG was added and incubated for 1 hr at room temperature.

Nanosphere - Peptide conjugation synthesis

The control 50 nm spheres were synthesised as above using 1% sodium citrate. 4 mL of the 3% nano sphere solution was diluted in 6 mL deionised water and moderately stirred. The particles were then either fabricated with the H3 or H6 peptides only or in the presence of PEG. The peptides were incubated with the nano spheres for 24 hrs, the PEG was subsequently added and incubated for 1hr.

The peptide: PEG volume ratios are shown in the table 4.2 that were used to achieve a 75:25 peptide: PEG molar ratio. All the peptide +/- PEG targeted nano structures were washed three times by centrifugation and stored at 4°C light protected.

	Nano Star		*Nano Sphere*	
Conjugation	**Peptide Volume, 2mg/mL (µL)**	**PEG Volume, 1 mM (µL)**	**Peptide Volume, 2mg/mL (µL)**	**PEG Volume, 1 mM (µL)**
Particle + PEG		125		250
Particle + H3	50		100	
Particle + H6	50		100	
Particle + H3 + PEG	37.5	31.2	75	62
Particle + H6 + PEG	37.5	31.2	75	62

Table 4.2 Peptide: PEG ratios for gold nanostars (left panel) and nanospheres (right panel).

4.2.3 Characterisation of the H3/H6 peptides on the surface of the nanostructures

The H3/H6 gold nanostructure conjugates were characterised to confirm the successful binding of the peptides to the nano structures and the overall stability of the nano – compounds.

Final peptide concentrations in the obtained suspensions were quantified by nanodrop protein measurement (described below).

Quantification of peptide

A Thermo Scientific NanoDrop One was used to confirm and quantify the peptide attached to the nano structures. The A280 application was used as this is the wavelength the peptides can be detected. As they are synthesised as single peptide chains, there is no risk of contamination from other proteins, so all values obtained are specifically for each of the H3 or H6 peptides. 2 µL of peptide-particle solution was dropped onto the Nanodrop and the absorbance was measured (against the corresponding blanks of either ultra-deionised water or 1 mM PEG solution), that then produced the wavelength peak indicating the concentration of peptide detected in the solution. The nanodrop was wiped with an ethanol wipe after each use to prevent cross contamination and the values were expressed as mg/mL.

Ultraviolet–visible spectroscopy (UV – Vis)

UV – Vis was used to determine the nano particle synthesis was successful and to characterise the size and shape and aggregation state based on the absorption peak. UV – Vis was used to determine if the peptides had attached to the nano structures by evaluating any shift in the absorption peak. 500 µL of nano particle solution was diluted in 500 µL deionised water and read by the UV – Vis spectrometer using the full spectrum of visible light.

X-ray Photoelectron Spectroscopy (XPS)

Gold nanoparticles and their binding to PEG and H3/H6 were investigated using X-ray Photoelectron Spectroscopy (XPS). Survey and core level spectra were recorded on a Thermo Scientific K-Alpha+ XPS system using its monochromated, microfocused Al K_α X-ray source (hv= 1486.7 eV). The base pressure was 2×10^{-9} mbar base pressure and an X-ray spot size of 400 µm was used. Data were collected at 200 eV pass energy for survey and 20 eV pass energy for core level spectra. The nanoparticles were dropcast onto Si wafer substrates (Si/SiO_2)

which were mounted on the sample holder using conducting carbon tape. A flood gun was used to minimize sample charging throughout. All data were analysed using the Avantage software package and for peak fit analysis, Voigt functions with Shirley-type backgrounds were used.

Zeta Potential

Zeta (ζ) potentials of the peptide fabricated nano-compounds were measured in the four conditions: deionized water (H_2O) pH 7.4, RPMI cell growth medium (RPMI) pH 7.43, neurobasal medium (NB) pH 6.76 and 1% bovine serum albumin (BSA) pH 6.44. For each condition, 20 µg/mL (peptide concentration) of each respective nano-compound was added to 1 mL of the medium and ζ potentials were measured using the Zeta sizer (Malvern instrument 2000) at 37°C. The pH varied depending on the medium. Each measurement was performed in triplicate, the average zeta potential measurement was calculated by taking three measurements after 100 runs per sample and the arithmetic mean reported.

4.2.4 Transmission Electron Microscopy (TEM)

Sample preparation for TEM

The morphological features of each of the nanostructures was examined by Transmission Electron Microscopy (TEM), using holey carbon 300 mesh Cu TEM grids. 50 µL of sample solution was dropped onto the grids and left to dry at room temperature. High resolution TEM was performed using Jeol 2100 F plus or the Joel 2100 + operated at 200 kV.

Uranyl Acetate (UA) staining

Uranyl Acetate negative (UA) stain was used to try and gain a visual of the peptides attached to the nano structures. The UA staining solution was prepared under the fume hood by dissolving 2% uranyl acetate (UA) in deionised water and stored for 24 hr at 4 ˚C. 50 µL of the nanoparticle – peptide sample solution was drop cast onto the holey carbon 300 mesh Cu TEM grids and left to dry at room temperature. Once dry, the grids were placed in the fume hood and 5 µl of 2% UA aqueous solution was added to the TEM grid for five minutes. The remaining UA solution was washed off using deionised water and the TEM grid was dried using filter paper until only a thin film was left on the grid which was left to dry overnight.

4.2.5 Statistics

The TEM images presented in this chapter and the statistical analysis performed on the particles were obtained by visual analysis and measured using ImageJ. Several Au nano spheres and nano stars were analysed from a minimum of 3 separate samples prepared under identical conditions.

4.3 Results and Discussion

Spherical (AuNP) and star-shaped (AuNS) nanostructures were prepared for comparison to determine the most effective particle morphology that allows optimal drug loading and to design a matrix of nanostructures for testing in neuronal cultures and, in future, on a BBB cell model (Chapter 5 and 6). For enhanced BBB crossing the particles need to be around 50 nm in size[67]. For the star like nano structures, it is vital to synthesize the seeds as small as possible to retain the star like morphology and to keep below the 50 nm overall size threshold.

4.3.1 Nano Seed Synthesis: Citrate – Capped Au Nano Seeds

Citrate capped spherical nano seeds were synthesised using the Turkevich method of using sodium citrate to reduce $HAuCl_4$ into gold particles[61]. Highly oxidised $HAuCl_4$, dissociates to form a covalently - bonded $(AuCl4)^-$ ion in water. In order to form metallic gold, this needs to be chemically reduced. However, simple reduction could produce bulk gold, rather than nanoparticles, so to obtain the desired nanoparticles, it was necessary to incorporate a molecule that would bind to the small gold particles when they formed, coating them and preventing them from combining into a bulk metal; this is known as a capping agent. Therefore, in this method used, the citrate ions acted as both the reducing agent and the capping agent. This capping is where the negatively charged citrate ions get absorbed onto the surface of the nano particles, thus, producing a negative electrostatic field that prevents the particles from aggregating and allows a stable dispersion of particles[61, 62].

Another important property of citrate, is that it also acts a 'stop agent'. This means that use of a reduced concentration of citrate reduces the citrate ions available for stabilizing the particles, which causes small particles to aggregate into bigger ones[61, 62]. Based on the deduction that the higher the citrate concentration, the smaller the particle size, the concentration of citrate trialled was 3% and 4%.

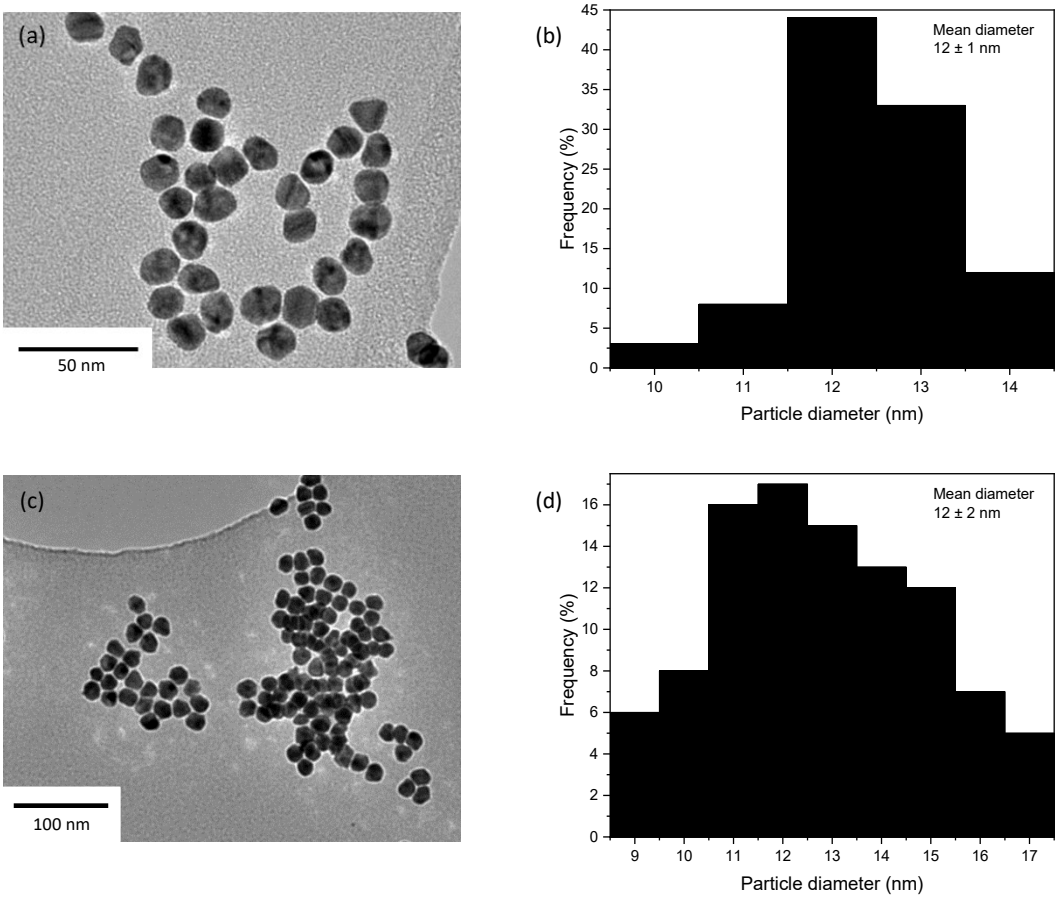


Figure 4.1 EM characterisation of Au nano seeds. (a) TEM micrograph imaged at 200kV of Au nano seed synthesised with 3% sodium citrate. (b) Histogram displaying the particle size distribution and identifying the mean diameter as 12 nm ± 1 nm with a uniform size distribution. (c) TEM micrograph image at 200kV of 4% citrate reduced nano seeds. (d) Histogram displaying the particle size distribution and identifying the mean diameter as 12 nm ± 2nm with a less uniform size distribution. n =200.

The overall mean diameter of both the 3% and 4% citrate reduced seeds was approximately 12 nm (Figure 4.1). However, it is clear the 4% did not produce an equal size distribution of 12 nm particles. The diameter of the 4% nano seeds varied between 9 and 17 nm, whereas the diameter of the 3% nano seeds varied between 10 and 14 nm, with the majority being 12 nm.

The size distribution is critical as this is the starting point at which to grow the seeds to stars of even morphological size and structure. It is also important to note that sodium citrate is not considered toxic to the body at low concentrations and is widely used in nanomedicine, however, the overall concentration was still taken into consideration when

deciding how to proceed. When evaluating all considerations; *i.e.* size distribution, uniformity and best yield, it was decided the 3% synthesised nano seeds were optimal to further functionalize into star like nano structures.

4.3.2 Effect of $AgNO_3$ on optimising the Nano Star Synthesis

For the nanostars, a surfactant - free method was used as this avoids use of polymers or surfactants in the synthesis which could be toxic[62]. As the optimal nano seed had been established and characterised for shape and size, by following and developing the protocol described in the methods section above, the nanostars were then optimised. To modify and optimise the morphology of the AuNS, the amount of silver nitrate ($AgNO_3$) was varied. The main mechanism of $AgNO_3$ in this scenario is to influence star geometry. By changing the volume or concentration of $AgNO_3$ it is possible to controllably tune the particle size and morphology, in particular, focusing on the quantity and size of the branches generated during synthesis.

In conjunction with the optimal spike size, which can be manipulated by the concentration of $AgNO_3$, the quantity of spikes is of equal importance. The volume and size of the spikes are the surface area for the peptide to bind to. The more surface area, the higher the concentration of drug per particle. There has to be the right balance, so that there are optimal spikes for surface area, but not too many that they are so close in proximity to each other that it would inhibit drug loading, which would in turn, require more stars per dose of drug.

Fine tuning the spike length was first explored by varying the concentration of $AgNO_3$. The influence this had can be seen in Figure 4.2. 300 µL of the $AgNO_3$ was used during this wet chemistry approach following the protocol written in the methods section and the resulting spike size is summarised in table 4.1 below.

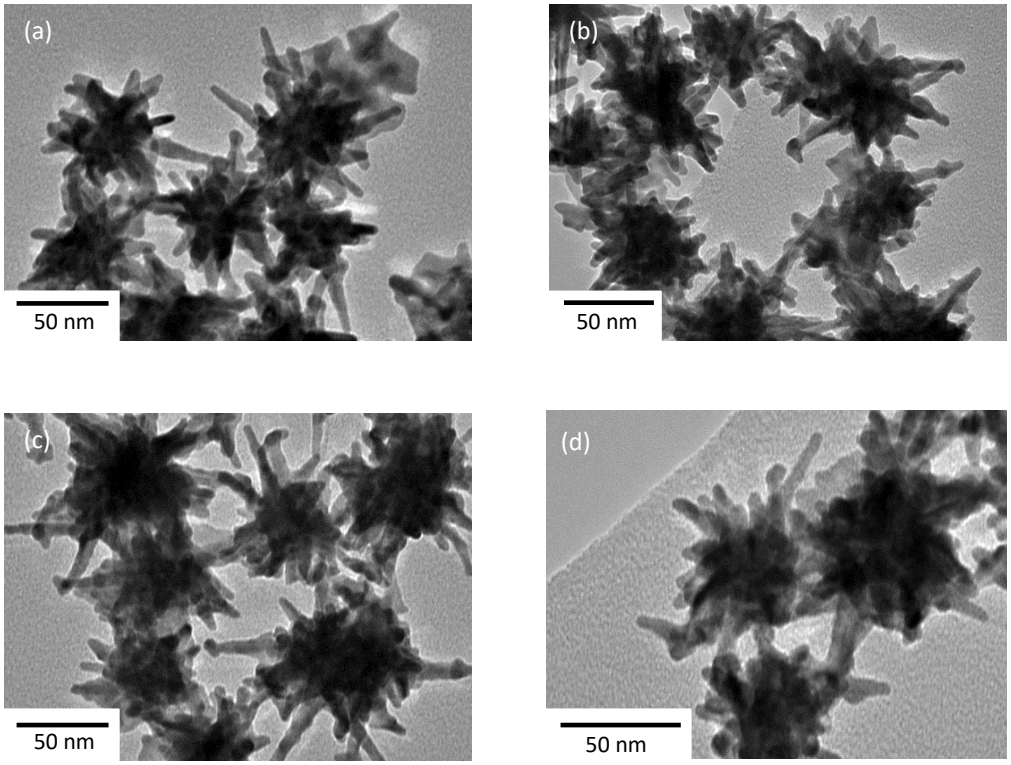


Figure 4.2 TEM characterisation of the morphological characteristics of the gold nano stars synthesised with varying concentrations of $AgNO_3$. Imaged at 200kV. 0.5 mM $AgNO_3$ (a), 1 mM $AgNO_3$ (b), 2 mM $AgNO_3$ (c) and 3 mM $AgNO_3$ (d). n = 200.

Concentration of $AgNO_3$ (100 µL)	Quantity of Spikes	Length of Spikes (nm)	Star diameter (nm)
0.5 mM	14 ± 3	20 ± 8	57 ± 11
1 mM	14 ± 3	19 ± 8	62 ± 22
2 mM	13 ± 2	21 ± 6	57 ± 10
3 mM	15 ± 4	23 ± 8	53 ± 9

Table 4.3 Table summarising the effect that changing the concentration of $AgNO_3$ had on the length of the spikes formed during synthesis. The spike length was measure from the core of the star to the tip of the spike by using ImageJ. n = 200

Initial observations of changing the $AgNO_3$ concentration showed no significant effect on the spike length. The biggest effect in spike length was between concentrations 0.5 and 3 mM. Table 4.1 summarises the difference in length as 3 nm. 3 nm is a significant difference, however, when visually analysing the TEM images in Figure 4.2, image (a) clearly shows quite short, stubby branches, whereas in image (c) overt elongated branches are observed. Adding 2 mM of $AgNO_3$ also reduced the number of spikes, and therefore, the spike proximity discerned when images (c) and (d) are compared.

The overall impact the $AgNO_3$ concentration had on the spike length was quite minimal, however there was a marked impact on overall formation of the nanostars. Moreover, it was intriguing that the 3 mM $AgNO_3$ produced the longest spikes but the overall smallest star, yet the 1 mM produced the smallest spike length, but overall the largest star diameter measured tip to tip. Based on these results, and having set the desired nano star to 50 nm, the 3 mM concentration was decided to take forward.

The next step was to explore the possibility of changing the quantity of spikes per star for optimal drug loading. 3 mM $AgNO_3$ was used in volumes of 5 µL, 25 µL, 50 µL and 100 µL. The influence this had can be seen visually in Figure 4.3 and the resulting spike quantity is summarised in table 4.2 below.

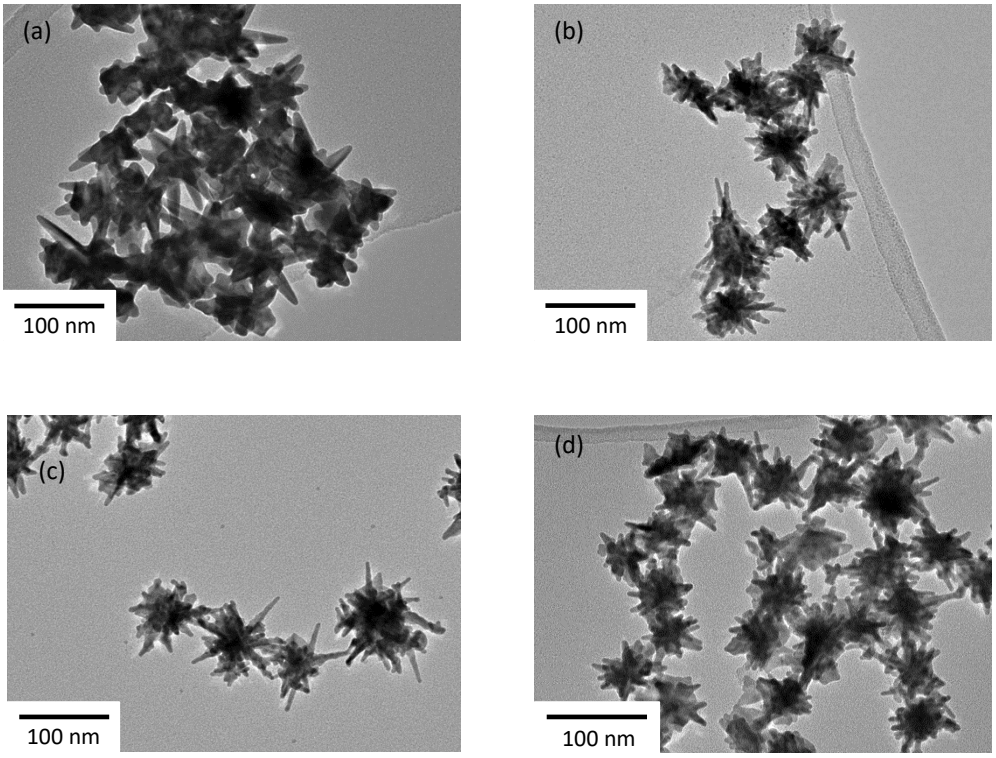


Figure 4.3 TEM characterisation of morphological characteristics of the gold nano stars synthesised with varying volumes of $AgNO_3$. Imaged at 200kV. 5 µL $AgNO_3$ (a), 25 µL $AgNO_3$ (b), 50 µL $AgNO_3$ (c) and 100 µL $AgNO_3$ (d). n = 200.

Volume of 3 mM AgNO3	Quantity of Spikes	Length of Spikes (nm)	Star diameter (nm)
5 µL	6 ± 2	20 ± 8	56 ± 16
25 µL	8 ± 3	18 ± 8	55 ± 15
50 µL	12 ± 4	18 ± 8	53 ± 17
100 µL	15 ± 3	23 ± 8	53 ± 9

Table 4.4 Table summarising the effect of changing the volume of $AgNO_3$ had on the quantity of spikes formed during synthesis. The quantity of spikes were measured by recording how many spikes were visible per star using ImageJ. n=200.

Figure 4.3 shows that changing the volume of silver nitrate had quite a dramatic effect on the star formation. Whilst there was a correlation between steadily increasing the volume of $AgNO_3$, producing an increase in spike formation. Reducing the volume of $AgNO_3$ to as low as 5 µL or 25 µL resulted in nano structures with very few uneven branch like features, which in turn limits the amount of drug loading. Using 100 µL of 3 mM $AgNO_3$ produced the desired nano star structure, both in terms of the quantity of spikes and the length of spikes produced.

Although it was previously stated that the 3% was the optimal percent strength of citrate to use to get the smallest seed size and the most uniform in size and shape, both the 2% citrate and 4% reduced seeds were explored to see if they had a better impact on the overall star morphology and size.

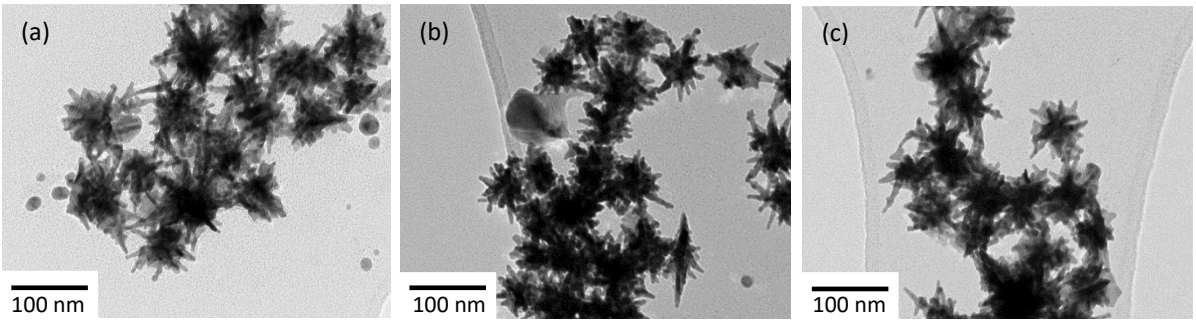


Figure 4.4 TEM characterisation of the morphological characteristics of the Au nano stars synthesised with varying sized nano seeds. Imaged at 200kV, 2% sodium citrate (a), 3% sodium citrate (b) and 4% sodium citrate (d) reduced nano seeds were used to subsequently synthesise nano stars. n = 200

sodium citrate	Nano seed Size (nm)	Quantity of Spikes	Length of Spikes (nm)	Star diameter (nm)
2%	20 ± 1	13 ± 3	22 ± 8	64 ± 19
3%	12 ± 1	15 ± 3	23 ± 8	53 ± 9
4%	12 ± 2	16 ± 2	19 ± 6	54 ± 12

Table 4.5 Table summarising the effect of changing the nano seed size on the overall formation and geometry of the nano stars. The nano stars were measured by visual representation measured by using ImageJ. n=200.

Figure 4.4 shows the geometry of the nanostars produced using different diameter nano seeds. The results are summarised in table 4.3. Varying the concentration of citrate capped nano seeds did influence the overall size of the nano stars. There was no significant difference in the overall star size from using the 3 and 4% nano seeds as expected as both concentrations produced the same size seeds, only that the 4% generated a higher standard error, which could easily be predicted as the seeds had a very uneven size distribution as shown in Figure 4.1. Reducing the citrate to 2% produced larger nano seeds, and hence larger nano stars, which is not optimal for this research. Table 4.4 describes the effects changing each of these parameters had on particle growth.

Parameter change	***Effects***
Concentration of $AgNO_3$	No significant difference shown in spike length when varying the concentration from 0.5 mM to 3 mM, there was a difference in star size. 1 mM $AgNO_3$ produced stars almost 10 nm larger than the 3 mM. The results show the higher the $AgNO_3$ concentration, the smaller the overall star size.
Volume of $AgNO_3$	Results demonstrated a significant difference in spike quantity when changing the volume of $AgNO_3$. From adding 5 µL to 50 µL, double the quantity of spikes were formed.
Nano seed size (citrate concentration)	Using 3% and 4% citrate capped nano seeds produced the same size nano stars, a higher overall variation of the size was seen from the 4% seeds. Reducing the concentration of citrate to 2% resulted in nanostars with a 10 nm larger diameter.

Table 4.6 Summary of the effects of different chemical parameters on the morphological characteristics of the gold nanostars.

4.3.3 Characterisation of the 50 nm Gold Nano stars

Systematically changing the properties of the nanostars by modifying synthesis conditions gave a better understanding of how to control and thus produce the optimal nano stars, and to select which candidates should be bought forward for testing *in vitro*. In summary from results section 4.3.2 above, synthesising the nano stars *via* the seed mediated growth method from the 3% citrate capped nano seeds, 100 µL of 3 mM $AgNO_3$ was the best option to grow the nano stars into the optimal geometry. Figure 4.5 below demonstrates full characterisation of the 50 nm nano stars.

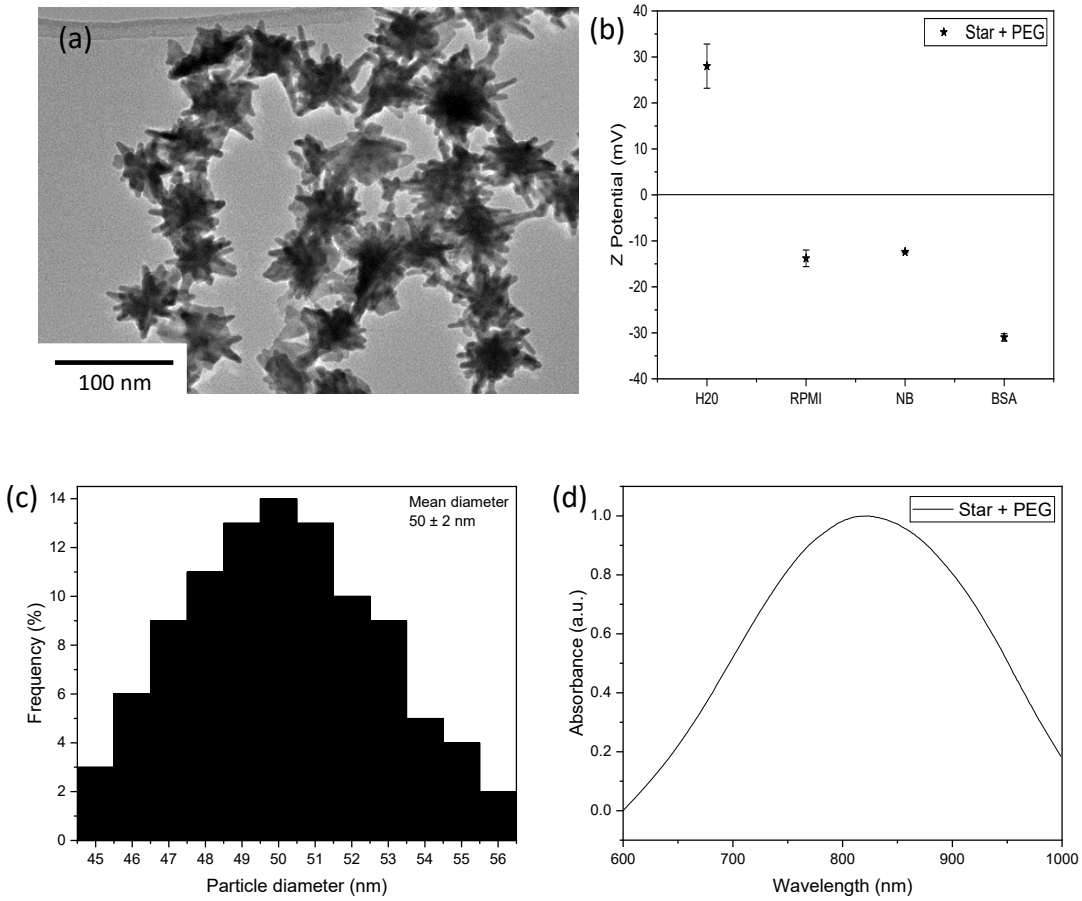


Figure 4.5 TEM micrograph image of the 50 nm nano stars, Imaged at 200kV (a); Zeta potential demonstrating the stability of the nano stars in different media, deionized water (H_2O) pH 7.4; RPMI 1640 growth medium (RPMI) pH 7.4; neurobasal neuronal growth medium (NB) pH 6.7; 1% bovine serum albumin (BSA) pH 6.4; measured at 37°, three independent experiments, values are shown as means ± SEM. (b); Histogram showing the size distribution of the nano stars, n = 200 (c) and (d) UV-Vis used to indicate if the stars are aggregated or non-aggregated and demonstrating the nano stars are uniform in size and shape.

As previously stated, this chapter aimed to directly compare the 50 nm star like nano structure with the same size spherical nano structure to determine which of the two morphology's would be the most effective drug delivery system for the neuroprotective peptides 'H3 and H6'. Reducing the concentration of sodium citrate to 1% allowed the formation of the 50 nm AuNPs (Figure. 4.6).

4.3.4 Characterisation of the 50 nm Gold Nano Spheres

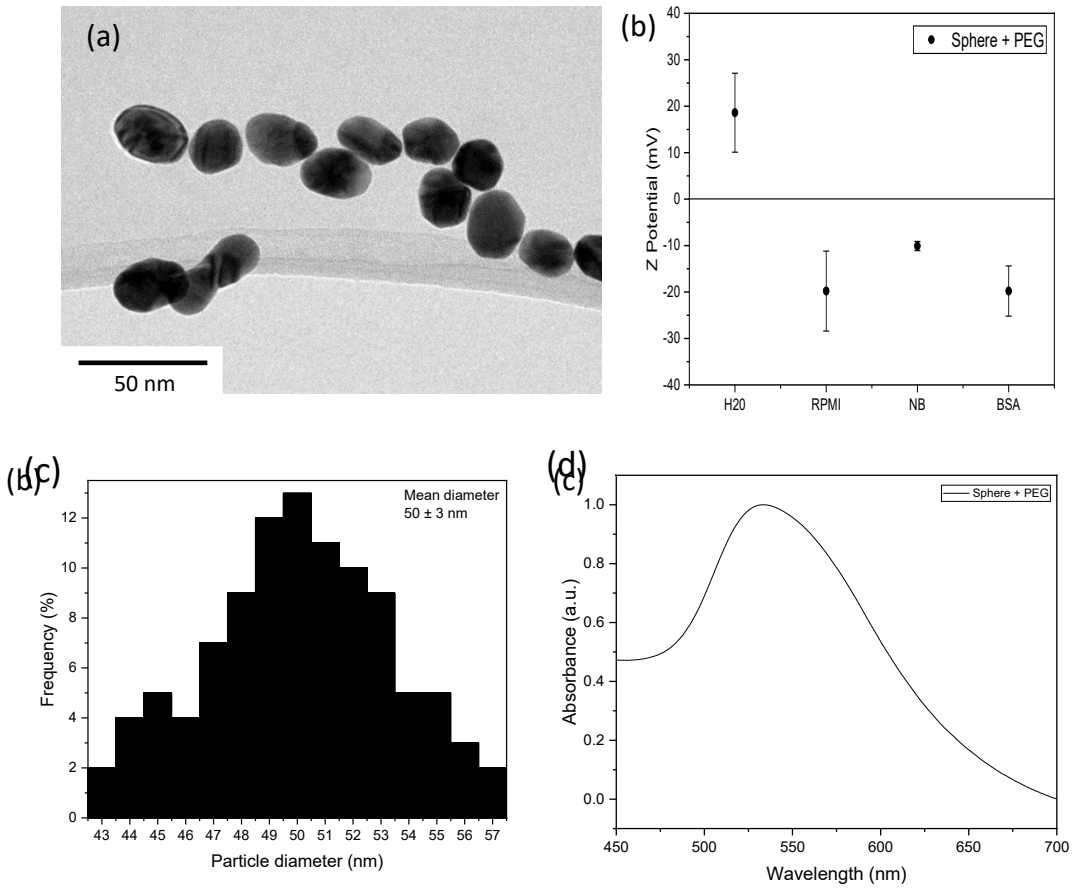


Figure 4.6 TEM micrograph image of the 50 nm nano spheres, Imaged at 200kV (a); Zeta potential demonstrating the stability of the nano stars in different media, deionized water (H_2O) pH 7.4; RPMI 1640 growth medium (RPMI) pH 7.4; neurobasal neuronal growth medium (NB) pH 6.7; 1% bovine serum albumin (BSA) pH 6.4; measured at 37°C, three independent experiments, values are shown as means ± SEM (b); Histogram showing the size distribution of the nano spheres, n = 200 (c) and (d) UV - Vis used to indicate if the nano spheres are aggregated or non - aggregated and demonstrating the nano spheres are uniform in size and shape.

The citrate capped stabilised nanospheres were approximately spherical in morphology (Figure 4.6, TEM images (a)). Reducing the citrate to 1% diminished the control over the size and shape uniformity of the AuNPs. However, as shown in the TEM images (Figure 4.6.a) the particles had not attained the curvature desired and were primarily 50 nm, indicated by the frequency distribution graph in Figure 4.5.c. The alkyl- polyethylene glycol (PEG2000) stabilised AuNS displayed the desired multi-branched morphology with multiple protruding spikes (TEM images, Figure 4.5.a). The morphological properties of the AuNP/NS including core size, the number of visible spikes, and the overall (tip-to-tip) AuNS size were quantified from multiple TEM images using Image J. The zeta potential of the nanostructures in deionised water (H_2O) pH 7.4, cell culture medias; RPMI/Neural Basal (NB) media pH 7.4/6.7 respectively and 1% BSA pH 6.4, were measured to determine the stability of the particles. Figures 4.5b and 4.6b confirm the zeta values for both the AuNPs and AuNSs in H_2O to fall within the stable range of + 10 to + 30 mV. Both the nano structures are also stable in all cell culture media and BSA tested, with zeta values of – 10 to -30 mV also.

4.3.5 Conjugation of H3 and H6 neuroprotective peptides onto the nanostructures' surface

The surface of the AuNPs and AuNSs were coated *via* covalent binding of either the thiol-modified H3/H6 peptides alone, or in the presence of thiol - modified PEG, as described in the methods above. Thiol to gold covalent binding is considered a strong bond with a k affinity of 126 kJ/mol and is almost irreversible. Figure 4.7 shows a visual representation of where the thiol modifications were localised. In both the peptide formulations, the thiol modifications were localized in the lysine backbone *via* the addition of the cysteine amino acid (Figure 4.7 b, d) this location should not affect the neuroactive peptide sequences (Figure. 4.7b). The H3-peptide is highly homologous within the S100 family, whereas, the H6-peptide (C-terminal of S100A4) shares little homology with other S100 members ('unique' motif)[8, 66] (Figure. 4.7).

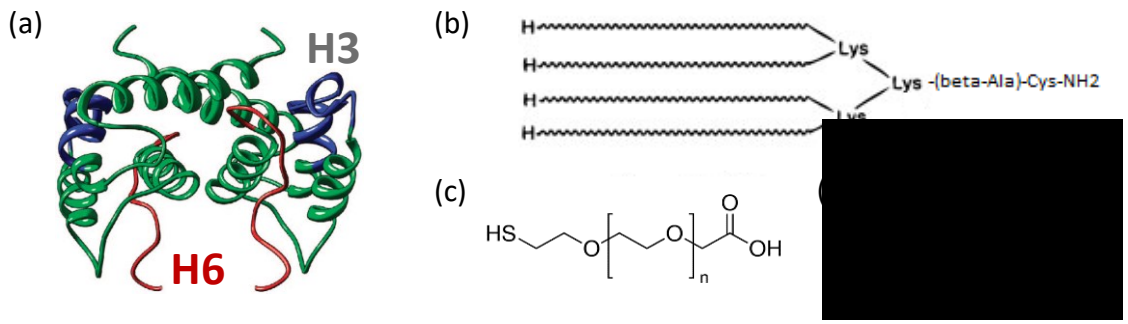


Figure 4.7 S100 A4 mother protein with the H3 and H6 peptide mimetics labelled (a). H3 and H6 peptides synthesised as tetramers for stability (b). (c) The chemical structure of PEG displaying the –SH thiol group that allows direct binding to gold and (d) is the structural representation of the cysteine amino acid used in the synthesis of the peptides that also contains the –SH thiol bond that allows direct binding to gold.

Physical Property	**Au nano Star**	**Au nano Sphere**
Core size	18 nm ± 5 nm	51 nm ± 9 nm
Diameter	53 nm ± 9 nm	51 nm ± 9 nm
Spike length	23 nm ± 8 nm	N/A
Quantity of Spikes	30 ± 6	N/A
Peptide content	1.29×10^{-5} mol	2.58×10^{-5} mol

Table 4.7 Table summarising the physical properties of the Au nanostars and nanospheres. Au nano star (middle panel) and Au nano sphere (right panel) physical properties including core size, particle diameter (measured tip to tip), quantity of spikes per stars and the length of the spikes measured by Image J. These calculations gave the surface available for drug binding. n = >200.



Figure 4.8. Schematic diagram showing the steps used to produce nanospheres and nanostars and conjugate H3/H6 (+/-PEG) onto the spherical and star shaped gold nanostructures.

The fabrication protocol developed for the synthesis of S100 peptide-conjugated AuNPs and AuNSs is depicted schematically in Figure 4.8 and in detail in methods section 4.2.2. As the H3/H6 nano constructs were synthesized *via* a surfactant-free seed-mediated wet chemical approach, this surfactant-free method does not use polymers or surfactants in the synthesis and thus results in highly biocompatible nano therapeutics that can be easily functionalized with the cargo drugs for biomedical applications. PEGylation of polypeptide drugs is widely used in pharmaceutics, protecting them from degradation by proteolytic enzymes, preventing generation of neutralizing antibodies, and increasing compound half-life[68].

4.3.6 Characterisation and functionalisation of the H3/H6 Peptide - Conjugated nano compounds

It is vital to fully characterise the nano constructs, to confirm the peptide has attached and how stable and functional these constructs are for further analysis as a drug delivery system for neurological disorders.

First step was to determine the exact moles of peptide required to cover the surface area of the nano structure and to confirm that there was no excess peptide in any of the solutions that could distort the results or give cause for concern over the accuracy of any

results going forward. The volume of 2 mg/mL peptide required for surface coverage for both the AuNPs and AuNSs generated in a 10 mL synthesis was estimated at 23 µL (calculated in methods section 4.2.2). This was further optimised to determine the actual volume of 2 mg/mL H3 or H6 that was required for full surface coverage.

The peptide content was measured via the NanoDrop one, A280 application, and as they are synthesised as single peptides, there is no risk of other protein contaminants. Both the sample and supernatant were measured during the initial trials to confirm there was no excess peptide/slight detection in the supernatant, and hence that all peptide measured in the sample was bound peptide. A low level detection of peptide in the supernatant was used to confirm that there was sufficient peptide/PEG molecules covering the surface of the particles *i.e.* that the surface was fully covered.

The Peptide volume was trialled to measure the exact volume of H3 or H6 peptide required for full surface coverage for both the nanostars and nanospheres as well as a 75:25 Peptide: PEG ratio reported in table 4.6. There were approximately 4.98×10^{16} particles formed in each of the AuNP and AuNS synthesis. To observe 100% surface area coverage of each particle, the AuNS required 50 µL of either the H3 or H6 (2 mg/mL) per synthesis and the AuNP synthesis required 100 µL of either the H3 or H6 (2 mg/mL) per synthesis. To functionalise the particles with H3 or H6 + PEG, the peptide coverage was reduced to 75%, with PEG molecules covering the remaining 25% of free surface space to complete 100% surface area coverage. The volume of H3/H6 was reduced by 25%, thus, required 37.5 µL and 75 µL of the H3/H6 peptides for the AuNS and AuNPs respectively and 31.2 µL and 62 µL of 1 mM PEG was required for the AuNS and AuNPs respectively.

	Nano Star		*Nano Sphere*	
Conjugation	**Volume of 2mg/mL Peptide (µL)**	**Volume of 1 mM PEG (µL)**	**Volume of 2mg/mL Peptide (µL)**	**Volume of 1 mM PEG (µL)**
Particle + PEG	n/a	125	n/a	250
Particle + H3	50	n/a	100	n/a
Particle + H6	50	n/a	100	n/a
Particle + H3 + PEG	37.5	31.2	75	62
Particle + H6 + PEG	37.5	31.2	75	62

Table 4.8. Peptide : PEG ratios for full surface coverage of gold nanostars (left panel) and nanospheres (right panel). To achieve 100% AuNS/AuNP peptide only full surface coverage, 50 µL/100 µL of 2 mg/mL H3/H6 peptide was required. To achieve 100% AuNS + peptide + PEG full surface coverage, 37.5 µL of 2 mg/mL H3/H6 peptide and 31.2 µL of 1 mM PEG was required. 75 µL of 2 mg/mL H3/H6 peptide and 62 µL of 1 mM PEG was required for AuNP + peptide + PEG 100 % surface coverage.

The next step was to obtain a visual of how the peptides were organised on the surface of the AuNS. To achieve this, uranyl acetate (UA) negative staining was used. UA takes advantage of the high affinity the electron dense uranyl ions have for proteins that contain carboxyl groups, which are contained in the peptides, thus would produce an enhancing contrast.

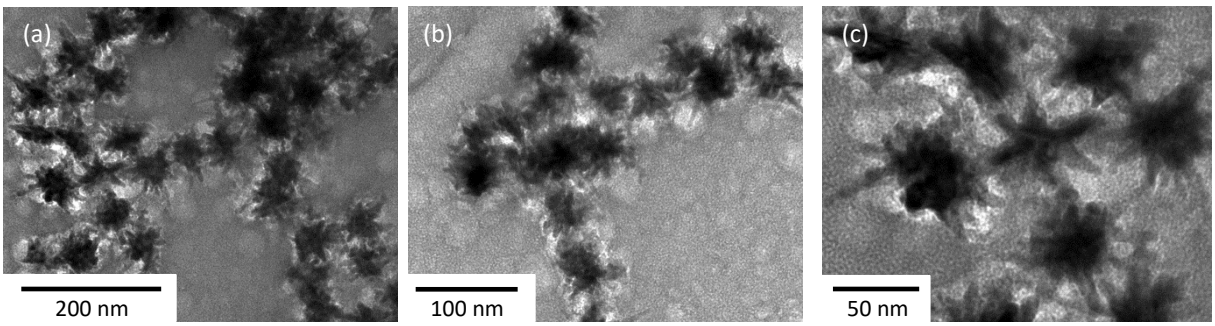


Figure 4.9 TEM Micrograph image of uranyl acetate (UA) contrast staining to visualise the peptide H6 bound to the nano stars. Imaged at 200 kV

The TEM images in Figure. 4.9 revealed a bright cast directly around the AuNSs, surrounded by a grey cake. These images suggest that some of the surface-bound peptide molecules had been positively stained. However, there is a lot of variability between nanostructures and this data set could not be used to unambiguously confirm the peptides had bound to the gold.

One of the appealing attributes the gold nano compounds is their plasmonic property and the fact that they can be imaged using fluorescence microscopy and micro CT that also enables their location to be tracked inside the brain. As the particles are plasmonic and reside in the visible light spectrum, UV-Vis was used to confirm peptide attachment, and any particle aggregation, seen by shifts in the spectral peaks and by how broad the spectrum is respectively.

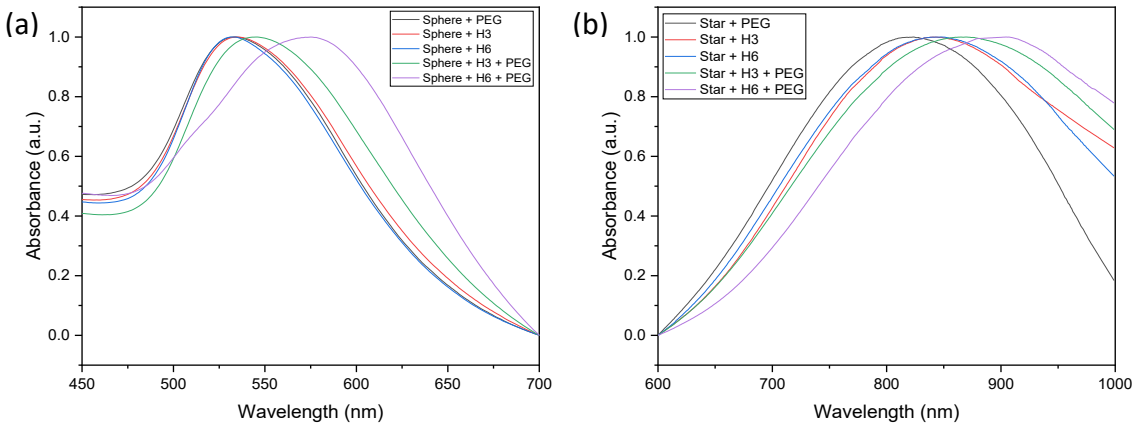


Figure 4.10 UV - Vis spectra identifying the plasmonic nano particles conjugated with the H3/H6 neuroprotective peptides +/- PEG nano spheres (a) nano stars (b). The colloidal solutions were measured after 24hr incubation with the peptides +/- PEG, washed by centrifugation three times, and measured in deionised water at pH 7.4.

The peptide targeted AuNPs (Figure.4.10.a.) displayed a peak shift for all the H3/H6 +/- peptide/PEG conjugations when compared to the AuNPs + PEG. The sphere + H6 + PEG demonstrated a larger shift to the right and a much broader spectrum than the other formulations.

The peptide targeted AuNSs (Figure 4.10 b) also displayed a shift in peak for all the +/- peptide/PEG conjugations, when compared to the PEG only AuNSs. The AuNS + H3 and AuNS + H6 displayed the same peak at 825 nm, as expected. This demonstrates they are the same size; the slight shift from the AuNS + PEG, indicated the overall particle size is slightly larger. The AuNS + Peptide + PEG constructs also shift further to the right.

The red shift (peak shifting to the right) was due to the refractive index of the particles that increased due to the functionalisation and thus, indicates a particle size increase, suggesting that the peptide did attach onto the surface on the nano structures. However, the conjugation of AuNP + H6 + PEG has an increased red shift that could be induced by some aggregation of the construct.

X-ray photoelectron spectroscopy (XPS) Confirmation of peptide attachment

X-ray photoelectron spectroscopy (XPS) was used to confirm the presence of and the actual binding of H3/H6 and PEG on the surface of the AuNPs/AuNSs. All samples showed the signals expected from their synthesis. The main core level spectra of AuNP and AuNS are shown in Figure. 4.12. The Au 4*f* core levels for both sample sets (Figure. 4.12 a, d) are typical for metallic gold, as expected for AuNP/NS. Small shifts in the binding energy (BE) on the order of 0.1 eV (AuNP) and 0.3 eV (AuNS) can be caused by either binding to H3/H6/PEG or are minor effects from sample charging. The C and N 1*s* (Figure 4.12 b,c,e,f) spectra were used to determine the presence of the peptides and the PEG through contributions specific to their intrinsic chemical states.

Aiding the identification of the chemical environments, reference measurements of H3, H6 and PEG were performed (Figure 4.11). This data shows high C – O / C – N (carboxyl) peaks to identify the presence of PEG and a high NH_2 peak that identifies with the amine grouping on the end terminus of the peptides while a medium peak for the carboxyl grouping (C – H) found located at the cysteine amino acid on the peptide backbone where the –SH thiol – Au binding takes place.

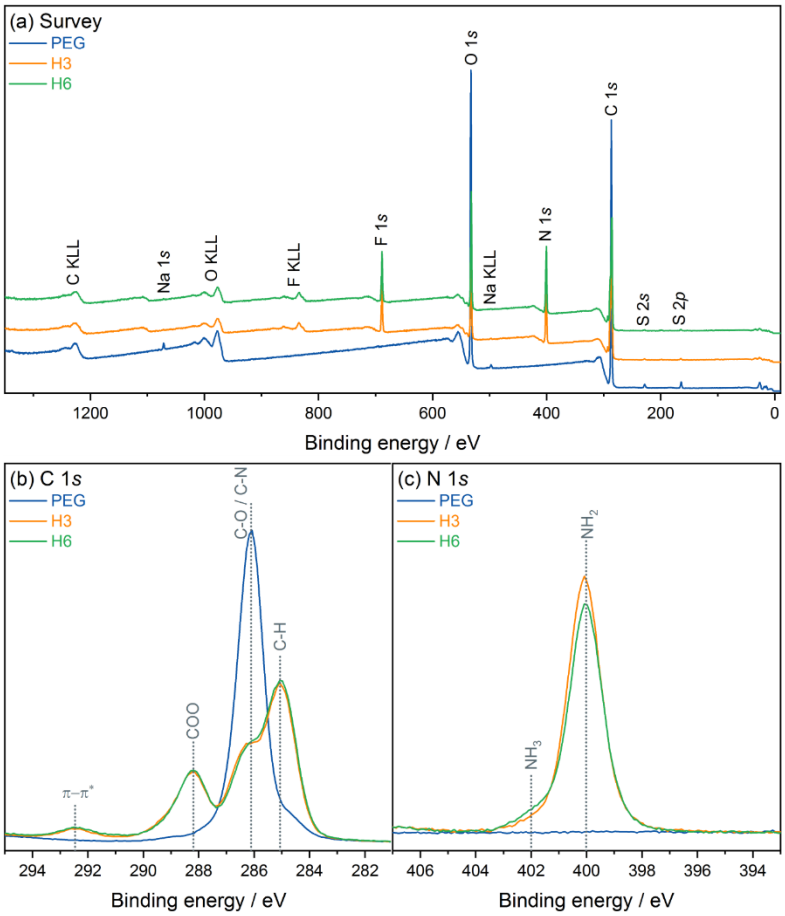


Figure 4.11 XPS reference datasets of PEG, H3 and H6, including (a) Survey, (b) C 1*s* core level, and (c) N 1*s* core level spectra. In the survey spectra, all major signals are indicated and for the core levels, chemical states are labelled. Data acquired and analysed in collaboration with Anna Regoutz, UCL.

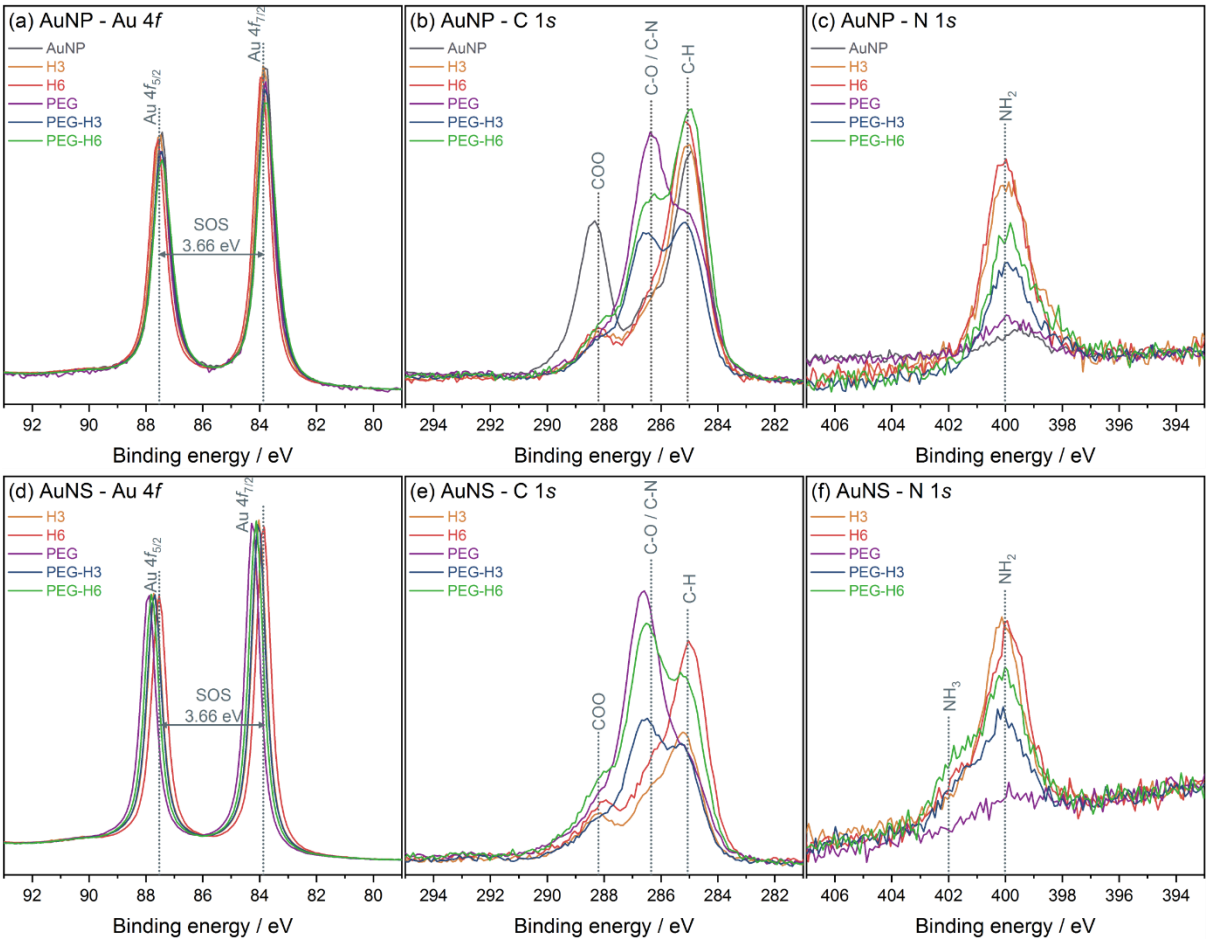


Figure 4.12 XPS data confirming peptide – particle attachment. Core level spectra including Au 4*f*, C 1*s* and N 1*s* for (a) - (c) AuNP and (d) - (f) AuNS samples. Data acquired and analysed in collaboration with Anna Regoutz, UCL.

The AuNPs and AuNSs conjugated with H3 or H6 showed three contributions to the C 1s core level (Figure. 4.12 b, e), which is typical for the peptides amino acid constituents. The lowest BE feature peaked at 285.1 eV and is typical for aliphatic carbon. This is followed by two further component peaks at 286.4 eV and 288.2 eV, which stem from the amine (N-H) and carboxyl (COO) functional groups, respectively. The binding energy's for these chemical environments agree well with previous reference data of amino acid spectra[63, 64]. The samples that included the PEG molecules demonstrated an increased intensity around 286.4 eV which is associated with the C-O environments, in which overlapped in BE with the N-H feature from H3/H6.

The N 1*s* core levels (Figure. 3C, F) showed significant amounts of nitrogen only for samples including H3/H6 at a binding energy of 400.0 eV typical of the amine group (NH_2). The unconjugated and PEG-only conjugated nanostructures only had trace amounts of nitrogen. In addition, the AuNS samples show an additional feature at higher BE (402.0 eV), which agrees with NH_3 environments. Thus, the XPS data confirmed specific immobilization of H3, H6 and/or PEG on the surface of the nanostructures.

4.3.7 Stability of the conjugated nano structures

As the peptides have successfully bound to the surface of the nanostructures, it is of high importance to confirm these conjugates are stable, as the colloidal stability and surface charge of these conjugations may have an impact on further biological studies especially the nanoparticle's toxicological profile. To determine this, zeta potential measurements were utilised in media that mimic the body's blood serum and mediums used in *in vitro* cell culturing. The zeta potential of the peptide targeted nano structures were measured in deionized water, RPMI 1640, neuronal neurobasal media, as well as in 1% bovine serum albumin solution (BSA), at 37°C to mimic the body's natural temperature.

The Zeta potential describes the electric potential that the nanoparticles have developed in the solutions mentioned above *via* the formation of a double electrical layer. In general, it is considered that a potential of. + 5 to + 20 mV and the respective negative counterpart −5 to −20 mV are minimally stable, and + 20 to + 40 mV and the respective negative counterpart of − 20 to − 40 mV are considered to be moderately stable, while + / - 30 mV and above/below, is an indication of a very stable particle[6].

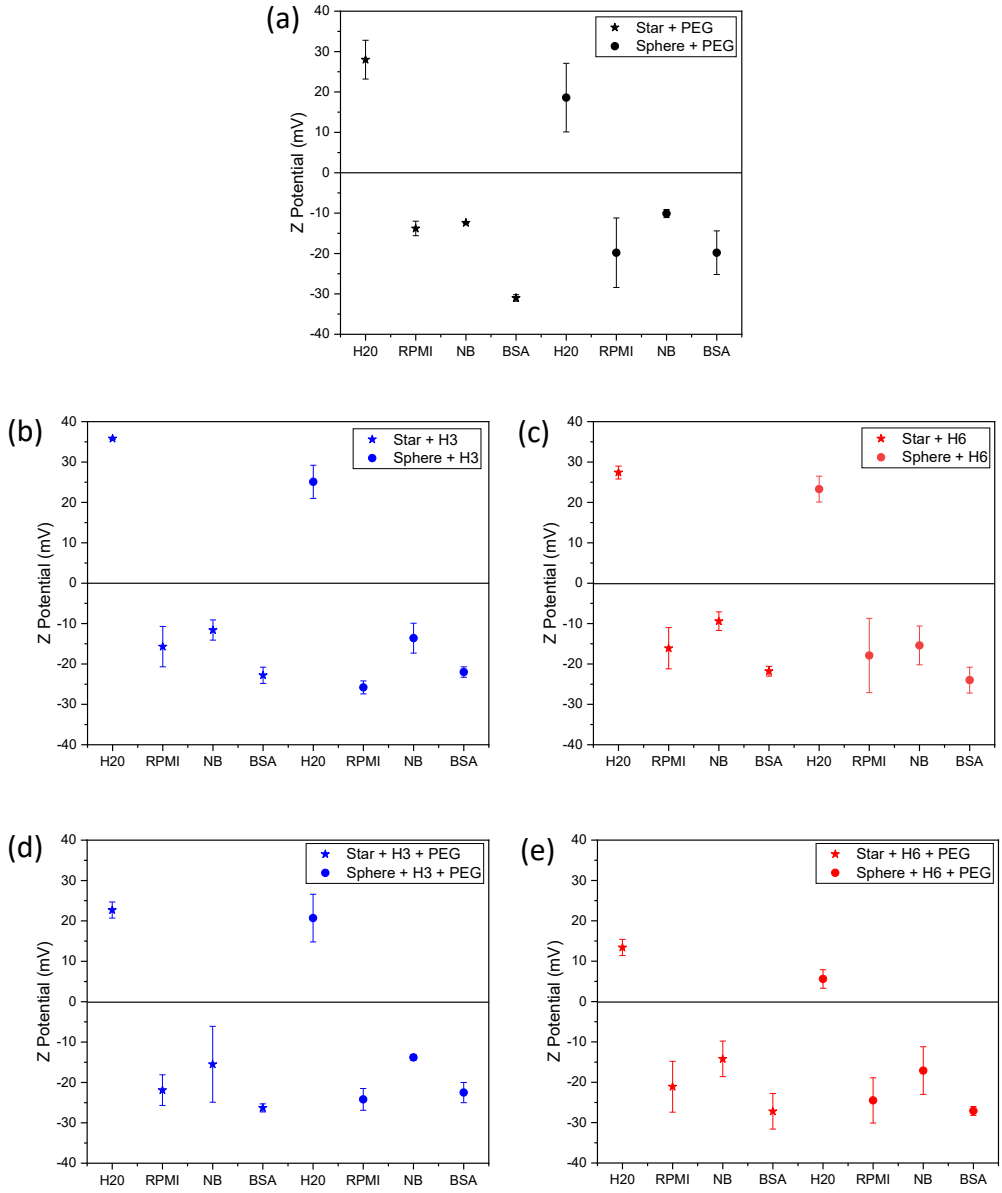


Figure 4.13. Zeta potentials of the conjugated nano structures in different media; deionized water (H_2O); RPMI 1640 growth medium (RPMI); Neurobasal neuronal growth medium (NB); 1% bovine serum albumin (BSA). Measured at 37°C, three independent experiments, values are shown as means ± SEM. n = 5.

Figure. 4.13 shows the zeta potentials, adding a 0 mV baseline for reference. If all the particles in suspension have a large negative or positive zeta potential then they will tend to repel each other and there will be no tendency for the particles to aggregate as explained by Van der Waals or electrostatic forces. It is possible that a change of pH can result in a change of the surface charge and nanoparticles' stability in a medium. However, the pH for media did

not vary significantly and was not a contributing factor in the surface charge of the conjugated nanostructures. The pH of the particles in the respective mediums are shown in table 4.7 below.

Particles in medium	***pH***
H_2O	7.4
RPMI	7.43
NB	6.76
BSA	6.44

Table 4.9 pH values of the media containing the peptide targeted nano structures measured for zeta potential analysis.

The results did not significantly vary based on the media types, particle geometry or PEGylation, with the zeta values remaining in the range of -10 -30 to mV, which would be considered stable.

Interestingly, the zeta value for the sphere + H6 + PEG shows the particles to be very unstable in water, with a value at almost 0 mV, which coincides with the broad spectra from the UV-Vis analysis suggesting the occurrence of particle aggregation. In contrast, the particles are far more stable when in the BSA media that mimics that found in the body.

The zeta potential of the peptide conjugated nanostructures measured in BSA, RPMI and NB were all negative, and positive when measured in deionised water. This could be explained by the fact that the body mimicking mediums; BSA, RPMI and NB have a higher viscosity value (3 cP) than water (0.88 cP), but also due to the cell culture media containing negatively charged ions that could result in the charge being screened.

4.4 Conclusions

In conclusion, this chapter achieved the initial aims set out. High quality and optically tunable gold nanostars and nanospheres were developed though optimising the synthesis conditions that produced highly controlled particles with tailorable sizes and morphologies. The fabrication of the H3 and H6 neurotrophic motifs onto the surface of the nanostructures was achieved. However, the H6 mimetic was difficult to work with, and at the close of this chapter, it was unknown the exact reason why, but believed to be due to the more linear structural format of the peptide that allowed it external interactions with apparatus used in the experiments, compared to the coiled structure observed in the H3 mimetic. It was found that the H6 peptide in the presence of PEG can alter the surface chemistry of the AuNPs that in turn significantly altered the aggregation state of the AuNPs that was not observed in the AuNSs. Moreover, the H3/H6 AuNSs were highly stable in water, cell culture media and BSA, thus prove promising as an emerging nano – neuroprotectant delivery system to deliver the drug therapeutics H3 and H6 to the brain.

5. Neurotrophic Effects of H3/H6 Targeted Nanoparticles on Primary Hippocampal Neurons and Immortalized Dopaminergic Neurons (N27's)

5.1 Introduction

At present, drug therapeutics for Parkinson's disease (PD) are severely limited and mostly only appease disease symptoms, and the development of new drugs is limited, mostly by the fact that the disease origin for sporadic PD remains unclear. A major challenge in PD and the majority of other neurodegenerative diseases (ND) is the complexity of ND pathophysiology that involves several contributing factors such as disruption of neuronal membranes, inflammation, oxidative stress, and excitotoxicity. Current therapies predominantly address the contributing aspects, which in turn alleviate the clinical symptoms, but fail to halt the disease progression. Another obstacle is the lack of small easily producible compounds able to cross the blood-brain barrier (BBB) and protect neurons with minimal side effects. There is an urgent clinical need to develop strategies that are capable of targeting multiple neurodegeneration mechanisms and thus, diminish neuronal damage.

Previously, the Porter group identified a multifunctional trophic factor in the nervous system; the S100A4 protein[6]. The protein was found markedly (over)expressed in rodent and human brains after injury and during neuro – pathologies[6, 46, 86, 87]. The S100A4 protein signals through the interleukin-10 and ErbB receptors[6, 43], which are involved in neuronal plasticity in brain disorders that promote neurogenesis, neuronal differentiation and neuronal survival[80, 81, 88, 92, 96]. These receptors were also found to aid in mediating neuroprotection in models of Parkinson's disease, and also cerebral ischemia, and Alzheimer's disease[75, 78, 82, 84, 89, 92].

Accordingly, previous literature has shown that S100A4 induces neurite extension[7, 47] and protects neurons against oxidative stress, apoptosis, and excitotoxicity *in vitro* and *in vivo*, thus representing a broad spectrum central nervous system (CNS) protectant[6]. The beneficial effects of S100A4 are reproduced by its two peptide mimetics, H3 and H6 that have been designed, encompassing the neuroactive motifs of the S100A4 protein. These peptides have proven to bind to ErbBs that in turn induces neurite outgrowth from hippocampal, dopaminergic, and motor neurons[6, 8, 43]. These peptides have also shown to protect neurons in cell and animal models of brain trauma and excitotoxicity[40], as well as against PD - associated neurotoxicity *in vitro*[43]. In contrast to the parent S100A4 protein, the peptide mimetics do not affect cell proliferation or motility[43] and thus have been synthesised as specific neurotrophic agents. In addition they are cheap and simple to synthesise.

Chapter 4 of this research optimised the conjugation of these novel therapeutic mimetics to both the nano star and nano sphere structures (NS/NP). The purpose of this study was to investigate the neuronal interaction, biological efficacy and neuroprotective properties of these nanostructures depending on geometry and determine if the H3 and H6 peptides retain the neurotrophic effects mentioned above once bound to the NS/NP delivery vesicles. This study aimed to prove or disprove the following hypothesis:

1. The nanostars will demonstrate improved efficacy compared to nanospheres because the spike like features could penetrate through the plasma membrane and deliver the peptide into the neuronal cytoplasm.

2. The peptides activate when in contact with the neuronal plasma membrane so delivery directly inside the cytoplasm is not necessary for neuroprotection, but could be more effective.

3. The spikes on the nanostars will be more effective in the tight intercalated neuronal network as the spikes can branch through and contact more neurons than the nanospheres.

The interface between the peptide conjugated nanoparticles and neurons was characterised for toxicity by examining how effective the H3/H6 – AuNS/AuNP +/-PEG were are protecting the neurons from toxin induced death. Neurite outgrowth assays were used to determine if H3/H6 – AuNS/AuNP +/-PEG could stimulate neurite projections that would aid in repairing damaged neurons often seen in Parkinson's disease pathology. ICP – OES, 2D and

3D electron microscopy techniques were used to detect and capture the interface between the neurons and the nano therapeutics. This chapter showed that the nanostructures efficiently interact with cell membranes, moreover, the nanostar morphology demonstrated a higher membrane binding/insertion affinity than the nanospheres, determined by electron microscopy. Both the peptide targeted nano compounds induced neurite extensions in cultured neurons and positively protected neurons against several models of neurodegeneration, with the H3/H6 - AuNS exhibiting higher neurotrophic potency/efficacy than the H3/H6 - AuNP formulations.

The data indicates that AuNS carrying multipurpose H3 and H6 synthetic peptides derived from the neurotrophic S100A4 protein are a novel, efficient platform for activating multiple neuroprotective pathways, that could be adapted in future studies to treat not only PD, but a broad spectrum of neurological conditions.

5.2 Methods

5.2.1 Peptide targeted gold nano particle synthesis

S100A4 peptide mimetic synthesis

Peptides (sequences H3: KELLTRELPSFLGKRT, H6: NEFFEGFPDKQPRKK) were synthesized as tetramers composed of four monomers coupled to a lysine backbone (purchased from Schafer-N, Denmark). Tetramerization was previously found to be necessary for the neuritogenic activity of S100A4[47].

Nano seed synthesis

12 nm spherical citrate-stabilized gold (Au) nanoparticles were synthesised *via* a Turkevich method of citrate reduction[4]. Following and modifying the protocol described by

Yuan *et al*, 2012[5], a 3% (w/v)) solution of sodium citrate was prepared by dissolving 0.3 g tri - sodium citrate in 10 mL of deionised water by bath sonication. 10 mM $HAuCl_4 \cdot 3H_2O$ was prepared by dissolving 0.394 g of gold(lll) chloride trihydrate in 100mL deionised water, then stored light protected at 4 ^{0}C. In an AR cleaned 250 mL erlenmeyer flasks with a 1-inch stir bar, 48.75 mL of deionised water and 1.25 mL of the 10 nM $HAuCL_4$ solution was added and bought to the boil. At boiling point, 1 mL of 3% (w/v) sodium citrate solution was added under vigorous stirring until the solution had changed colour to red. At this point, the colloidal solution was quickly cooled, washed by centrifugation three times.

The peptide - only fabricated NS/NP nanostructures were completed by diluting 4 mL of the nano seed solution in 6 mL deionised water, then adding 50 µL of either the 2 mg/mL H3 peptide or the 2 mg/mL H6 peptide and left to stir for 24 hrs at room temperature.

The NPs functionalized with the peptides in the presence of PEG, at a ratio of 75 : 25 peptide : PEG molar ratio, were synthesized as mentioned above and 31.2 µL of 1 mM PEG was added whilst stirring for 1 minute, then incubated whilst stirring for 24 hr at room temperature with 37.5 µL of either H3 or H6 peptide. They were then washed 3 times by centrifugation, and stored at 4^{o}C light protected.

Nanostar synthesis

The Yuan *et al*, 2012[5] protocol was followed for the subsequent synthesis of the AuNS. A 10 mL acidified 0.1 mM $HAuCl_4 \cdot 3H_2O$ solution was prepared by adding 100 µL of 10 mM $HAuCl_4$, 10 µL of 1 M HCL and 9890 µL of deionised water into a vial and placed under moderate stirring at room temperature (RT). 200 µL of the 12 - nm Au seeds were then added, quickly followed with 100 µL of 3 mM $AgNO_3$ and 50 µL of 100 mM ascorbic acid. The colour of the solution changed from faint red to blue as soon as the ascorbic acid was added, this indicated the AuNS had formed and the synthesis was complete.

The H3/H6 - NS/NPs were completed by adding 50 µL (AuNS) or 100 µL (AuNP) of either the 2 mg/mL H3 or the 2 mg/mL H6 and left to stir for 24 hrs at RT.

The nanostars functionalized with the H3/H6 peptides and the PEG, at a ratio of 75:25 peptide : PEG molar ratio, were synthesized as mentioned above and stabilized with 37.5 µL of either H3 or H6 and incubated for 24 hr, then 31.2 µL of PEG was added and incubated for 1 hr at room temperature. They were then washed 3 times by centrifugation, and stored at 4^{o}C light protected.

5.2.2 Quantifying the volume of Au per drug dose.

Inductively Coupled Plasma Optical Emission Spectroscopy (ICP-OES)

ICP – OES was used to detect and quantify the Au content that would be administered alongside the H3 and H6 peptides when the peptide functionalised NP/NSs were administered in doses of 2 µg/ml, 5 µg/ml, 10 µg/ml, 20 µg/ml and 40 µg/ml.

H3/H6 - NS/NPs +/- PEG were measured by NanoDrop for protein/PEG content then the required volume of each sample that amounted to the desired concentrations of 2, 5, 10, 20 and 40 µg/ml were placed into 15 mL falcon tubes. 500 µL of concentrated aqua regia (AR) (HCL : HNO_3, 3 : 1 v/v) was added to the samples and left to digest overnight. 10 mL deionised water was then added to dilute the AR and the samples were then run on a ThermoScientific iCAPTM 7400 ICP - OES platform against a set of standards of known varying concentrations of gold. The absorbance was measured to characterise and quantify the Au.

Protein measurement by NanoDrop

A Thermo Scientific NanoDrop One was used to confirm and quantify the peptide attached to the Au nano structures. The A280 application was used as this is the wavelength the peptides can be detected. As they are synthesised as single peptide chains, there is no risk of contamination from other proteins, so all values obtained are specifically for each of the H3 or H6 peptides. 2 µL of peptide - particle solution was dropped onto the NanoDrop and

measured against the corresponding blanks of either ultra - deionised water or 1 mM PEG solution. The NanoDrop was wiped with an ethanol wipe after each use to prevent cross contamination and the values were expressed as mg/mL.

5.2.3 Ethics statement

Animals were handled in accordance with European Union legislation (European Directive 2010/63/EU). Pregnant Wistar rats (E18) were from Charles River (UK).

5.2.4 Cell culturing

Primary Neurons

Hippocampal neurons were isolated from Wistar rat embryos at gestational day 18 (E18). Isolated hippocampal tissue was homogenized, trypsinized, and incubated in the presence of DNase I (Sigma) and soybean trypsin inhibitor (Sigma). Cells were seeded in 60-well microtiter plates (NUNC, Roskilde, Denmark) at a density of 50,000 cells/well in a volume of 15 µl. For low density cultures, dissociated neurons were seeded in 8-well LabTek cover slides (NUNC) at a density of 5000 cells/cm^2. Cultures were maintained at 37 °C, 5% CO_2 in neurobasal medium supplemented with B27, 4 mg/ml bovine serum albumin, 100 units/ml penicillin, and 100 µg/ml streptomycin (all from Invitrogen).

N27 cell line

The rat immortalized mesencephalic dopaminergic neuronal cells 1RB3AN27 (N27) were used, derived from day 12 rat fetal mesencephalic tissue and positive for tyrosine hydroxylase2. N27 were grown and maintained at 37 °C, 5% CO_2 in RPMI 1640 medium

supplemented with 10% FBS, 1% penicillin (100 U/mL), and streptomycin (100 µg/mL). All experiments were performed between passages 10 and 20 and at 60 - 80% confluence in Gibco Roswell Park Memorial Institute RPMI 1640 with 1% serum.

5.2.5 Neuronal Survival Assay

Rat hippocampal (E18) cultures were prepared as stated above. To evaluate neuroprotection in the oxidative stress and 6-OHDA models, hippocampal neurons (7 DIV) or N27 cells were treated with H3, H6 or H3/H6 - based nano formulations, challenged with H_2O_2 (60 mM, hippocampal neurons) or 6-OHDA (100 µM, N27 cells, both from Sigma Aldrich, UK), further cultured for 24 h, fixed, and stained with Hoechst 33258 (1:1000; Invitrogen). To evaluate neuronal survival, images of 1,000 – 1,200 cells were recorded in systematic series of fields of view across the whole area of a well for each group in each experiment employing a Nikon Eclipse E800 microscope with a Nikon Plan ×20 objective (Nikon, Tokyo, Japan) coupled to a video camera (QImaging, Surrey, Canada). Neuronal survival was evaluated as the ratio of live (non - pyknotic) neurons to the total number of cells using the PlabApp software (Protein Laboratory, University of Copenhagen, Denmark, 2002). The obtained viability levels were normalized to those in untreated controls (CTL, set to 100%).

5.2.6 Neurite Outgrowth

Rat hippocampal neurons (E18) were isolated as described above and plated at a density of 5,000 cells per well in eight - well LabTek Permanox slides (NUNC, Roskilde, Denmark) coated with laminin (5 µg/mL; Sigma-Aldrich). The cells were stimulated with the peptide conjugations at does 2, 5, 10, 20 and 40 µg/mL and incubated for 24 hrs.

To evaluate the neurite outgrowth of the hippocampal neurons, the LabTek cover slides were fixed in 4% w/v paraformaldehyde for 15 minutes, then stained with Coomassie Blue R250 (4 g/litre in 45% v/v ethanol and 45% v/v acetic acid) for 20 min, and cover slides

were examined under a Nikon Diaphot 300 inverted microscope using Nikon Plan × 20 phase - contrast optics.

ProcessLength software package was used to digitally analyse the images. This software analyses using an unbiased counting frame containing a grid with a user - defined number of test lines was superimposed on the images of the cell cultures. The number of intersections of cellular processes with the test lines was counted and related to the number of cell bodies, thereby allowing quantification of the total neurite length per cell. Between 150 and 250 cells were analysed in each group in each individual experiment.

5.2.7 Nanoparticle – Neuron interaction

Cell binding

Immortalized dopaminergic neurons (N27s) were grown as stated above to high confluence (70 – 80%), then plated in 24 well plates and incubated with each of the nano structures (NP + peptide +/- PEG, NS + peptide +/- PEG and NS/NP + PEG) for 24 hrs under all dose concentrations (2, 5, 10, 20 and 40 µg/mL). After 24 hrs, the supernatant was carefully removed so not to disturb any membrane bound/embedded, or internalised particles and placed in individual 15 mL falcon tubes. The cells were dislodged *via* trypsinization, and placed in individual 15 mL falcon tubes, spun down in a centrifuge, and lysed. All samples were then digested in 500 µL of Aqua Regia (HCL: HNO_3 3:1 v/v) for24 hr. Samples were then diluted with 10 mL deionised water. The gold content in both the samples (cell associated and supernatant) for each construct at each dosing, was confirmed and quantified by ICP-OES.

Cell seeding

Cells were plated in 48 well plates, seeded at approximate 50,000 cells per well. The cells were manually counted, by mixing 100 µL of cell solution with 100 µL of trypan blue stain.

50 µL of this solution was placed on a haemocytometer; the improved Neubauer, 0.01 mm depth, 1/400 mm^2 Bs.748 by Hawksley cell counter. Cells were then counted under a light microscope at x10 magnification and seeding accordingly and incubated at 37 °C, 5% CO_2 in RPMI 1640 medium supplemented with 10% fetal bovine serum (FBS), 1% penicillin (100 U/mL), and streptomycin (100 µg/mL).

Cell preparation for electron microscopy

To study the neuronal interaction with the nano-neuro therapeutics, 7 DIV cultures of dissociated hippocampal neurons were treated with either 20 µg/mL AuNS + Peptide +/- PEG or AuNPs + Peptide +/- PEG and incubated for 24 hrs, then rinsed with 0.1 M 4-(2-hydroxyethyl)-1-piperazineethanesulfonic acid (HEPES) buffer (pH 7.2), fixed with 2.5% glutaraldehyde in HEPES for 2 hrs at 4 ^oC, and washed 3 × 10 min with HEPES. The samples were then stained with osmium tetroxide (1% OsO_4 in HEPES × 1 hr at RT), then washed 5 times with deionised water. The samples were treated with 1 ml saturated thiocarbohydrazide (THC(aq)) for 1 hr. The THC acts as a cross linker to bind the osmium ions to further enhance the contrast from cellular organelles. The samples were washed 3 times with deionised water and stained again with osmium tetroxide (1% OsO_4 in HEPES × 1 hr at RT). After washing 6 × deionized (di) H_2O, cells were dehydrated in a graded ethanol concentration (50%, 70%, 95%, and dry 100%, volume ratio of ethanol to diH_2O), 3 × 5 minutes, followed by 3 × 10 minutes in acetonitrile (Sigma-Aldrich, UK). The samples were then resin embedded *via* progressively infiltrating the samples with 50% and 75% solutions of Taab 812 resin (Sigma) in acetonitrile at RT and 100% Taab 812 resin at RT. Samples were incubated with 50% resin for 2 hrs, 75% resin overnight and 100% resin for 12 hrs, with three consecutive changes. The samples were then cured at 60 °C for 72 hrs.

Transmission Electron Microscopy (TEM)

The embedded neurons were cut using a Leica UC7 ultramicrotome (Leica, Austria) with a 35° diamond knife (Diatome, CH) to a thickness of 70 nm for TEM and 400 nm for STEM. Sections were immediately collected on 2 × 1 mm slot grids, formvar and carbon coated TEM copper grids (Agar Scientific, UK), dried and stored until TEM analysis. TEM imaging of hippocampal neurons was performed at 120kV (JEOL JEM 1400Plus, JEOL, Japan) with a 2k by 2k format CCD camera (JEOL Ruby CCD Camera, JEOL, Japan). Tilt series were collected at 200kV (JEOL JEM F200 JEOL, Japan) with the Recorder software in STEM mode using the Bright Field Imaging detector (JEOL, Japan) from -60 to +60 degrees, with 1 degree tilt increments.

Quantification of AuNP/AuNS neuronal interaction

To quantify the AuNP/AuNS neuronal interaction, non - overlapping TEM images were examined for localization of each particle geometry, The localisation were assigned to four compartments: *extracellular* (not interacting with cell membranes), *membrane bound/surface associated* (interacting with the cell membranes without changes in membrane curvature, no embedding or piercing), *membrane embedded* (embedded into and/or piercing cell membranes) and *internalized* (detected within cells). The AuNP/AuNSs were counted by visual analysis and the counts in each compartment were normalized to the total count for each particle type (set to 100%).

Focused Ion Beam - Scanning Electron Microscopy (FIB-SEM)

Resin embedded samples were prepared as mentioned above and were cut and mounted onto SEM stubs and coated with 5 - 10 nm carbon film immediately before imaging to aid with electrical current charging and protection of the neuronal network. The Zeiss Auriga SEM, fitted with a gallium focussed ion beam, was utilised to obtain micrographs. The images were obtained using a back scattered electron (BSE) detector with an SEM probe of

1.49 keV at a working distance of 5 mm. Milling was performed at a 20° angle, images at 0.5 µm intervals with a grid voltage of 775 V.

Cryo – EM

N27 cells were grown directly on formva coated 300 mesh gold grids in 48 well plates, by drop casting the N27 cell solution directly onto the grids and incubating at 37 °C, 5% CO_2 for 1 hr. Subsequently the wells were filled with 200 µL RPMI 1640 medium supplemented with 10% FBS, 1% penicillin and further incubated at 37 °C, 5% CO_2 for 24 hrs. The cells were treated with the H3 - AuNS at concentration 20 µg/mL and incubated for 24 hrs. The grids were then placed in to a Leica EM GP cryo plunge and then blotted using blotting paper to prevent any excess liquid from crystalizing. The sample was then quickly plunged into liquid nitrogen to fix the cells and freeze - dried conditions for 24 hrs. Images were then obtained by High resolution TEM, performed using Jeol 2100 f, operated at 200 kV.

5.2.8 Statistics

Statistics was performed using Origin 8 pro software (OriginLab) and excel by one - way ANOVA or two - way ANOVA. Unless indicated otherwise, results are expressed as means ± SEM, *$p < 0.05$; **$p < 0.01$; ***$p < 0.001$.

5.3 Results

5.3.1 Volume of gold per drug dose

As therapeutics are given to patients in doses, it was crucial to evaluate exactly how much Au would be administered along with the peptide dose. The peptides in this research were administered at doses of 2, 5, 10, 20 and 40 µg/mL. Au has been FDA approved for medicinal use, however, when designing a drug delivery system, it is imperative to keep the non – therapeutic elements entering the body to a minimum where possible. To determine the volume of Au associated with each peptide dose for the nano conjugates, ICP - OES was used. Since no detectable amounts of free peptide/PEG were present in any of the AuNP/NS suspensions, the ICP-OES measurements provided a good estimate of the amount of gold corresponding to a given peptide dose for the AuNP/NSs and thus of the efficiency of the functionalization. Figure 5.1 shows a parallel volume of Au when comparing the H3 only bound to the NSs and NPs to the H6 + NSs, but not of any significance (Figure 5.1, c). There was minimal increase observed in gold content up to dose 20 µg/mL when comparing both the H3/H6 only conjugated nano structures (Figure 5.1, b, c), with a slight difference at 40 µg/mL, but of non - significance. There was a steady increase in Au content when administering the nano spheres with either of the peptide (H3/H6) in the presence of PEG compared to the AuNS, and a significant 5 - fold increase at 40 µg/mL, (Figure 5.1, d, e). The optimal drug delivery vector based on the volume of Au per dose was the AuNSs conjugated with H3/H6 with PEG, as the Au per dose remained under 10 mg/L (Figure 5.1, d, e).

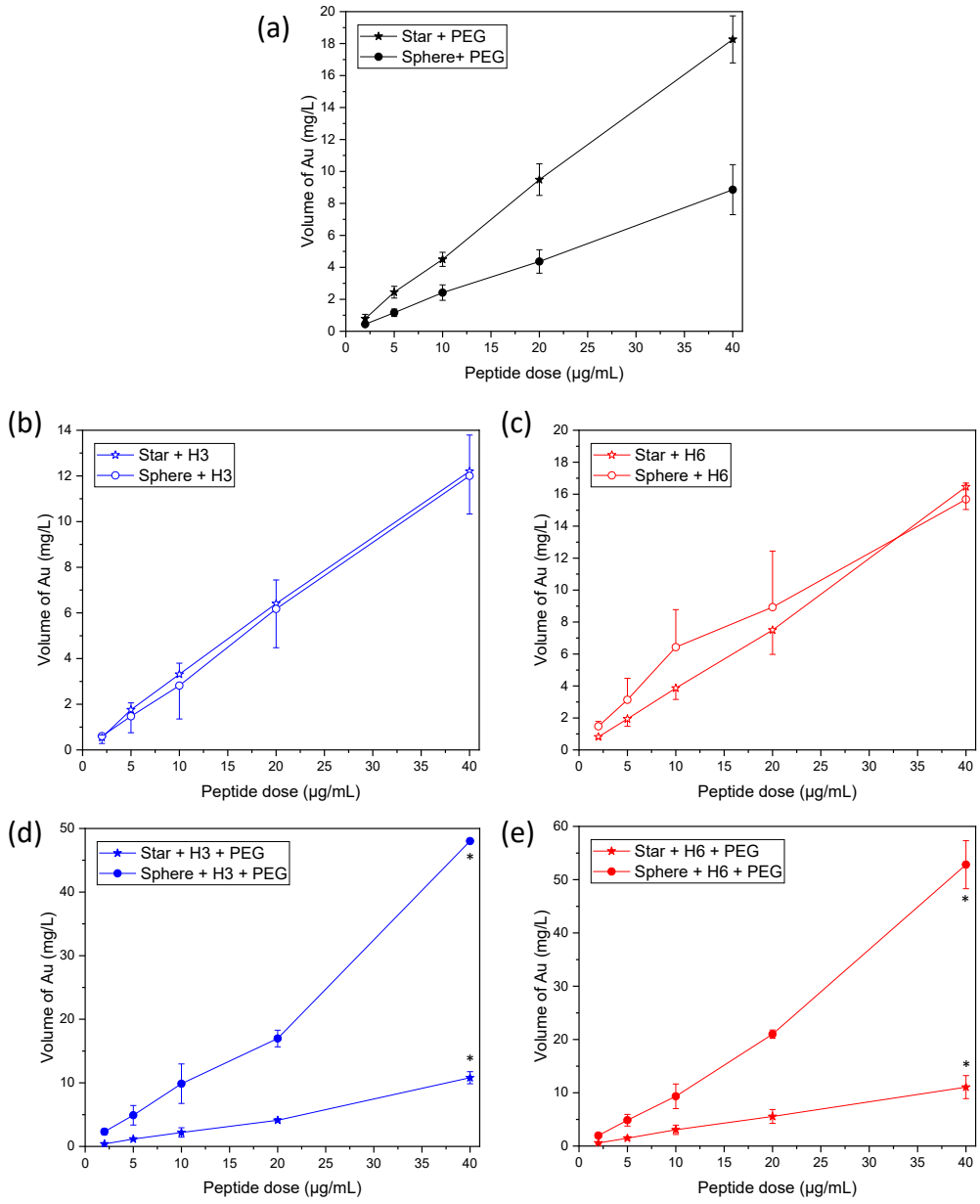


Figure 5.1 Quantification of Au administered along with the peptide doses of 2, 5, 10, 20 and 40 µg/mL as determined by ICP – OES. PEG only functionalised particles (a) AuNS + H3 vs AuNP + H3 (b), AuNS + H6 vs AuNP + H6 (c). AuNS + H3 + PEG vs AuNP + H3 + PEG, (d) and AuNS + H6 + PEG vs AuNP + H6 + PEG, (e). Significant difference found in the volume of Au administered per peptide dose between the AuNS/AuNP + H3/H6 + PEG at 40 µg/mL. *p < 0.05. Results are expressed as means ± SEM. n = 6.

5.3.2 Evaluating the toxicity of the peptide targeted nanoparticles.

To determine if the S100 peptide - targeted nanostructures were neuroprotective *in vitro*, two survival assays were performed. The first assay was to determine protection against a neuronal model of oxidative stress, which is a key neurodegeneration factor, not only in Parkinson's disease, but in several brain disorders[73, 76]. The model neurotoxin used was hydrogen peroxide (H_2O_2), an oxidant commonly employed in oxidative stress models[76, 85, 94] and previously proven to induce neurodegeneration in multiple cell types[6, 43]. Figure 5.2, A, confirms a profound decrease in neuronal viability when treated with 60 µM H_2O_2 (Figure 5.2 A, CTL vs H_2O_2). The hippocampal neurons were efficiently protected from the H_2O_2 - induced death in a dose - dependent manner, (Figure 5.2 A, CTL vs H_2O_2 + H3 - AuNS), with the H3-AuNSs displaying a significantly higher survival rate when treated with low doses of H3 peptide concentrations (2 and 5 µg/mL) than spherical H3 - AuNP treated at the same dose (Figure 5.2, B). At the higher dose of 20 µg/mL, all three peptide targeted nano structures (AuNS + H3 +/- PEG and AuNP + H3) equally protected the neurons from H_2O_2 induced death.

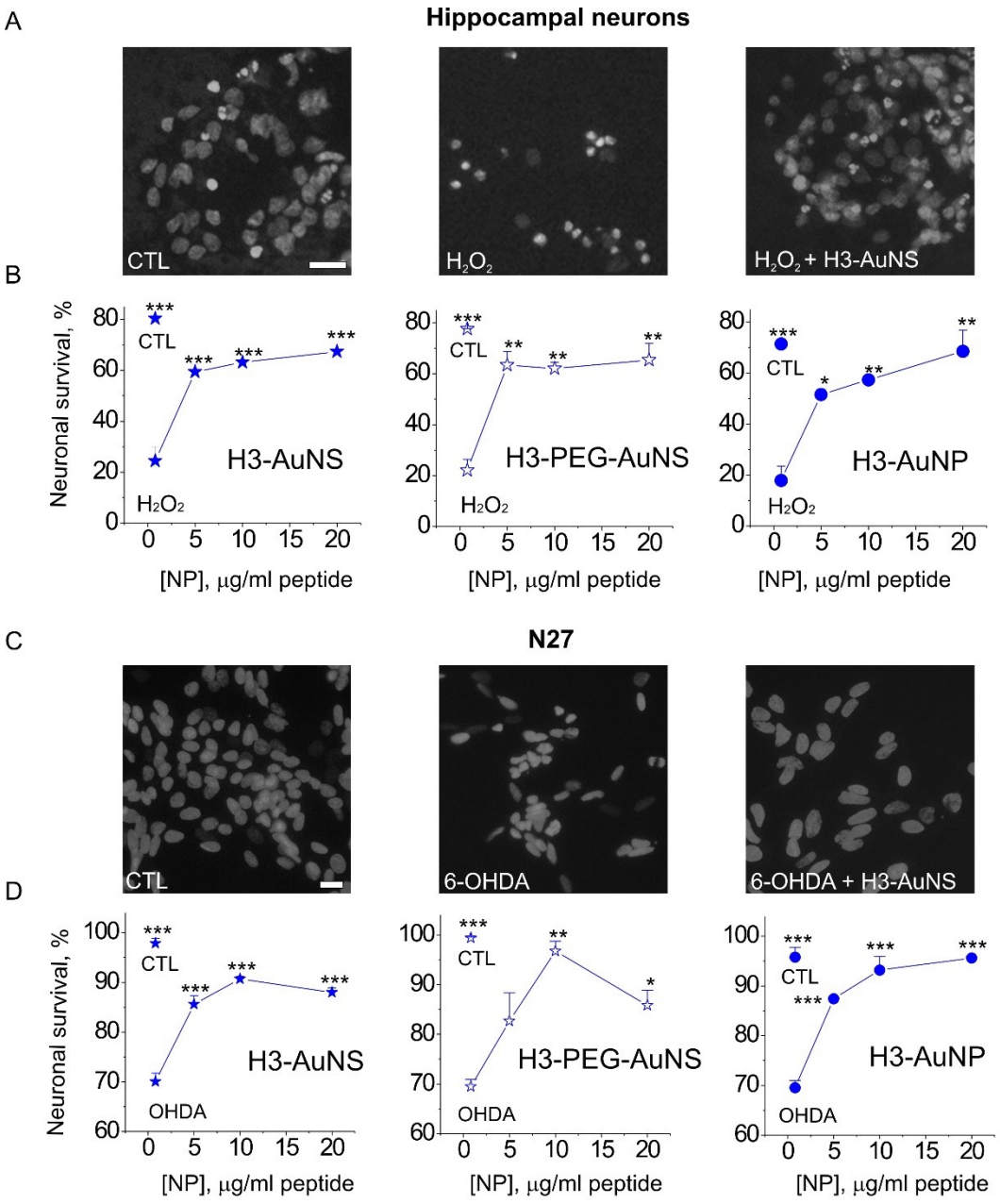


Figure 5.2 Effect of the peptide – targeted nano particles in cell survival. (A, C) Representative images of Hoechst - stained hippocampal neurons (A) or N27 cells (C) left untreated (CTL) or treated with H_2O_2/6-OHDA (A or C, respectively) in the absence or presence of H3 - AuNS (10 μg/mL). Scale bar, 20 μm. (B, D) H3 - functionalized AuNP protect cultured hippocampal neurons and N27 cells against the H_2O_2 (B) and 6-OHDA (D) induced neurotoxicity. CTL, untreated cells; H_2O_2/6-OHDA, neurotoxin only (60 and 100 μM, respectively) treated cells. One - way ANOVA vs H_2O_2 (C) or 6-OHDA (D), three to four independent experiments, *p < 0.05; **p < 0.01; ***p < 0.001. Data images and analysis obtained in collaboration with Darya Kiryushko (Imperial College London).

The second assay was to determine the effectiveness of the H3 targeted nanostructures +/- PEG in protecting cells from cytotoxicity induced by the model PD neurotoxin, 6-hydroxydopamine *(*6-OHDA)[43]. 6-OHDA has shown to trigger cell death in cultured primary and immortalized Dopaminergic (DA) neurons (N27 cells)[43, 79, 90, 95] and induce many pathological hallmarks of PD in animals, including, but not limited to; dopamine depletion, selective degeneration of DA neurons and neurological deficits[72]. N27 cells are similar to dopaminergic neurons, as they are positive for the dopamine marker tyrosine hydroxylase (TH) and dopamine transporter[70, 91] and so are widely used as an *in vitro* PD model[71, 74, 77] and thus the cell line chosen in this research. Figure 5.2 C, images demonstrate a depletion of N27 cells by around 30% after being treated with 100 µM 6-OHDA (Figure 5.2 C, CTL vs 6-OHDA). All three H3 functionalised nano formulations (AuNP/NS + H3 +/- PEG) had a significant pro - survival effect in this model. However, there was no significant difference in either potencies or efficacies of either the AuNP + H3, AuNS + H3 or AuNS + H3 + PEG (Figure. 5.2D).

5.3.3 Neurite outgrowth

The S100A4 derivative peptides, H3 and H6 are neuritogenic i*n vitro*[6, 8, 43]. For this reason it was necessary to determine if the peptides could still trigger the same neurite outgrowth from hippocampal neurons without any inhibition from the delivery nano structures. Three conjugations were examined: AuNS + H3/H6, AuNS + H3/H6 + PEG and AuNP + H3/H6 (Figure 5.3). The positive control used was the H3 only unconjugated at the dose 10 µg/mL, as previous literature has confirmed that has been the most effective concentration[6, 8, 43]. The negative control was the PEG - only conjugated AuNS, as PEG does not trigger any neuritogenic properties.

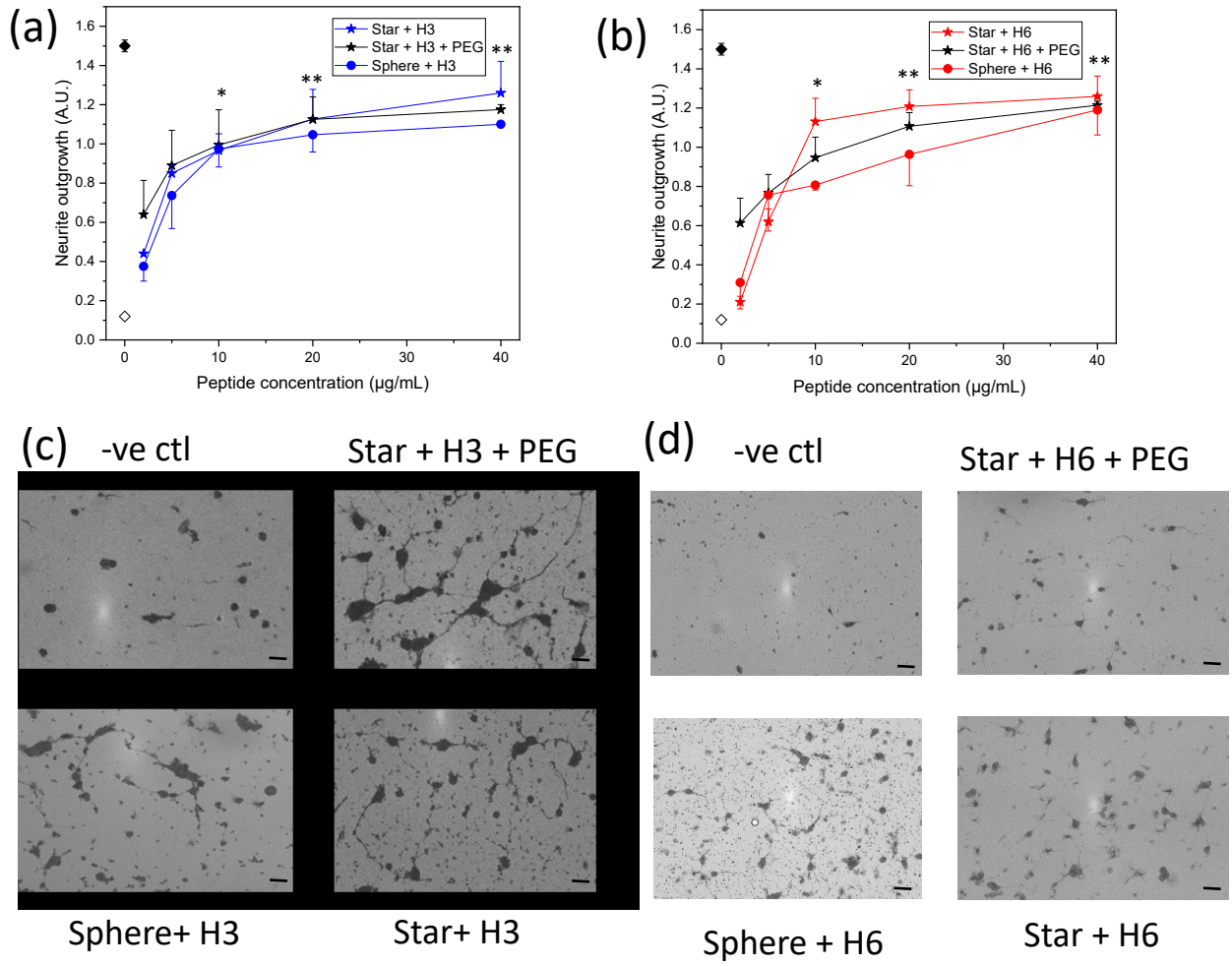


Figure 5.3 H3 and H6 - functionalized nanoparticles promote neurite outgrowth from hippocampal neurons. AuNS + H3 +/-PEG vs AuNP + H3 +/-PEG (a), Stars + H6 +/-PEG vs Spheres + H6 +/-PEG (b). (c/d) Representative micrographs of hippocampal neurons treated with AuNS + H3, AuNS + H3 + PEG and AuNP + H3 (c) and AuNS + H6, AuNS + H6 + PEG and AuNP + H6 (d). Conjugated nano constructs (10 µg/ml) and untreated control. Scale bar, 10 µm. One - way ANOVA vs CTL, four independent experiments. Results are expressed as means ± SEM. *p < 0.05; **p < 0.01

After 24 hr incubation shows that all the H3/H6 peptide conjugated nano structures induced neurite extensions in hippocampal neurons (Figure 5.3). The potency or efficacy of either of the H3 or H6 functionalized AuNS were not significantly affected by the addition of the PEG molecules. However, when comparing the geometries of the nano structures and any effect the particle morphologies had on inducing neurite outgrowth the H3/H6 AuNSs +/- PEG marked an increase on growth of neurite projections. This suggests the AuNS morphology did have an impact on neuronal targeting and interaction and thus, deemed more efficient at enhancing neurite outgrowth than the AuNPs. As the AuNS + PEG construct did not induce

neurite outgrowth (Figure 5.3 –ve CTL), a direct comparison was made against the H3/H6 AuNS/AuNPs +/- PEG nano compounds, where the results proved there was a significant increase in neurite extensions from all three nano structures at concentrations from 10 µg/mL (Figure 5.3, a,b).

Moreover, there was no significant difference in the H3 only positive CTL. Vs. the H6/H3 -NS/NPs, indicating that the Au nano structures do not impede the neuritogenic action of the peptides and have the same neuritogenic effect on the neurons bound or unbound to the delivery vehicles.

5.3.4 Neuronal interaction

Neuronal interaction was first evaluated in N27 cells (immortalized dopaminergic neurons). The assay performed was designed to ascertain if and how the peptide targeted nanostructures interacted with the neurons. As literature has described previously, the peptides signal their effects *via* the ErbB receptors located on the cell membrane surface[6, 43]. However, it is unknown if the NPs or NSs bind to the cell membranes or internalise. Since this chapter already demonstrated that the nanostructures do not inhibit any of the novel therapeutic effects of either of the peptides, it was important to understand the role the constructs played in the intracellular delivery of the peptides.

The N27 cells were grown to high confluence, plated and incubated with each of the nano compounds (NP + peptide +/- PEG, NS + peptide +/- PEG and NS/NP + PEG) for 24hrs under all dose concentrations (2, 5, 10, 20 and 40 µg/mL). The supernatant was carefully removed, so not to disturb any membrane bound/embedded, or internalised nanostructures and set aside for analysis, while the cells were dislodged, spun down, and lysed. The gold content in both the samples (cell associated and supernatant) for each construct at each dosing, was confirmed and quantified by ICP-OES. The results shown in Figure 5.4 confirmed there was a cell - association for all of the peptide conjugated nano structures and very minimal from the PEG only nano structures.

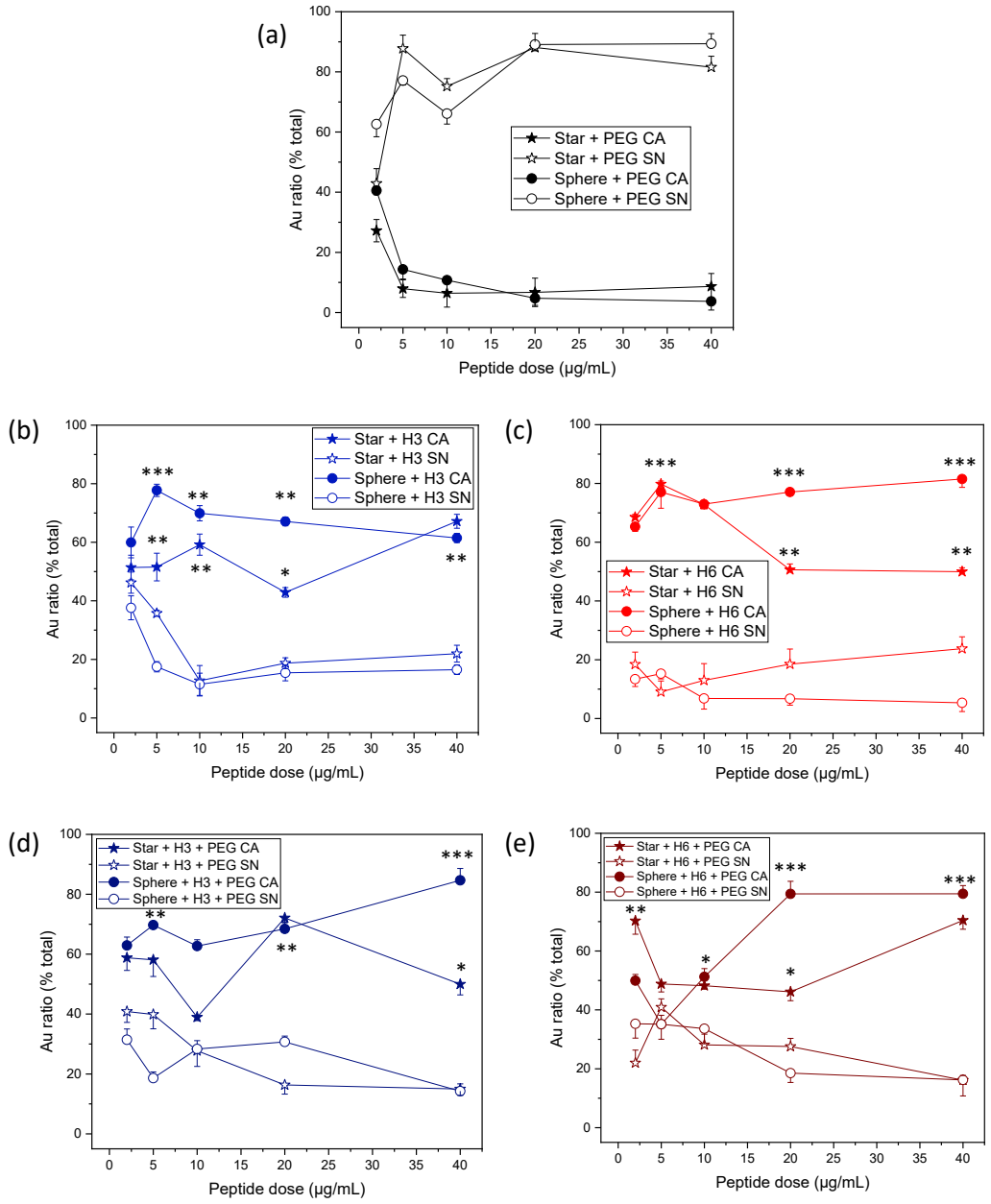


Figure 5.4 Cell association studies. Evaluating the N27 cell membrane binding/insertion properties of the two different drug delivery geometries, NS vs NP. In each graph, the ratio (%) of total gold content is shown detected in the cell - associated (CA) fraction or in the supernatant (SN) for the two nanostructure geometries. PEG only constructs (a). H3 only conjugated NS/NPs (b). H6 only conjugated NS/NPs (c). H3 + PEG conjugated NS/NPs (d). H6 + PEG conjugated NS/NPs (e). One - way ANOVA vs four independent experiments. Results are expressed as means ± SEM. *p < 0.05; **p < 0.01; ***p < 0.001. n = 3

Very limited particle + PEG was found to be cell associated (5 – 10%) (Figure 5.4, a), this would be due to PEG molecules having no specific neuronal membrane receptor site targeting expression. Whereas when compared to the H3/H6 – AuNS/AuNP that do express specific site targeting for the membrane bound ErbB receptors, there was a significant increase of Au found in the cell associated fractions (40-80%) (Figure 5.4, b-e). There was no significant difference found in the cell associated fractions when comparing the PEGylated and un - PEGylated H3/H6 AuNS/AuNPs, therefore the addition of the PEG molecules does not inhibit or enhance the H3/H6-functionalized AuNS/AuNPs from efficiently binding to the cell membranes.

Figure 5.5 is a summary of the cell binding behaviour of the AuNS/AuNP + H3/H6 +/- PEG constructs, in which the respective findings show that more than 50% of the H3/H6 AuNS/AuNPs fall within the cell associated fractions and the H3/H6 AuNS/AuNPs found in the supernatant was below the 40% mark.

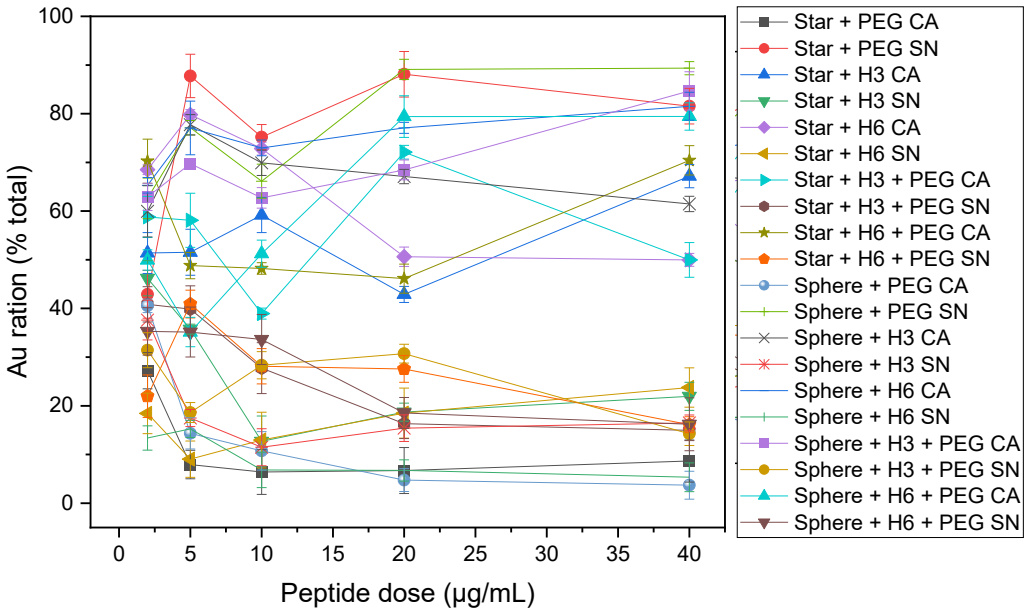


Figure 5.5 Cell binding activity of all peptide bound constructs, graphing both cell associated (CA) nano compounds and the nano structures found in the Supernatant (SN) after 24 hr cell treatment. Experiment formed in triplicate with the mean +/- SEM reported.

These results give a good indication for H3/H6 AuNS/AuNP neuronal interaction, however, as the cell associated values cannot differentiate between the particles inserting into the cells or are membrane associated only, clearer guidance was required.

Various electron microscopy protocols and techniques were trialled to gain a full understanding of whether the peptide compounds insert into the neuronal cells or stayed surface-bound. Cryogenic Transmission electron microscopy (cryo – TEM) (Figure 5.6) was first used with the aid of Professor Roland Fleck, and his team at Kings College London Centre for Ultrastructural Imaging, to study the interaction.

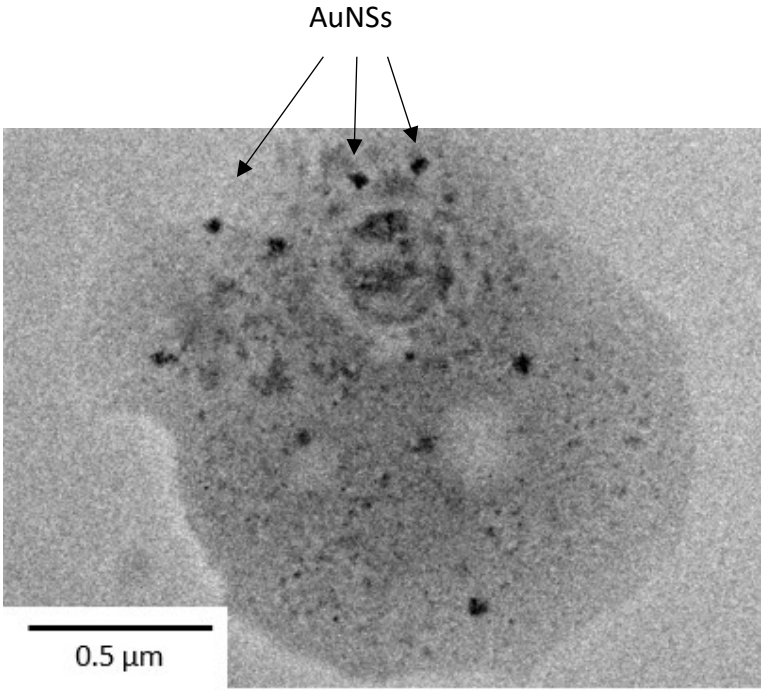


Figure 5.6 Immortalized dopaminergic neuron (N27), treated with H3 - AuNSs for 24 hrs at concentration 20 µg/mL. The cells were plunged into liquid nitrogen for fixation, then freeze dried for 24 hrs. Imaged using TEM operated at 200 kV. Image obtained in collaboration with Professor Roland Fleck, KCL.

N27 cells were grown directly onto Formvar - coated Au TEM grids and treated with the H3 - AuNS for 24 hrs. The grids were then plunged into liquid nitrogen to fix the cells then freeze dried for 24 hrs. Figure 5.6 provided a visual confirmation, obtained using TEM, of the H3 - NSs interacting with an N27 cell, however, the image is 2D and cannot unambiguously show that the NSs have become internalised; in addition the cell ultrastructure was poor. For this reason a focused ion beam scanning electron microscope (FIB – SEM) was used to image heavy metal stained cells to further examine the relationship between the nanostructures and hippocampal neurons (Figure 5.7).

The SEM images showed H3 - NS associated with the neuronal projections (Figure 5.7). The images gave preliminary evidence of two stages of neuronal – particle association. Figure 5.7, (a) demonstrates the particles embedded themselves into the neuronal membrane, while Figure 5.7, (b) shows surface associated/membrane bound nanostructures. However, it was difficult to pick out characteristic features of neurons in this data-set.

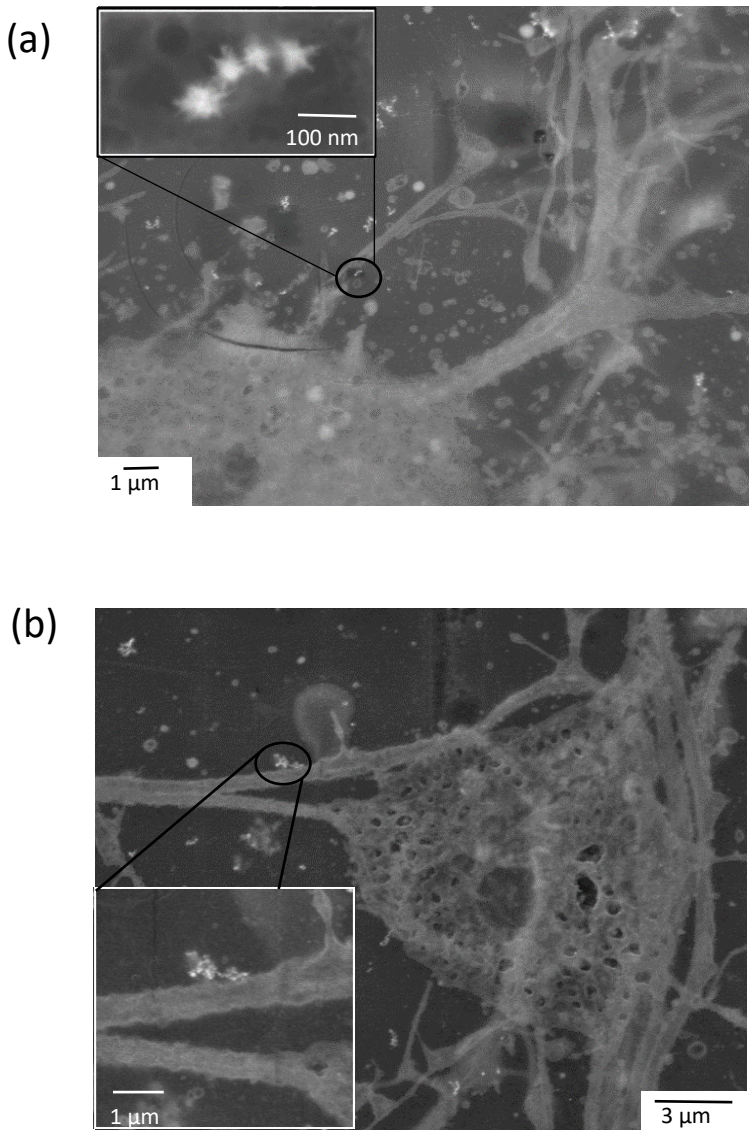


Figure 5.7 FIB – SEM images acquired at 10 kV *via* Auriga showing H3 - AuNSs interacting with the hippocampal neuronal network. Image (a) demonstrates nanostars embedded in the dendrite membrane of the neuron. Image (b) shows the nanostars are membrane bound.

The final analysis for the neuronal interaction study was performed in collaboration with Dr Pedro Machado, at the Centre for Ultrastructural Imaging, Kings College London.

Figure 5.8 reveals that the H6 - AuNS frequently associated with the neuronal membrane. The H6 - AuNSs were also internalised by the neurons and found in vesicle - like structures after 24hrs, although these events were also observed in the H6 – AuNPs, it was seen much less frequently (Figure 5.8, a, b).

To quantify the AuNP/AuNS neuronal interaction (Figure 5.8, b), a total of 33 NP + H3, 38 NP + H6 and 43 NS + H6 non-overlapping TEM images from multiple neurons were generated and examined for localization of each particle geometry, with the total number of AuNP/NS analysed n = 1000 - 1300 for each particle type. The nanostructures were assigned to four compartments: *extracellular* (not interacting with cell membranes), *membrane bound/surface associated* (interacting with the cell membranes without changes in membrane curvature, no embedding or piercing), *membrane embedded* (embedded into and/or piercing cell membranes) and *internalized* (detected within cells). AuNP/AuNS counts in each compartment were normalized to the total count for each particle type (set to 100%).

Unfortunately the AuNS + H3 samples were subjected to severe sample damage and were not viable for detailed analysis. This meant the H6 conjugated compounds were the focus of this next investigation to determine the effect or difference between the two nano structures (stars v spheres). H6 is a unique motif in the sequence of its parent protein, S100A4, and S100A4 has both extra - and intracellular receptor targets, and moreover, is internalized in several cell lines[40]. Previous literature has also showed that AuNS has a higher probability of binding to cell surface and/or internalization of cells due to their multi - spiked geometry[60,67].

Both the geometries (AuNP + H6/AuNS + H6) were quantified by intracellular distribution across the four compartments mentioned previously, (*extracellular*, *surface associated*, *membrane embedded* or *internalized*). Figure 5.8 b, confirms a significant difference between the volume of particles found extracellular and internalised fractions. 2 - fold more H6 - AuNPs than H6 - AuNSs were found in the extracellular space (77% vs 31%, respectively, Figure 5.8 b), *extracellular*). Significantly more H6 - AuNSs than H6 - AuNPs found internalised (36% vs 7%, respectively, Figure 5.8 b *internalized*). Moreover, when analysing the AuNS + H6 and AuNP + H6 separately, 31% of the AuNS + H6 were found extracellular, 36% were found internalized and 33% were found either membrane embedded or associated. Whereas, 74% of the AuNP + H6 were found extracellular, 7% were found internalized and 19% were found either membrane embedded or associated. Thus, overall suggesting that the drug delivery geometry does have an impact on neuronal interaction and inserting into the cells.

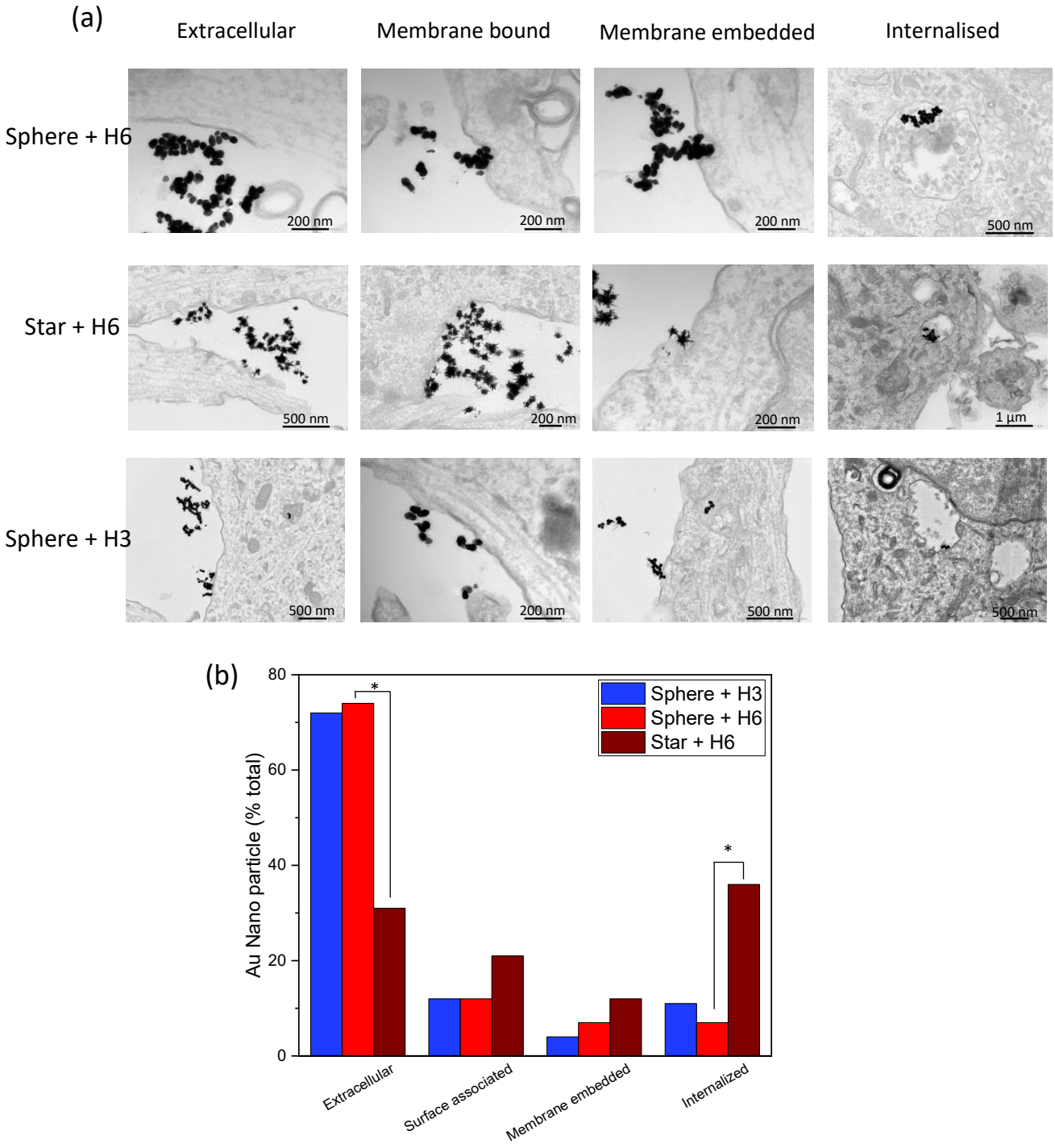


Figure 5.8 TEM micrograph images showing the interactions between the H3 and H6 NS/NPs and cultured hippocampal neurons (20 µg/mL) (A). (B) Quantification of AuNP/AuNS distribution across cell compartments. Total number of NSs and NPs analysed: H6 NPs, n = 1291; H6 NSs, n = 1260; H3 NPs, n = 1041. AuNP/AuNS counts in each compartment are normalized to the total AuNP/AuNS count for each particle type (set to 100%). One - way ANOVA Star + H6 vs Sphere + H6 particles found internalised and extracellular *p < 0.05. Images obtained in collaboration with Dr Pedro Machado, Centre for Ultrastructural Imaging, Kings College London.

5.4 Discussion

5.4.1 Biological effects of the peptide bound Nano – Neuro therapeutics

After the successful conjugation of the peptides to the delivery vehicles (NPs/NSs), it was necessary to examine whether these novel nano - neuro therapeutics would still exhibit the same neuroprotective effects as previously described[6, 8, 43]. The H3 nano compounds actively protected neurons against oxidative stress and against cytotoxicity induced by Parkinson's (PD) toxins. However, the H3 - AuNS were more potent in the oxidative stress model than the spherical H3 - AuNPs.

The H3/H6 nanostructures also interacted with and promoted neurite extension in hippocampal neurons, however, the neuritogenic effect of the nanostars was markedly higher. In particular, H3/H6 - AuNS had a potency and efficacy similar to those of unconjugated peptides being 1.5 - 2 times more efficient than spherical nano formulations. This could be explained by the enhanced AuNS - neuronal surface interaction/insertion compared to the AuNPs, resulting both in a strong activation of neuritogenic signalling and in a robust neurite adhesion to the substrate. Additionally, interaction of AuNS with plasma membranes is known to induce a slight increase of neuronal electrical activity[93] and, thus, local Ca^{2+} 'hotspots', which can promote neurite extension.

Both neuroprotection and neurite outgrowth results were conclusive of previous findings by Dmytriyeva *et al.* Moldovan *et al.* and Pankratova *et al*. that confirms that H3 and H6 launch multiple neuroprotective pathways by activating plasma membrane receptors such as ErbB[43] and/or preventing toxin - induced plasma membrane disruption. The data presented in this work has also provided evidence to show that there was no detriment to the peptide activity when bound to the delivery nanostructures. The addition of the optional PEGylation to increase compound half – life, also did not affect the neurotrophic properties of either of the peptide targeted nanostructures, thus suggesting the PEGylation of the compounds adds a useful option for increasing the compound half - life and circulation time *in vivo*.

5.4.2 Effect of particle geometry on drug delivery

It was hypothesised, that the stars should improve the peptide efficacy of either the H3 or H6 peptide as they activate when in contact with the neuronal membrane receptors, therefore, the spikes on the star would be more effective in the tight intercalated neuronal network as the spikes can branch through and contact more neurons than the spheres in their 'ball like' morphology. However, the spikes could also potentially penetrate through the plasma membrane and deliver the peptide into the neuronal cytoplasm. Although delivery directly inside the cytoplasm is not necessary for neurotrophic effects of the peptides, it could be more effective.

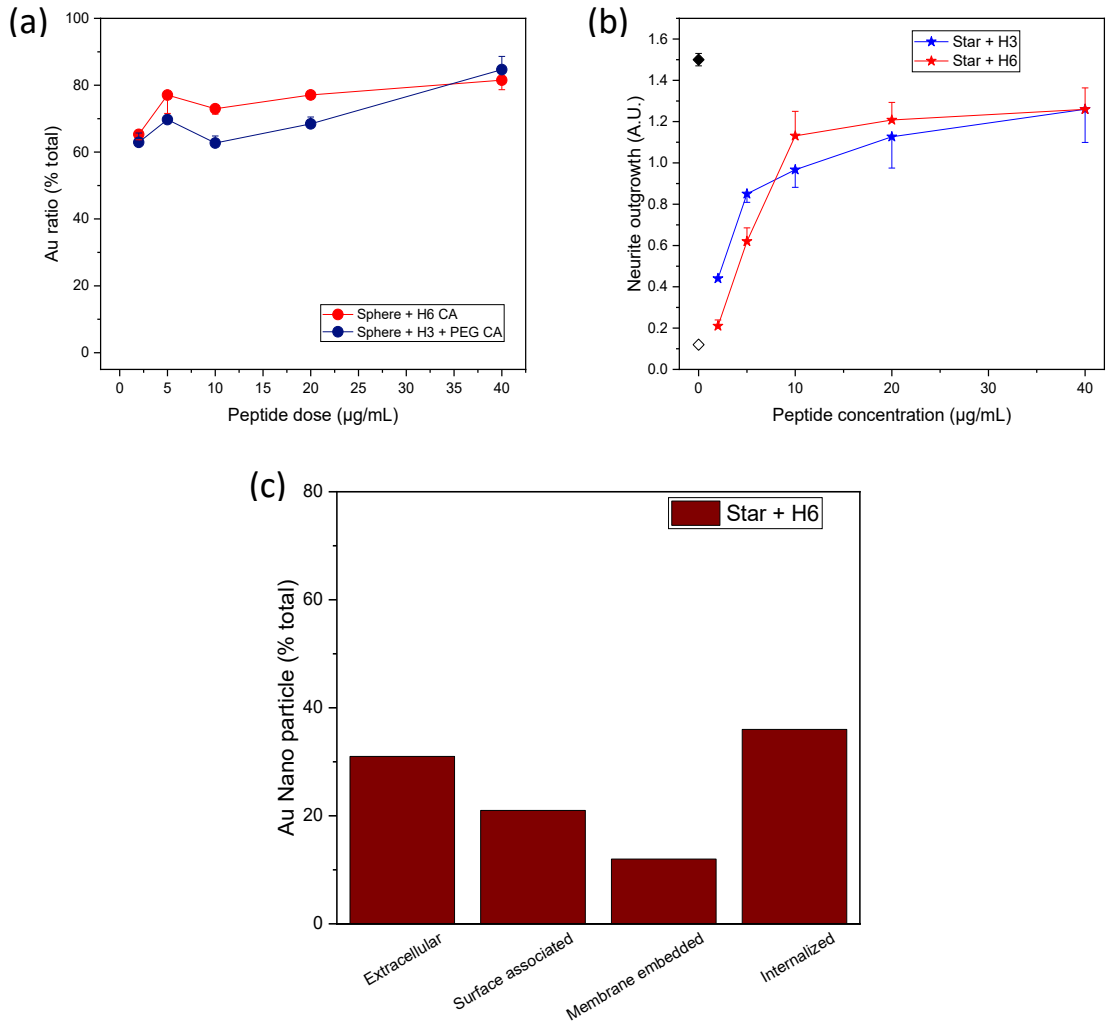


Figure 5.9 Summary of the best performing nano structure for drug delivery. (a) Demonstrates the AuNPs + H3/H6 were the better performing structure in the cell association studies *via* ICP analysis. (b) AuNS + H3/H6 were the best performing delivery system for neurite outgrowth. (c) Demonstrates the NSs as the better performing structure in the neuronal interaction studies *via* TEM analysis.

Figure 5.9 highlights the best performing nano structures to determine the most effective geometry for delivering the novel therapeutic peptides to the brain. Comparison of the H3/H6 – NP/NSs indicated that they were not significantly toxic to the hippocampal neurons or the N27s. As only the H3 peptide was analysed in the neuroprotection assay, only effects of geometry (spherical vs. star shaped) can be compared. The results confirmed that neither of the constructs (stars/spheres) inhibited the neurotrophic actions of the peptide, however, the stars were more potent for neuronal survival than the spheres and the addition of the PEG molecules had no impact. The neurite outgrowth data (Figure 5.9 b) also supports the finding that the star shaped nanostructures were optimal in the stimulation of neuronal projections This correlates with the quantitative TEM analysis (Figure 5.9 c) suggesting that the star structure efficiently interacts with cell membranes with a higher affinity of membrane binding/insertion than nanospheres and thus, exerting the neurotrophic effects of the peptides on a wider scale, and so proving the initial hypothesis to be true.

In contrast, quantification of cell compartmentalisation of each nanostructures by ICP - OES (Figure 5.9 a) gave evidence that the spheres had the optimal morphology for neuronal interaction. However, there was no significant difference between the NS and NPs.

Another important aspect to take into consideration when comparing the nano structures, is the drug per dose. The H3/H6 only bound nanostars and nano spheres equally administered the same Au content per peptide dose. However, when PEGylated, there was a drastic difference between AuNS + H3/H6 + PEG and AuNP + H3/H6 + PEG. The nano spheres could not be effectively functionalised and for this reason, it is suggested that the PEG molecules in some way removed or replaced the peptide molecules from the nano structure, resulting in less peptide molecules immobilized on the surface of the spherical structures compared with the PEGylated stars of the same Au mass, which leads to more Au particles required to achieve the equal peptide dose. The nano stars, however, did perform optimally when PEGylated. In this case, there were no signs or evidence that the PEG competed with, removed or replaced the peptide and the Au content per dose was lowest, effectively making the NS + peptide + PEG formulation the best performing neuroprotective nanostructure.

It was noted that the H6 - conjugated nano constructs (stars and spheres) demonstrated a higher degree of time - dependent aggregation in the stock solutions, culture medium and through experimentation than the H3 - based formulations. The H6 was difficult

to functionalise onto the nano particles both in the presence and absence of PEG because of this aggregation. This may, in part be due to the differing amino acid sequence of the peptides and the fundamental differences in the peptides' origins. H6 is a "unique" motif in the S100A4 sequence with little homology to other S100 proteins, that can be seen in the structure itself, as more linear. Whereas the H3 is a "common" motif for many S100 proteins demonstrating a more coiled structure mimicking more of the S100A4 structural format[35]. This finding advocates that the H3 neuro – therapeutic peptide as the optimal drug to further functionalise future *in vivo* studies.

5.5 Conclusions

In conclusion, the findings presented in this research suggest that the nanostars have advantages over spherical shaped NPs, by improving the potency and efficacy of the neurogenic cargo drugs (H3/H6). This multifactorial neuroprotection may be an important advantage for future translational studies providing therapeutic effects in a wide window of pathological conditions. In combination with the neurotrophic peptides, nanostars hold promise as a novel theranostic platform with multiple functions, such as neuroprotection, delivery of high drug loads across the BBB, and bio imaging capability.

This novel NS - peptide platform has the potential to act as both a versatile neuro - protectant and also as a technology to improve the efficiency for neuronal targeting small molecule drugs that cannot cross the BBB unaided, which may lead to a great change in the treatment of neurological diseases.

6 Fabricating and Optimising Au Nano Stars for Blood Brain Barrier Crossing *via* L - dopa LAT1 Trans membrane Protein

6.1 Introduction

The Blood Brain Barrier (BBB) is a term used to describe the unique properties of the microvasculature barrier formed by capillary endothelial cells surrounding the central nervous system (CNS). These vessels tightly regulate the movement of molecules, ions, and cells between the blood and the CNS. The BBB endothelial cells tightly regulate CNS homeostasis which allows healthy neuronal function and restricts toxins and pathogens from entering the brain and thus limiting neuronal inflammation, injury, and disease. However, this tightly controlled barrier also inhibits drug delivery to the brain, so the ability to treat neurological disorders is challenging[130]. The need for new technologies to modulate or bypass the BBB for delivery of therapeutics is of paramount importance.

Current dopamine replacement therapies, such as Levodopa (L - dopa) are currently the most popular forms of Parkinson's disease (PD) treatment, as they have the ability to improve motor functions by controlling the symptoms of the disease, in particular the slow movements and stiff, rigid body parts that inhibit the everyday life for PD patients. However, levodopa has major shortcomings as it is short acting and only treats the disease symptoms, having no impact on preventing or slowing the disease progression. Therefore, it is necessary to design a successful particle to shuttle drugs across the BBB and target the neurons that would have a major impact on treatment prognosis and quality of life for PD patients.

Au nanomaterials are biocompatible and therefore constitute a highly attractive option for various theranostic applications. The two most researched methods of shuttling nanomaterials across the BBB are *via* BBB receptor mediated transcytosis (insulin, transferrin) or the use of transport proteins (glucose, amino acids, i.e. LAT 1). AuNPs functionalised with transferrin[103, 111], glucose[112] and insulin[54] have demonstrated effective *in vitro* and *in vivo* penetration of the BBB, however, each of these methods bought potential unwanted

inadequacies, such as the lack of brain specificity and unwanted accumulation in peripheral organs which could lead to off – target side effects.

Functional groups, which can target both the BBB and neurons are highly sought after as a highly effective approach for drug delivery. The large amino acid (LAT - 1) transporter transports large neutral amino acids with bulky or branched side chains across the BBB and is physiologically expressed at the BBB[113]. The LAT - 1 transporter has a much higher affinity for amino acids at the BBB, than in peripheral tissues, and so is a highly promising target to cargo NPs across the BBB. The LAT - 1 transporter is also used to deliver dopamine replacement therapies, such as L - dopa inside the dopaminergic neurons *via* the dopamine active transporter to treat PD symptoms[113, 114].

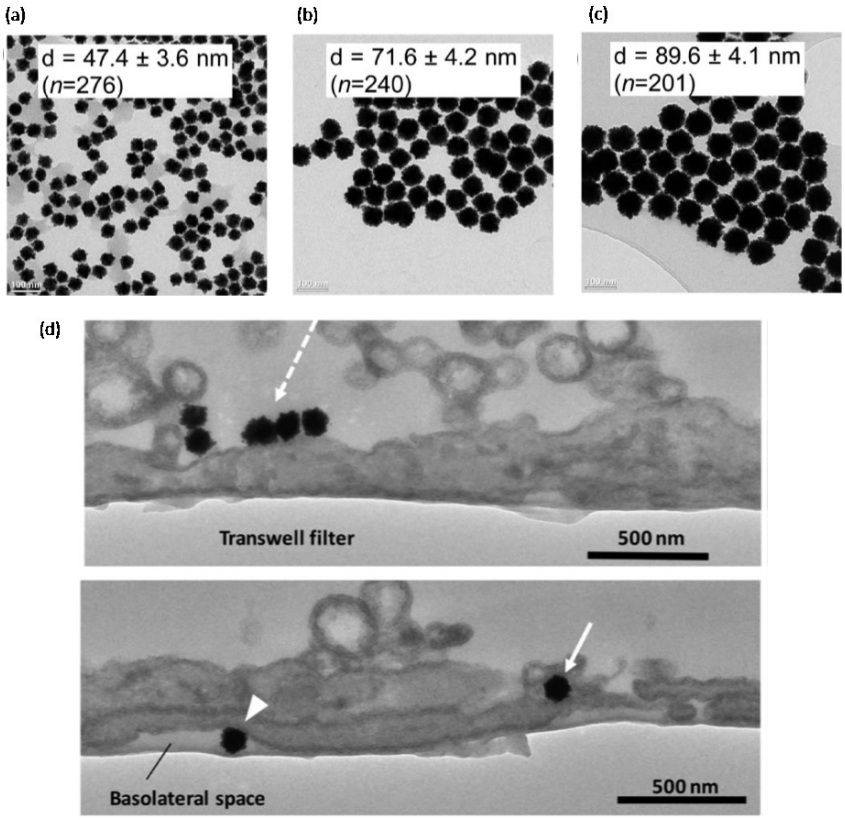


Figure 6.1 TEM micrograph displaying successful synthesis of L - dopa nano flowers (AuNFs) by the Porter group[59, 60]. Use of 4 mL of 15 mM L - dopa and varying the volume of 0.1 M $HAuCL_4$ (12.5 µL (a), 50 µL (b), 100 µL (c)) allowed chemical control of the particle size. (d) TEM images confirming transport of L - dopa gold nanoflowers (AuNF) across BBB endothelial *via* LAT - 1 transporter protein using *in vitro* primary brain endothelial cells. Images adapted from Zhan Yuin Ong *et al*[59].

Recent research has indicated that the large amino acid (LAT - 1) transporter can efficiently transport gold nano flowers (AuNFs) functionalised with L - dopa across the BBB *in vitro*[60] (Figure 6.1). However a limitation of the synthesis protocol was that the AuNS were more "flower-like" than "star-shaped", i.e. the spikes were not well pronounced, which could significantly influence their interaction with cells and ability to enhance fluorescence for imaging. In addition it was difficult to tailor their shape, size or the amount of functional groups and they could not be post - functionalised with H3/H6 peptides as a one - pot synthesis was used. Recent research has also demonstrated a correlation between spike length and transcytosis across the BBB (Figure 6.2)[67].

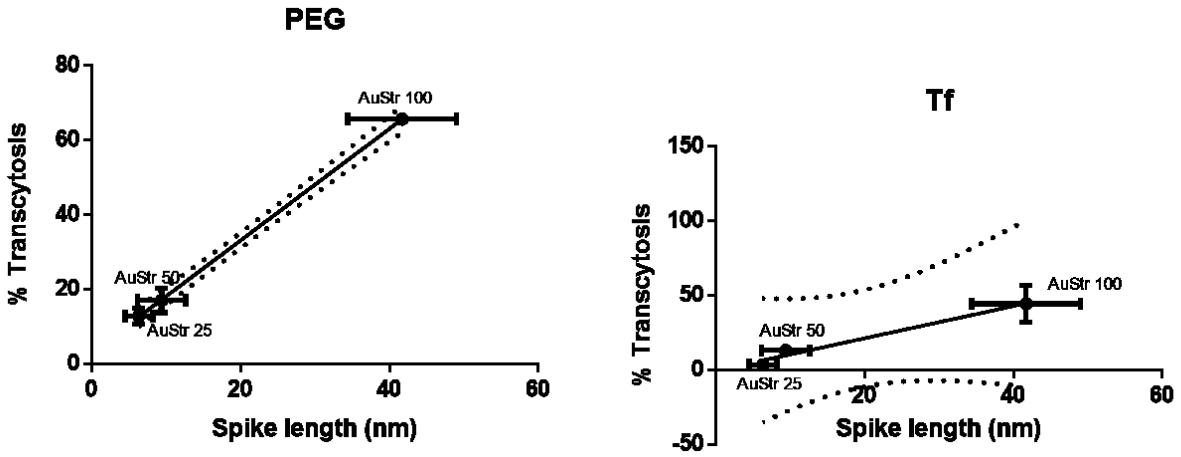


Figure 6.2 Transcytosis of AuNS by diameter for PEGylated (left) and Transferrin (Tf) coated nanostructures (right). Results showed that D3 cell crossing increases linearly with spike length. Image adapted from Rodrigues *et al*[67].

As the blood brain barrier (BBB) is semi permeable, it is, in turn, semi selective in what molecules/ions can pass into the brain parenchyma, so there are very few ways in which particles can cross the BBB. The overall objective of this chapter was to synthesise and further develop the AuNF into AuNS vectors functionalised with L - dopa to shuttle the novel neuroprotective drugs H3 and H6 across the BBB. The target diameter of 50 nm was previously chosen as past and present literature has demonstrated 50 nm to be the optimal size NS to enable effective drug loading and the enhanced BBB transcytosis allowing delivery of drugs across the BBB and inside the brain[14, 54, 67, 102, 103, 111, 112]. This study has shown the

synthesis protocol was successfully optimised to generate a platform technology with the flexibility to tune the geometry of the AuNS and to allow post – functionalisation of the particles with other molecules such as the H3/H6 peptides and fluorescent dyes to impart additional imaging capabilities such as the conjugation of a fluorescent dye for deep tissue imaging in the NIR2 range.

6.2 Methods

Nano star synthesis

First, spherical citrate - stabilized gold (Au) nano seeds were synthesised using a Turkevich method of citrate reduction[5]. Following and modifying the protocol described by Yuan *et al*, 2012[2], solutions of sodium citrate were prepared by dissolving 0.3 g (3% (w/v)) tri - sodium citrate in 10 mL of deionised water by bath sonication. 10 mM $HAuCl_4 \cdot 3H_2O$ was prepared by dissolving 0.394 g of gold(lll) chloride trihydrate in 100 mL deionised water, then stored light protected at 4 ^{0}C. In an aqua regia (AR) cleaned 250 mL Erlenmeyer flasks with a 1 - inch stir bar, 48.75 mL of ultra - deionised water and 1.25 mL of the 10 mM $HAuCL_4$ solution was added and bought to the boil. At boiling point, 1 mL of 3% (w/v) sodium citrate solution was added whilst under vigorous stirring until the solution had changed colour to red. At this point, the colloidal solution was quickly cooled, washed by centrifugation three times then stored at 4^{0}C light protected. These nano seeds were then used to form the nano stars.

Yuan *et al*, 2012[2] protocol was followed for the subsequent synthesis of the gold nanostars. A 10 mL acidified 0.1 mM $HAuCl_4 \cdot 3H_2O$ solution was prepared by adding 100 µL of 10 mM $HAuCl_4$, 10 µL of 1 M HCL and 9890 µL of deionised water into a vial, placed under moderate stirring at room temperature (RT). 200 µL of the L - dopa Au seeds were then added, then quickly followed with 100 µL of 3 mM $AgNO_3$ and 50 µL of 100 mM ascorbic acid. The color of the solution changed from faint red to blue as soon as the ascorbic acid was added, which indicated the nano stars had formed and the synthesis was complete. Whilst till stirring 125 µL of 1 mM of Polyethylene glycol (PEG) was added after completion of synthesis to

stabilise the nanostars. They were then washed three times by centrifugation, and stored at 4^{o}C light protected.

6.2.1 L - dopa Functionalized nanostars

L – dopa

15 mM 3,4-Dihydroxy-L-phenylalanine (L - dopa) solution was prepared by dissolving 0.06 g of L - dopa in 20 mL ultra - pure deionised water by bath sonication at room temperature.

Substituting Ascorbic acid for L - dopa to form nanostars

To make the nano stars via substituting the reducing agent ascorbic acid for L - dopa, A 10 mL acidified 0.1 mM $HAuCl_4 \cdot 3H_2O$ solution was prepared by adding Varying volumes of 10 mM $HAuCl_4$, 10 µL of 1 M HCL and 9890 µL of deionised water into a vial and placed under moderate stirring at room temperature (RT). Varying volumes of the nano seeds were then added, then quickly followed with 100 µL of 3 mM $AgNO_3$ and varying volumes of 15 mM L - dopa, (refer to table 6.1 Below). The color of the solution changed from faint red to blue as soon as all the ingredients was added, this indicated the nano stars had formed and the synthesis was complete. Whilst till stirring 125 µL of 1 mM of PEG was added after completion of synthesis to stabilise the nanostars. They were then washed three times by centrifugation, and stored at 4^{o}C light protected.

Synthesis	*Volume of $HAuCl_4$ (µL)*	*Volume of 3% nano seeds (µL)*	*Volume of 15 mM L - dopa (µL)*	*Volume of 3 mM $AgNO_3$ (µL)*
A	12.5	200	200	100
B	50	200	300	100
C	100	200	150	100
D	200	200	150	100
E	100	100	150	100
F	200	100	150	100

Table 6.1 Table showing the varying volumes of the synthesis components to produce L - dopa functionalised nano stars

L - dopa Nano seed synthesis and star formation

Spherical L – dopa - stabilized gold (Au) nanoparticles were synthesized in an AR cleaned 250 mL Erlenmeyer flask. A 1 - inch stir bar was added to 48.75 mL of ultra - deionised water and 1.25 mL of the 10 mM $HAuCL_4$ solution and bought to the boil. At boiling point, 1.25 mL 15 mM L - dopa solution was added whilst under vigorous stirring until the solution had changed colour to a blueish colour. At this point, the colloidal solution was quickly cooled and washed by centrifugation three times. These L - dopa NPs were then grown into AuNSs by the Nano star synthesis seed mediated growth method mentioned above, then washed by centrifugation three times then stored at 4^0C and light protected

L - dopa capped nanostars

Principle of this synthesis was to use the L - dopa to stabilize the nano stars, but also, the L - dopa attached to the outside of the nano structure would allow post functionalisation of the nano stars to further incorporate the H3 and H6 peptides.

The 12 nm nano seeds were prepared as stated above. Following the nano seed synthesis, the nano stars were formed by adding 10 mL acidified 0.1 mM $HAuCl_4$ solution into a glass vile and moderately stirred. The solution was prepared by adding 100 µL of 10 mM $HAuCl_4$ and 10 µL of 1 M HCL into 9890 µL of deionised water. 200 µL of the 12 - nm Au seeds were then added, then quickly followed with 100 µL of 3 mM $AgNO_3$ and 50 µL of 100 mM ascorbic acid. The color of the solution changed from faint red to blue as soon as the ascorbic acid was added, this indicated that the nano stars had formed and the synthesis was complete. Whilst till stirring varying volumes of 15 mM L - dopa was added after completion of synthesis to stabilise the nanostars, (see table 6.2 below).

Synthesis	*Volume of 15 mM L - dopa*
A	100 µL
B	250 µL
C	500 µL
D	1 mL
E	2 mL

Table 6.2 Table showing the volume of L - dopa trialled to stabilise the nanostars per synthesis.

Functionalising the nanostars via EDC/NHS coupling of L - dopa to PEG

Functionalising the nano stars with L - dopa *via* EDC/NHS chemical coupling, would also mean post – functionalisation would be possible and the L - dopa is at the best placement on the nano stars for LAT1 recognition and BBB crossing.

Nano star synthesis

The 12 nm nano seeds were prepared as described above. Following the nano seed synthesis, the nano stars were formed by adding 10 mL acidified 0.1 mM $HAuCl_4$ solution into a glass vile and moderately stirred. The solution was prepared by adding 100 µL of 10 mM $HAuCl_4$ and 10 µL of 1 M HCL into 9890 µL of deionised water. 200 µL of the 12 - nm Au seeds were then added, then quickly followed with 100 µL of 3 mM $AgNO_3$ and 50 µL of 100 mM ascorbic acid. The color of the solution changed from faint red to blue as soon as the ascorbic acid was added, this indicated the nano stars had formed and the synthesis was complete. 125 µL of 1 mM PEG was used to stabilize the nano stars, then washed three times by centrifugation.

EDC/NHS coupling of L - dopa to PEG

The process of EDC/NHS coupling works by EDC activating carboxyl groups (—COOH) for direct reaction with primary amines (—NH_2) via amide bond formation. The N-hydroxysulfosuccinimide (Sulfo - NHS) aids in controlling and modifying the carbodiimide crosslinking reactions that involves the activation of carboxylates (—COOH) and primary amine (—NH_2) binding. For the purpose of this experiment, the – COOH group on the PEG that was activated to bind to the – NH_2 group on the L - dopa, as the PEG did not contain the amine group.

For the EDC/NHS coupling to be effective, there needed to be enough moles of EDC to activate the carboxyl group (-COOH) group on the PEG, therefore, the EDC was in 10 - fold excess to the PEG.

The EDC : Sulfo - NHS ratio used was 1 : 1.5. Then for every one mole of PEG there were equal moles of L - dopa.

Once the nano stars were synthesised, stabilised with 1 mM PEG and washed, the nanostars were re - suspended in 10 mL of 0.1 M 2-(N-Morpholino)ethanesulfonic acid (MES) buffer, pH 4.7. 10 mM EDC was made up in either ultra - pure deionised water, or in MES buffer with a pH of either 4.7 or 7, with 125 µL of either added to the solution (see table 6.3 below). 125 µL of 14 mM Sulfo - NHS was then added to aid in the carboxyl group activation and was left to stir at room temp for 15 minutes. The nanostars were then washed three times by centrifugation to remove the excess EDC/NHS, so that it cannot activate the carboxyl group on the L - dopa molecules. The nanostars were re - suspended in 3 mL 0.1 M MES at either pH 7 or 4.5 (see table 6.3 below) and 125 µL 1 mM L - dopa was added and left to stir at room temperature for two hours to allow the carboxyl - amine binding. They were then washed three times by centrifugation, and stored at 4^{o}C light protected.

Sample	*EDC*	*Re-suspended in MES pH*
1	MES pH 4.7	4.7
2	MES pH 7	4.7
3	H2O	4.7
4	MES pH 4.7	7
5	MES pH 7	7
6	H2O	7

Table 6.3 showing the different modifications trialled during the six different variations used to couple the L - dopa to PEG *via* EDC/NHS chemistry.

6.2.2 Characterisation of the L - dopa fabricated nanostars

Transmission Electron Microscopy (TEM)

The morphological features of each of the nanostructures was examined by transmission electron microscopy (TEM). 50 µL of sample solution was dropped onto holey carbon 300 mesh Cu TEM grids and left to dry at room temperature. High resolution TEM was performed using Jeol 2100 F plus or the Joel 2100 +, operated at 200 kV.

X-ray Photoelectron Spectroscopy (XPS)

Gold nanoparticles and their binding to PEG and L - dopa were investigated using X - ray Photoelectron Spectroscopy (XPS). Survey and core level spectra were recorded on a Thermo Scientific K-Alpha+ XPS system using its monochromated, microfocused Al K_α X-ray source (hv= 1486.7 eV). The base pressure was 2×10^{-9} mbar base pressure and an X-ray spot size of 400 µm was used. Data were collected at 200 eV pass energy for survey and 20 eV pass energy for core level spectra. The nanoparticles were dropcast onto Si wafer substrates (Si/SiO_2) which were mounted on the sample holder using conducting carbon tape. A flood gun was used to minimize sample charging throughout. All data were analysed using the Avantage software package and for peak fit analysis, Voigt functions with Shirley-type backgrounds were used.

6.2.3 Statistics

The TEM images presented in this chapter and the statistical analysis performed on the particles were obtained by visual analysis and measured using ImageJ. Several Au nano spheres and nano stars were analysed from a minimum of three separate samples prepared under identical conditions.

6.3 Results

6.3.1 L - dopa

The L - dopa molecule consists of an amine functional group (NH_2), carboxylic functional group (COOH-) and a catechol group, that is an organic chemical compound where two hydroxyl groups are substituted onto a benzene ring, depicted in Figure 6.2 below. Previous studies have shown that the positively charged amine group of the L - dopa has a tendency to adsorb onto the negatively charged AuNPs that results in the catechol group attaching onto the Au particle surface. The catechol group has also shown to facilitate the nucleation of gold to form the NPs themselves, dependent of synthesis method utilized[20, 106, 107, 108].

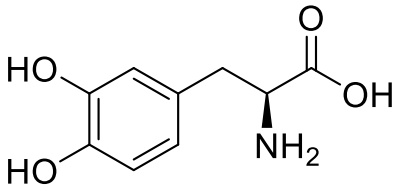


Figure 6.3 Schematic displaying the chemical structure of L - dopa

Several mechanisms have been proposed to explain how L - dopa shuttles nano particles across the BBB. These principally suggest that one or both the functional groups (amine/carboxyl) function jointly or in tandem. Past research has confirmed L - dopa can aid in delivering NPs across the BBB however, the exact mechanisms by how L - dopa shuttles particles across the BBB remains undefined, although it is suggested that this process occurs *via* the LAT 1 transmembrane protein[20, 106, 107, 108].

6.3.2 Nano Star synthesis

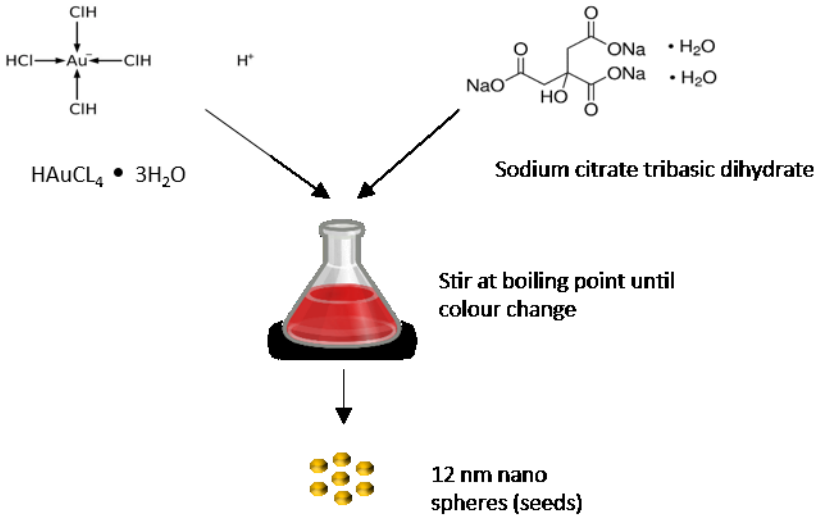


Figure 6.4 Schematic diagram demonstrating the synthesis procedure used to produce 12 nm seeds. 3% sodium citrate was used to reduce the oxidised $HAuCL_4$ to form bulk gold particles with a mean diameter of 12 nm.

Figure 6.4 and Figure 6.5 provide a schematic overview of the nano seed synthesis (Figure 6.4) and nano star synthesis (Figure 6.5), optimised in chapter one of this study and used throughout this research. These schematics provide a visual benchmark for understanding how and where future chemical manipulation in this study took place to form and optimise the L - dopa functionalised nano stars.

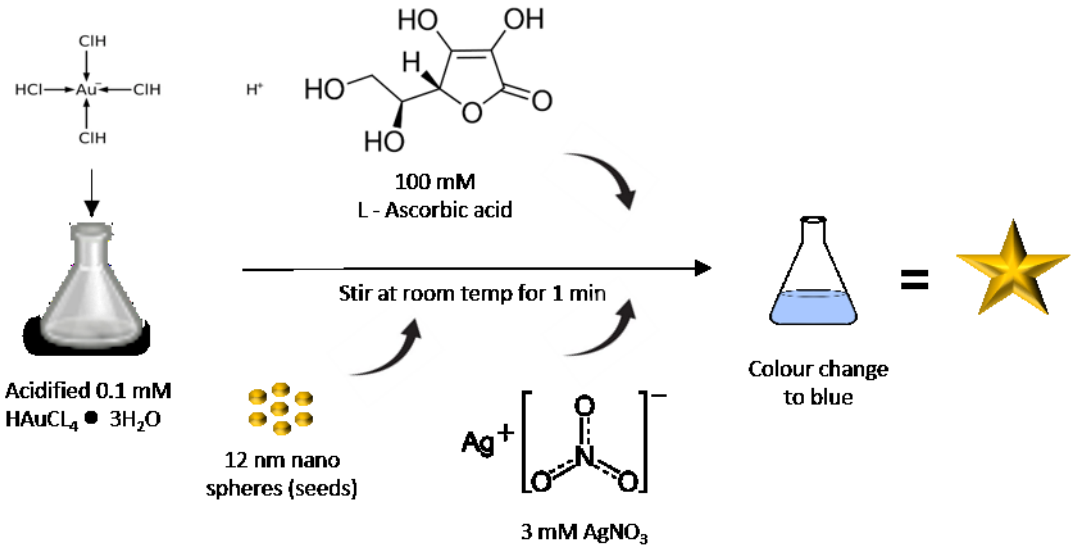


Figure 6.5 Schematic diagram demonstrating the chemical synthesis procedure used to produce the 50 nm stars. 12 nm nano seeds were grown into stars *via* seed mediated growth by the addition of 100 mM L - Ascorbic acid and 3 mM silver nitrate, stabilized with 1 mM PEG.

6.3.3 L - dopa functionalised Nano Stars

6.3.3.1 Substituting Ascorbic Acid for L - dopa functionalization.

TEM images of the successful L - dopa functionalised gold nano flowers (AuNFs) synthesised by Gonzalez-Carter *et al* are shown in Figure 6.1. The wet chemistry approach of substituting the L - ascorbic acid for L – dopa allowed the catechol functional group of the L - dopa to efficiently reduce the Au^{3+} to Au^{0} on the surface of gold seeds and adsorb onto the surface of the AuNFs[60]. The schematic diagram of this synthesis can be seen below in Figure 6.6 and thus provides the starting point for the optimisation of the L - dopa functionalisation route used in this chapter.

Figure 6.6 provides a schematic overview of the synthesis and specific elements that were adapted from the AuNS synthesised in chapter four (shown in Figure 6.5) to produce L - dopa reduced nano stars.

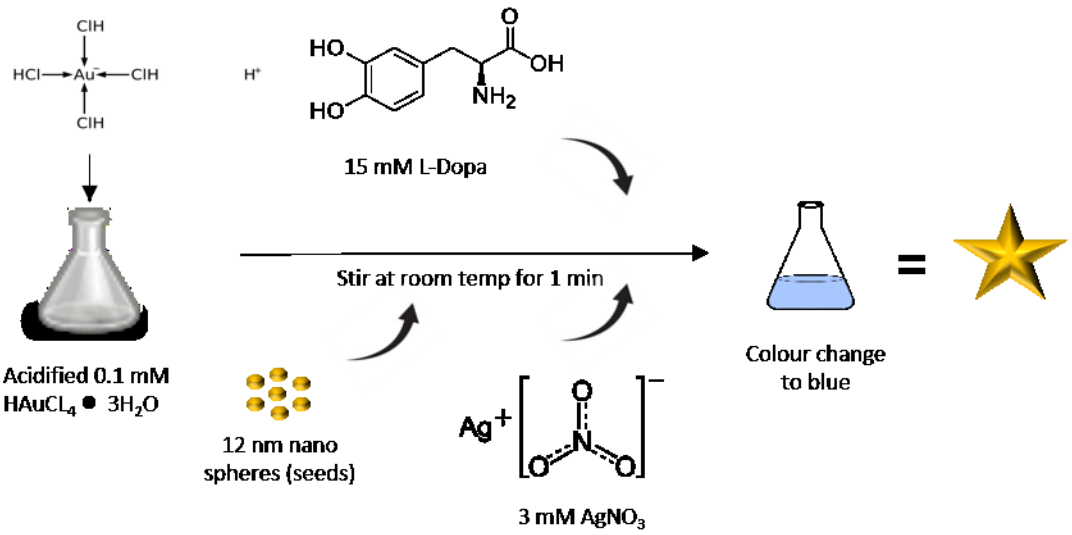


Figure 6.6 Schematic Diagram displaying the substitution of reducing agents - 100 mM L - ascorbic acid for 15 mM L - dopa to form the 50 nm nano stars. The molarity of silver nitrate (3 mM) was kept the same to enable the formation of the branch like structures. The stars were stabilised with 1 mM PEG.

Various chemical manipulations were trialled to develop the L - dopa reduced nano stars (Figure 6.7). The volumes of 12 nm nano seeds, 10 mM $HAuCL_4$ and 15 mM L - dopa were all subjected to modification in these trials. The first attempt at synthesis was to make only minor changes to the AuNF protocol and work on extending the flower - like projections into spike - like projections.

Testing the 15 mM L - dopa at a volume of at least 200 µL reduced the particles to a diameter of ~ 50 nm size; there were signs of branch like features trying to form, but the overall morphology was more similar to the AuNFs than AuNSs (Figure 6.7 a, b). An excess of nano seeds did not undergo seed mediated growth into nano stars (Figure 6.7, b), which could possibly have been due to the ratio of $HAuCl_4$: L - dopa 100 µL : 300 µL respectively, (Figure 6.7 b) vs 100 µL : 200 µL respectively (Figure 6.7 a) leaving an excess of L - dopa and not enough $HAuCl_4$ to reduce onto the seeds to enable the growth.

Therefore, the next trial decreased the volume of L - dopa (Figure 6.7 c). Reducing the volume of L - dopa interestingly caused mass aggregation of the gold particles forming around

150 – 200 nm in diameter with very little resemblance to stars or spheres. By only halving the L - dopa volume from 300 µL (Figure 6.7 b) to 150 µL (Figure 6.7 c) produced an extreme undesirable aggregation effect, so the next step was to increase the $HAuCl_4$ volume for the L - dopa to chemically reduce onto the individual stars and thus, reduce the mass aggregation of the particles binding together (Figure 6.7 d).

The images in Figure 6.7 d show the nano structures formed were less aggregated than those in Figure 6.6 c, with an average diameter of 100 – 150 nm in diameter. However, nano spheres of approximately 50 nm in diameter were observed to form, which suggests the L - dopa may have reduced the excess gold to form spherical nano particles instead of being utilised for seed mediated growth of the 12 nm nano seeds in to stars. It could be argued that the $AgNO_3$ should have been re - trialled in this investigation alongside the other chemical elements, however, chapter 4 established the optimal volume/concentration of silver nitrate to form the desired star like nano structure, so the current investigation continued with the change in reducing agents. The final trial was to reduce the quantity of the nano seeds going into the solution (Figure 6.7 e, f). The volume of 12 nm nano seeds were halved to 100 µL in an attempt to reduce the aggregation seen in the previous trials. Reducing the volume of nano seeds also sought to reduce the surplus of seeds and potentially prevent the seeds from developing into larger NPs instead of NSs. Figure 6.7 e and f confirm that reducing the volume of seeds was successful, demonstrating very little, if any surplus of NPs.

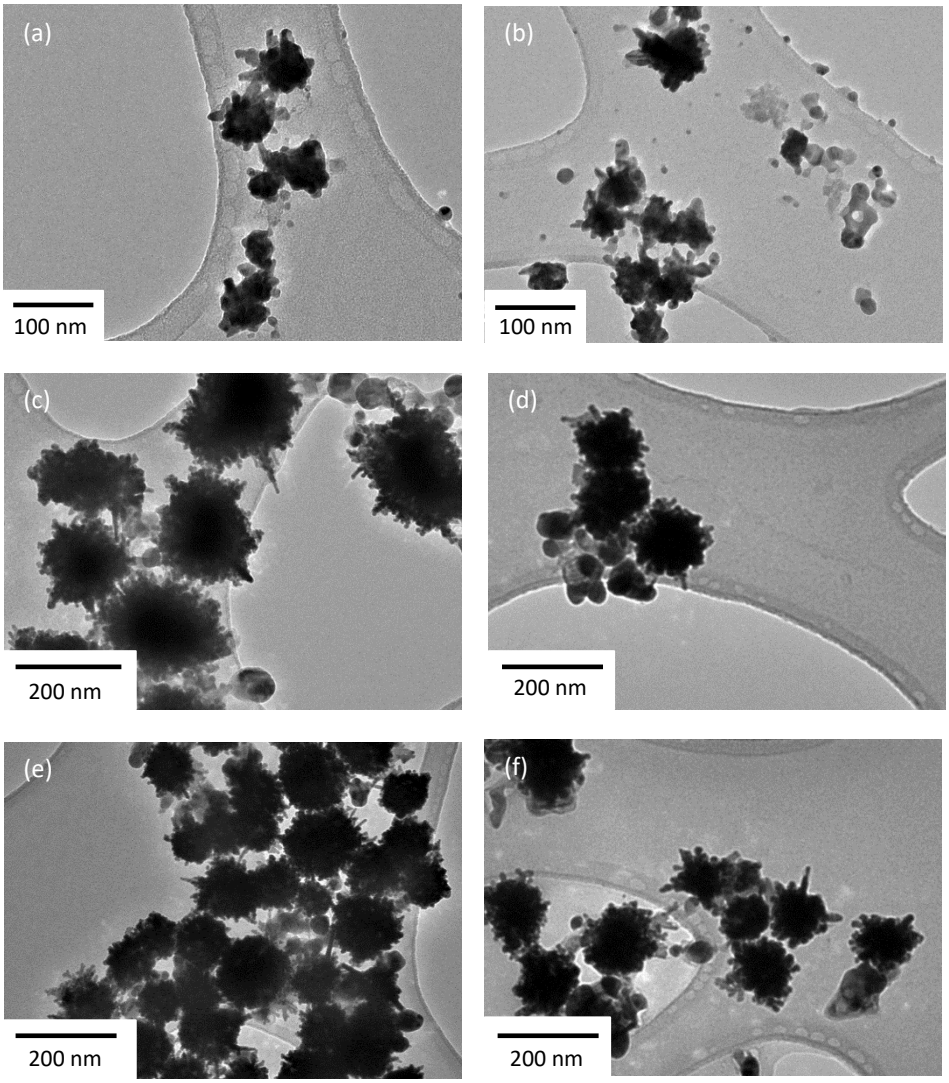


Figure 6.7 TEM micrograph images of L - dopa reduced nano stars. 100 µL 3 mM $AgNO_3$ remained constant throughout the trials, with the following chemical modifications: (a) 200 µL NP seeds, 100 µL $HAuCL_4$ and 200 µL 15 mM L - dopa (b) 200 µL NP seeds, 100 µL $HAuCL_4$ and 300 µL 15 mM L - dopa (c) 200 µL NP seeds, 100 µL $HAuCL_4$ and 150 µL 15 mM L - dopa (d) 200 µL NP seeds, 200 µL $HAuCL_4$ and 150 µL 15 mM L - dopa (e) 100 µL NP seeds, 100 µL $HAuCL_4$ and 150 µL 15 mM L - dopa (f) 100 µL NP seeds, 200 µL $HAuCL_4$ and 150 µL 15 mM L - dopa. Imaged using Joel 2100f operated at 200 kV.

This suggested that the L - dopa reduced the $HAuCl_4$ onto the individual seeds, to stimulate the seed mediated growth into circa star like structures. There was still an element of aggregation noted, however, on sporadic occasions, spiked projections can be seen, which indicates the silver nitrate volume and concentration (100 µL 3 mM) was at the optimal for this particular experiment but the reducing agents were very difficult to optimise.

To sum up the findings from 'Substituting Ascorbic Acid for L - dopa functionalization' synthesis section of this chapter, this synthesis did not create well controlled/defined nanostructures. The reason for this was probably the issues with particle aggregation through either the surplus of seeds, not enough $HAuCl_4$ or even too much, or the volume/concentration of L - dopa was not optimal to the volume/concentration with respect to the volume/concentration of the $HAuCl_4$. Many minor adjustments were made throughout the trial to try and counteract any negative results and improve the synthesis, from varying the volume of the compounds, stirring speeds and incubation times. Branches did appear on some particles, but seems in most of the results the excess of $HAuCl_4$ may only have bound to a small amount of the particles to make extra - large stars or larger nano particles, as opposed to spreading out onto all the seeds to form smaller stars.

An interesting concept, taken as a positive indication from this first initial trial, was the ability of the L - dopa to reduce the $HAuCl_4$ to form nano particles shown in Figure 6.7 d. This concept was further explored to determine if the L - dopa could replace the reducing agent, sodium citrate, and simultaneously be used to form 12 nm Au nano seeds.

6.3.3.2 L - dopa reduced Nano seeds to star formation

Advancing on from 6.3.3.1 that demonstrated that L - dopa could reduce $HAuCl_4$ to form nano particles of approximately 50 nm in diameter, this method was tried to determine if particles as small as 12 nm could be produced and thus, form the basis of L - dopa functionalized nano seeds that, in turn, would grow to form nano stars. Figure 6.8 provides a schematic overview of the synthesis process.

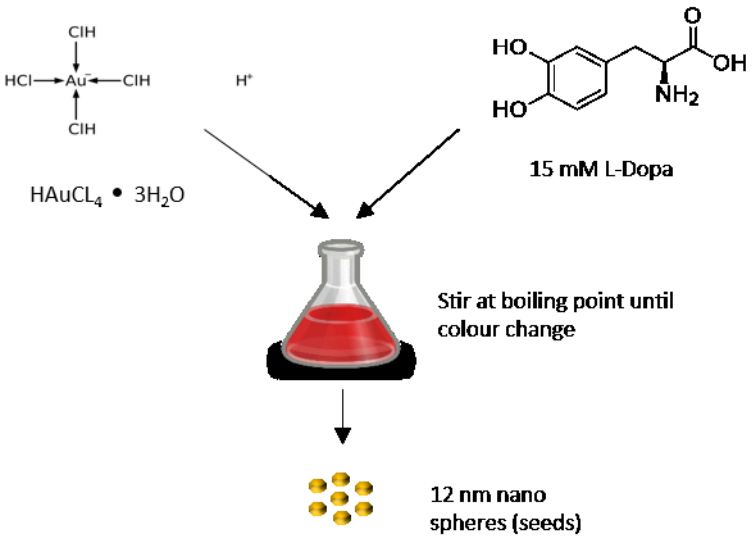


Figure 6.8 Schematic diagram demonstrating the chemical synthesis procedure used to produce L - dopa reduced Au nano seeds.

Previous literature has also confirmed that L - dopa can successfully act as a reducing and capping agent, as the Catechol has a reduction potential (E_o) that enables the formation of small scale AuNPs (ca. 530 mV) [100, 101, 104]. The method trialled here used 15 mM L - dopa to chemically reduce 10 mM $HAuCl_4$ in the same principle as displayed in Figure 6.4 to form stable spherical nano structures. The results are shown in Figure 6.9.

Figure 6.9, a, illustrates how the particle size varied when 15 mM L - dopa was used to reduce 10 mM $HAuCl_4$ into NPs. The size distribution was uneven and the smallest particle size produced was 50 nm in diameter. It was visually evident that clusters of particles were forming believed to be due to the positively charged amine group of the L - dopa that has a tendency to adsorb onto negatively charged gold nanoparticles, resulting in the attachment of the catechol group on the particles surface, thereby causing an aggregation state of AuNPs[102]. It was then sought to dramatically reduce the concentration of L - dopa to limit this affect as it was speculated that the cause was due to the excess L - dopa molecules.

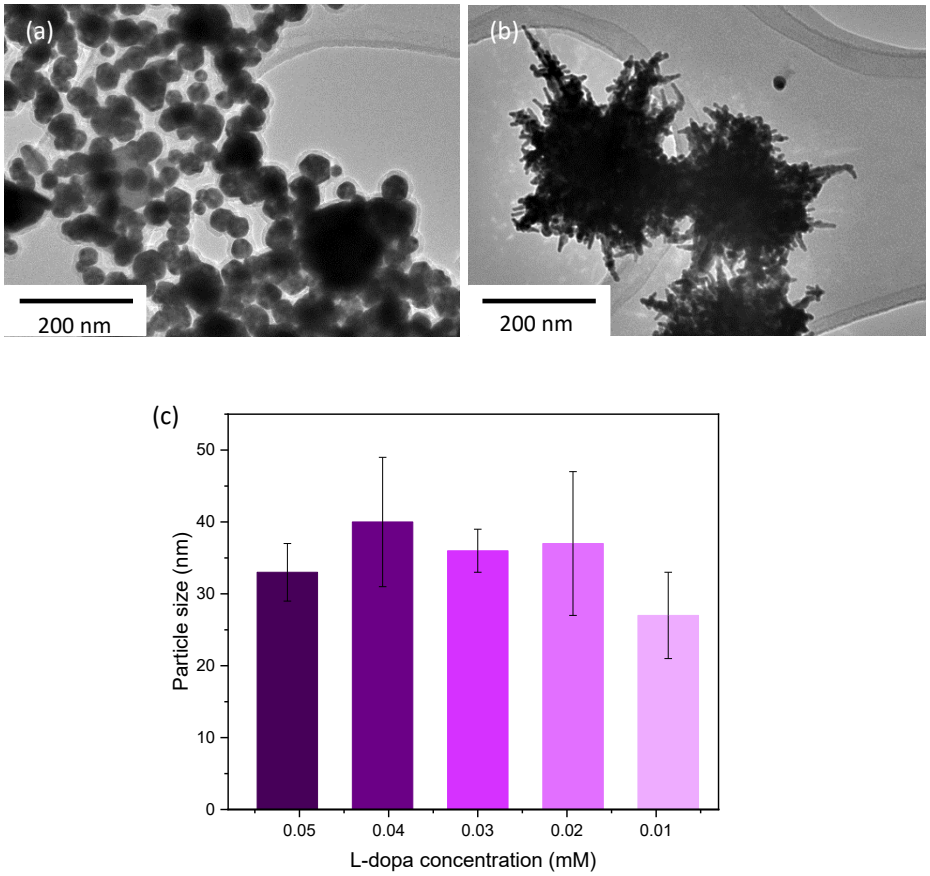


Figure 6.9 L – dopa functionalised nano particles produced *via* reducing 10 mM $HAuCl_4$ with 15 mM L - dopa (a) particles then gown into stars *via* the seed mediated growth method of reducing acidified $HAuCl_4$ bound to the NPs with ascorbic acid while forming branches with the addition of $AgNO_3$ (b). (c) Graph displaying the size variation of the L - dopa reduced NPs formed when changing the L - dopa concentration parameters, n = 200.

Varying concentrations of L - dopa from 0.05 mM to 0.01 mM was tested to determine if dramatically lowering the L - dopa dose from 15 mM would have an impact on the nano particle aggregation state and thus, on the overall NP size. The nano particles were analysed by Dynamic Light Scattering (DLS) (Figure 6.9 c). The results confirmed that the particles formed between 27 and 40 nm in diameter and there was no significant difference between reducing the concentration of L - dopa and the size of the NPs produced. The idea of this synthesis method was to produce nano seeds around the size of 12 nm, which unfortunately could not be achieved. This suggested either that the L - dopa is not a strong enough reducing agent to form particles small enough to use as base nano seeds intended for seed mediated growth synthesis into nano stars or that undesirable aggregation of the particles is still occurring.

Nevertheless, the nano particles were still grown into stars as per the protocol shown in Figure 6.5 to complete the full synthesis and to determine the morphological structure obtained when using L - dopa reduced nano seeds. Figure 6.9 b illustrates TEM images of the as – formed particles. As expected, the size of the particles were measured as 200 nm+. The particles did however form the branch like structures that resemble the star like properties, but they are without doubt an amalgamation of clustered NPs and not singular NSs.

The aggregation state in both the NPs and NS in this method was very high, therefore, in an attempt to limit this, the particles, after centrifugation, were re - suspended in various media, such as ethanol and culture mediums to try and combat the aggregation issue and to allow the particles to re disperse. However, none of these approaches worked.

6.3.3.3 L - dopa capped nano stars

In a simpler synthesis, it was next tried to see if the L - dopa could stabilise the NSs in the similar fashion to PEG. As previously shown the L - dopa can reduce Au and work as a capping agent, *albeit* it is not highly effective as a reducing agent as explained in 6.3.3.2. However, it was it was decided to trial replacing the PEG with L - dopa and to functionalise the NSs by immobilizing the L - dopa particles onto the external surface of the NSs. Figure 6.10 provides a schematic overview of the synthesis method used.

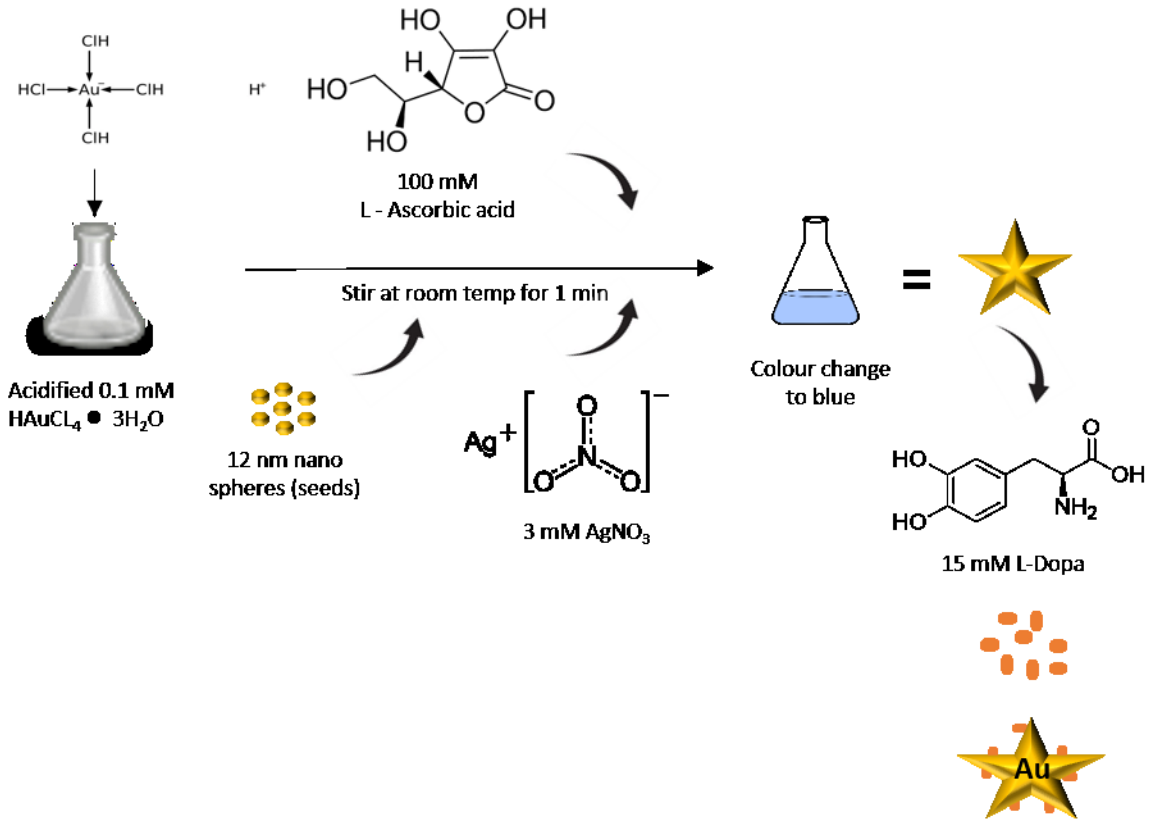


Figure 6.10 Schematic diagram demonstrating the chemical synthesis procedure used in attempt to produce L - dopa capped Au nano stars.

Sample	*Volume of 15 mM L - dopa (mL)*
1	0.1
2	0.25
3	0.5
4	1
5	2

Table 6.4 The different volumes of 15 mM L - dopa used to bind to the Nanostar surface in an attempt to form L - dopa capped functionalised nano stars.

Previous literature has shown that catechol has an exceptional binding affinity to various metallic substrates *via* metal − catechol complex - action. In the presence of tetrachloroauric ions ($AuCl_4$−), catechol can undergo rapid oxidative conversion into catechol Quinone through the transfer of two electrons to the ionic precursor, thus allowing the L - dopa to immobilise onto the surface of the gold particle[105, 106, 107, 108, 109]. This concept was attempted and the volumes of L - dopa used in each of the synthesis are noted in table 6.4.

Unfortunately the L - dopa alone did not stabilise the particles in solution, nor was there any indication that any L - dopa molecules had bound to the surface of the particles, as once the L - dopa was added to the solution, as the stars were forming, the L - dopa appeared to cause 'crashing out' of the particles from solution. The blue coloured solution that was used to confirm the nano star formation, changed to a clear colour and the remaining gold ions formed a precipitate. This occurred in all five procedures of the differing volumes of L - dopa trialled set out in table 6.4.

Previous studies have proved that attempting to control the synthesis of AuNPs or AuNSs in water using catechol's is very challenging due to the very fast reduction kinetics. The electron transfer kinetics need to be reduced to modulate the morphology of the nanostructures when a catechol is used as a reducing agent whilst still allowing the reduction potential to be maintained[104]. The nucleation and growth of AuNPs are influenced by the presence of water, which can in turn facilitate the dissociation of $AuCl_4$−, this may, in part give an explanation as to why the L - dopa in water caused the dissociation of the Au ions that caused the particles to potentially dismantle and precipitate as there was no organic solvent to act as a reaction medium to modulate the kinetic transfer rate.

However, the principle of having the L - dopa bound/immobilized on the particle surface was still of interest as a target property for BBB crossing of these particles. For this reason, the next step in this study was to explore the possibility of ligand binding to functionalise the nano stars with L - dopa.

6.3.3.4 EDC/NHS coupling L - dopa to PEG

The concept of using this EDC/NHS coupling method allowed the synthesis of the PEGylated nanostars optimised in chapter 4 to be utilized. The process of EDC/NHS coupling works by EDC activating the carboxyl groups (—COOH) for direct reaction with primary amines (—NH_2) *via* amide bond formation. The N-hydroxysulfosuccinimide (Sulfo - NHS) aids in controlling and modifying the carbodiimide crosslinking reactions between the carboxylate (—COOH) and primary amine (—NH_2) binding. Although NHS and Sulfo - NHS are not required for carbodiimide reactions, their use greatly enhances coupling efficiency. Figure 6.11 provides a schematic overview of how this protocol was used to activate the – COOH group on the PEG that is immobilized onto the AuNS surface to bind to the – NH_2 group on the L - dopa.

NHS and Sulfo - NHS are used to prepare amine - reactive esters of carboxylate groups for either chemical labelling, crosslinking or solid - phase immobilization applications. As this study used the crosslinking application, Sulfo – NHS was chosen for this application. Sulfo - NHS esters are identical to NHS esters except that they contain a sulfonate (–SO_3) group on the N-hydroxysuccinimide ring. This charged group has no effect on the reaction chemistry, but does preserve or increase water - solubility of the modified carboxylate molecule and the cross linkers containing them, whereas, NHS alone decreases water - solubility of the modified carboxylate molecule. In addition, the charged group prevents Sulfo - NHS cross linkers from permeating cell membranes, enabling them to be used for cell surface crosslinking methods[110]. Furthermore, Sulfo - NHS makes it possible to perform a two - step reaction.

The carboxylate (-COOH) group on the PEG molecule reacted to the Sulfo - NHS in the presence of a carbodiimide (EDC), resulting in a semi - stable Sulfo - NHS ester. This ester was then reacted with primary amine (-NH_2) group on the L - dopa molecule to form an amide crosslink. Sulfo - NHS esters are sufficiently stable but will hydrolyse within hours or minutes, depending on water - content and pH of the reaction solution. NHS esters have a half - life of 4 - 5 hours at pH 7, 1 hour at pH 8 and only 10 minutes at pH 8.6. The activation reaction with EDC and Sulfo - NHS is most efficient at pH 4.5 - 7.2, with the EDC reactions performing more efficiently in MES buffer at pH 4.7 - 6.0. Reaction of Sulfo – NHS - activated molecules with

primary amines is most efficient at pH 7 - 8, in phosphate-buffered saline (PBS) at pH 7.2-7.5[110].

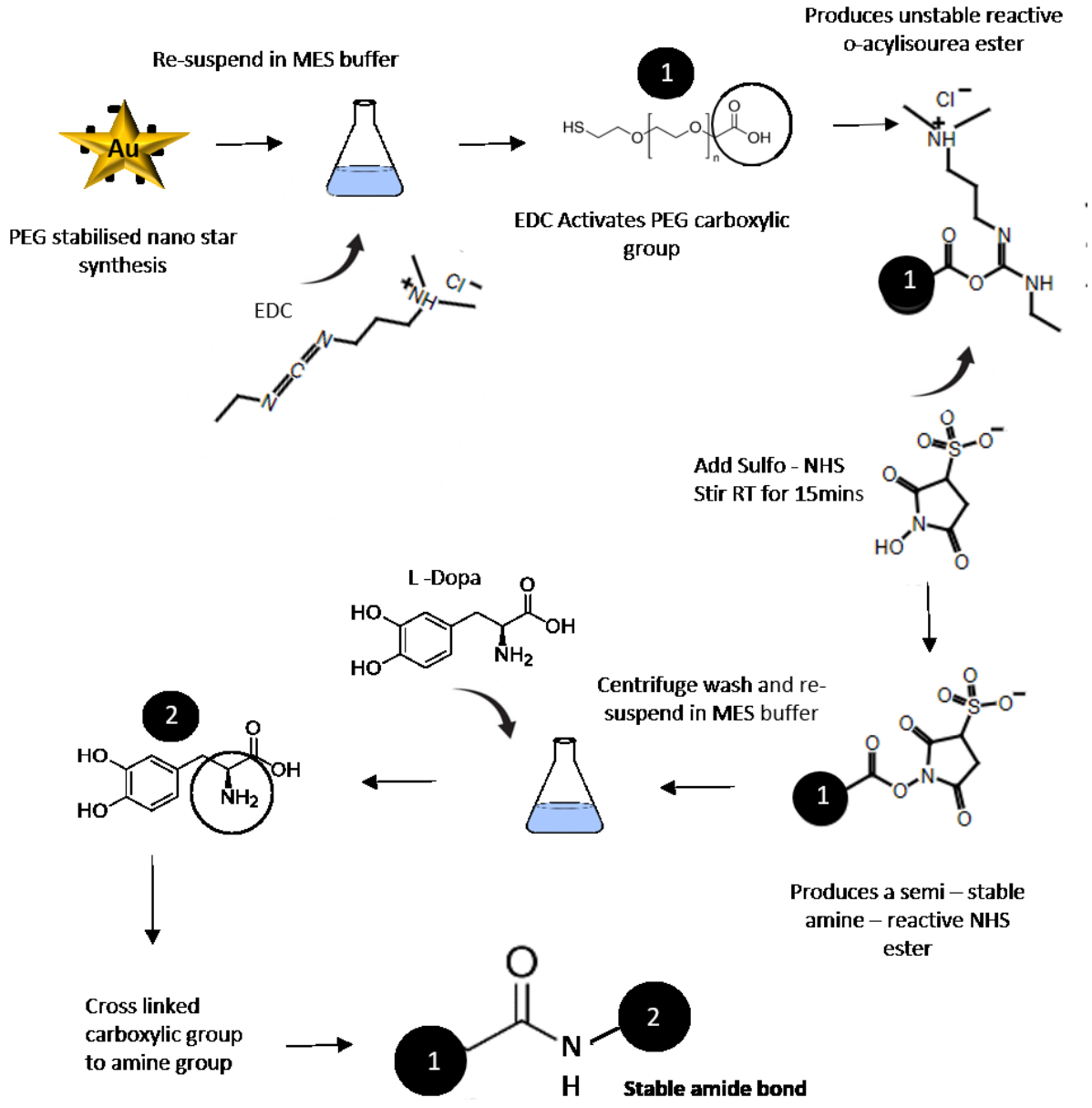


Figure 6.11 Schematic diagram providing a visual overview of the EDC/NHS coupling method used to couple L - dopa to the immobilised PEG on the surface of the nano stars.

As the coupling is very pH dependent, a number of different variations of the coupling protocol were trailed to evaluate which pH of what solution at what point of the protocol yielded the best outcome. Table 6.5 (below) summarises the changes trialled.

Experiment	*EDC*	*Re-suspended in MES pH*
1	MES pH 4.7	4.7
2	MES pH 7	4.7
3	H2O	4.7
4	MES pH 4.7	7
5	MES pH 7	7
6	H2O	7

Table 6.5 Table showing the different pH values of the solutions. Middle panel, showing which medium in which the EDC was dissolved and pH. Right panel, at the point in the protocol shown in Figure 6.11 after the Sulfo – NHS was added to form the amine ester, the particles were re - suspended in MES buffer with different pH.

TEM micrograph images of the completed coupling of L - dopa functionalised nano stars are shown in Figure 6.12. The nano stars were synthesised *via* the routes shown in Figure 6.4 and 6.5. The PEG molecules were initially present on the AuNS surface prior to being subjected to the coupling experiment. Based on the visual analysis, it is evident, that this procedure had no detriment to the morphology of the particles and that the structural integrity remained when compared to the AuNS generated in chapter 4 and 5 of this study. Experiment 6 (Figure 6.12, f), did not successfully produce the spike like features shown in the other five experiments, however, the result of this study was required to verify if the L - dopa had successfully coupled to the PEG and that both molecules were bound to the AuNSs, which cannot be detected by TEM analysis. As the L - dopa, PEG and Sulfo – NHS all absorb strongly at around 260 – 280 nm, Ultraviolet Visible Spectroscopy (UV – Vis) was not a viable option to distinguish between each of the compounds so X-ray Photoelectron Spectroscopy (XPS) analysis was adopted. The XPS results are displayed in Figures 6.13 and 6.14.

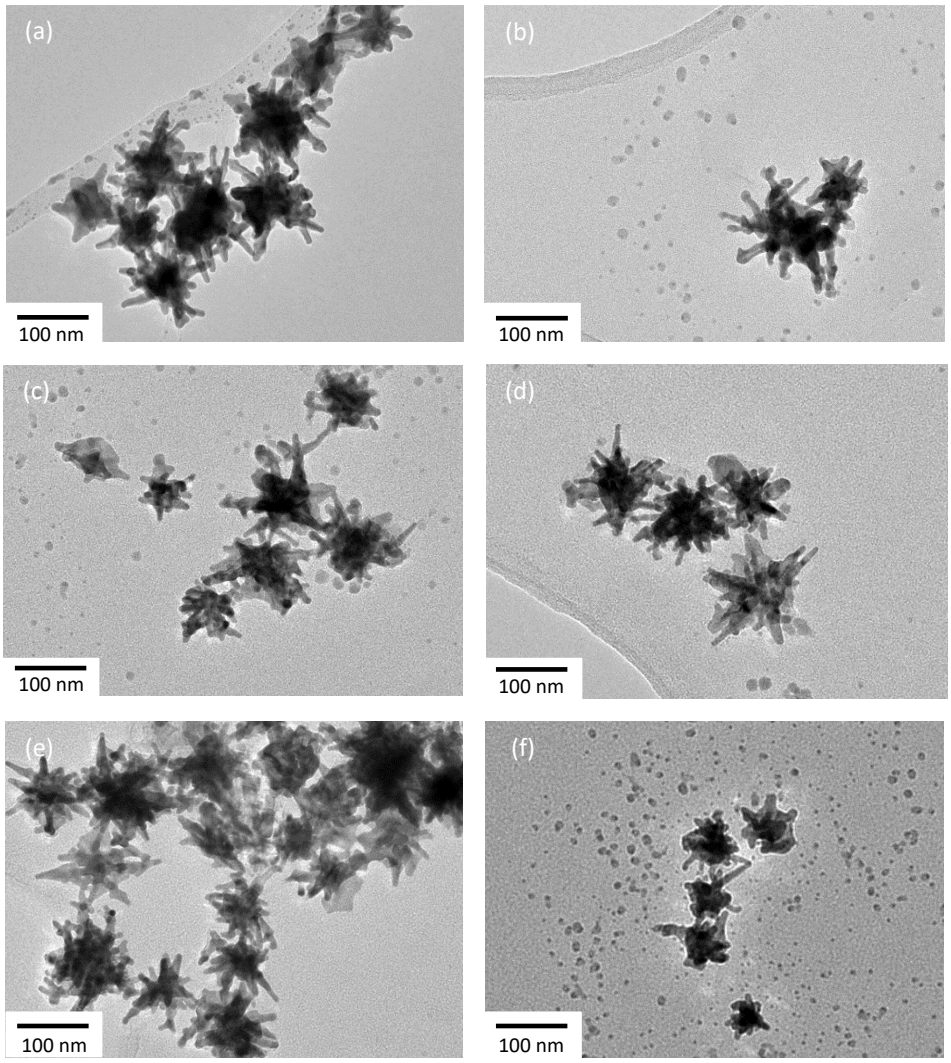


Figure 6.12 TEM images representing a visual analysis of the EDC/NHS L - dopa coupled PEG functionalised AuNSs. The individual results are as follows: Experiment 1 (a), Experiment 2, (b), Experiment 3 (c), Experiment 4 (d), Experiment 5 (e), Experiment 6 (f). Joel 2100f operated at 200kV.

Figure 6.13 shows the binding energies detected in the PEG only and L - dopa only compounds and allows confirmation of the presence of each of the molecules and binding observed between the two compounds. There is a high level of oxygen detected in the PEG compared to the L - dopa (Figure 6.13 b) due to the difference in chemical make - up of the two compounds. As PEG does not incorporate any nitrogen in its structure, none were detected, but nitrogen was detected in the L - dopa only sample (Figure 6.13 c). Figure 6.13 a, demonstrates peaks in C-O / C-N in reference to PEG detection and no peaks found in that region for L - dopa, however, the peak in the C-H region is the detection of the catechol ring found in the L - dopa structure, which would not be found in PEG. This data provides a clear

differentiation between the two molecules, in that they do not overlap or peak at the same points, which will enable the presence or absence of each molecule to be confirmed.

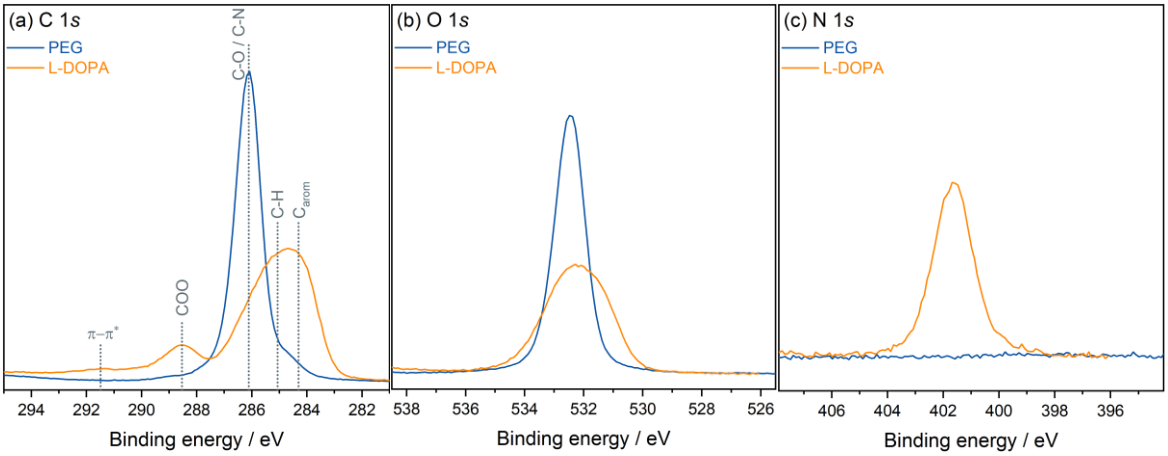


Figure 6.13 Reference XPS demonstrating the binding energy peaks to enable differentiation between L - dopa and PEG

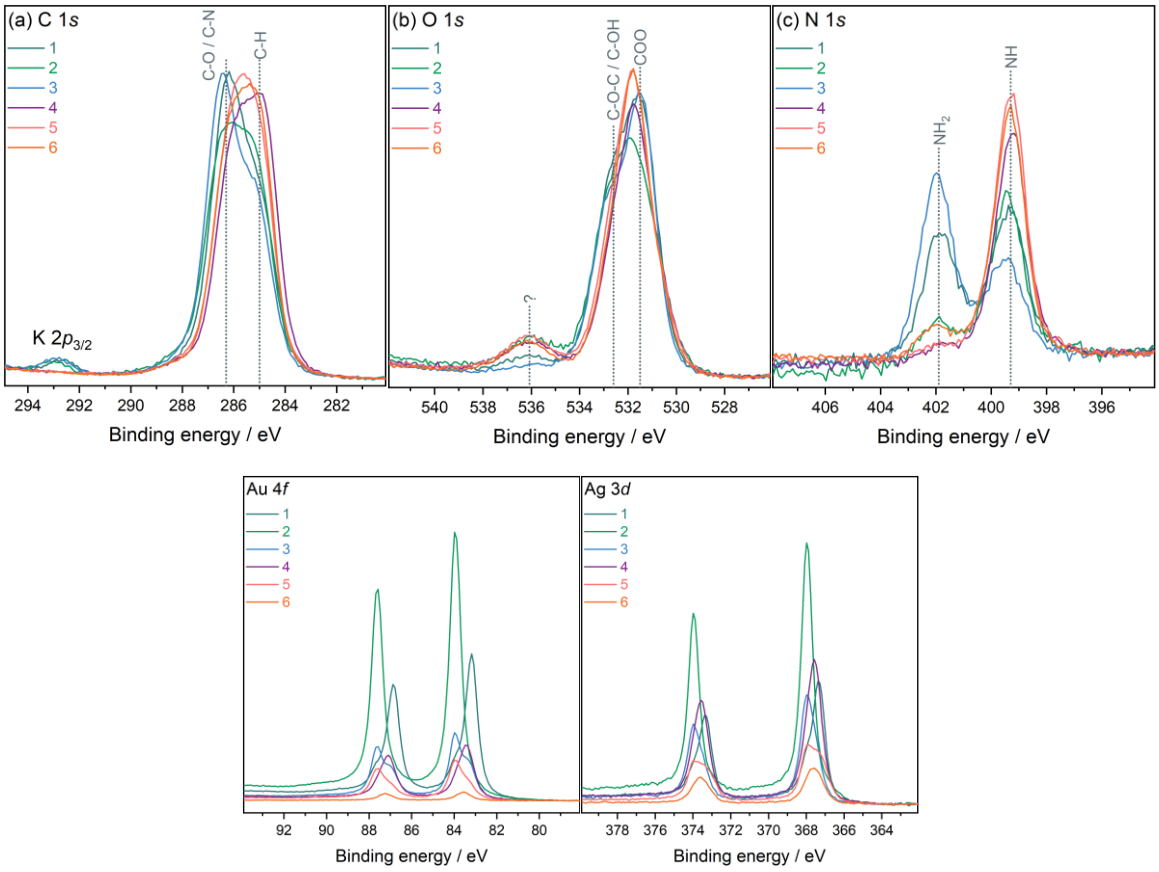


Figure 6.14 XPS data demonstrating the attachment potential for organic material binding. (Au 4f/Ag 3d) Data normalised to carbon, the strength of the peak determines bound material.

The data set Au 4f and Ag 3d (Figure 6.14) is normalised to carbon. This data shows the attachment potential of the organic matter bound to the AuNSs. The size of the peak is relative to the carbon signal, in which the higher the peak, the less organic material is attached, whereas, the lower the peak, the more organic material bound. Figure 6.14 (Au 4f and Ag 3d) demonstrates experiment 1 had very high peaks in Au and Ag, thus suggesting limited binding of organic material (PEG and/or L - dopa). Whereas, sample 6 displays very small Au and Ag peaks suggesting a high load of bound PEG/L - dopa.

The peaks demonstrated in the O 1s and N 1s XP analysis are the organic fractions, the PEG and L - dopa respectively (Figure 6.14 b, c). Figure 6.13 c displays the NH_2 peak as the L - dopa and the NH peak represents the amide bond coupling the L - dopa to PEG. Experiment 3 shows a high peak in the NH_2 region and a low peak in the NH region suggesting very little amide coupling took place in this trial. However, experiments 2, 4, 5 and 6 display low NH_2 peaks but high NH peaks suggesting a high yield in L - dopa activation/coupling. Experiment 1 demonstrates a mid - peak in both NH_2 and NH suggesting the presence of L - dopa, with only half coupled with PEG.

Figure 6.14 b, O 1s data is confirmation of PEG detection. As PEG is made up of Hydrogen (H), carbon (C) and Oxygen (O) elements, this data confirms that PEG molecules were detected on all 6 experiments, thus, confirming that the coupling protocol did not remove or inhibit any of the PEG bound to the AuNSs.

Figure 6.14 a, C 1s data represent the change in Carbon. The binding energies show a high peak in C-O/C-N in reference to PEG detection and the peak in the C-H region detects the catechol found in the L - dopa. This data suggests an increased presence of L - dopa on samples from experiments 4 - 6 as the shift is more towards the C-H and samples analysed from experiments 1 - 3 are more on the C-O/C-N PEG side, thus suggesting more PEG only attachment. Interestingly, a very mild energy Peak in the K (potassium) detection region for experiments 1-3 only was observed. This is potentially due to reducing the pH in the MES solution to a more acidic environment (pH 4.7) for all three samples when they were re – suspended in MES before the L - dopa was added. This production of potassium ions could have potentially been the cause of the limited PEG – L - dopa coupling observed in experiment 1 - 3. The summary of all effects can be found below in table 6.6.

Experiment	*(a) Binding of organic matter*	*(b) Detection of PEG (C-O/C-N)*	*(c) Detection of L - dopa (C-H/NH_2)*	*(d) Detection of amide bond formation (NH)*
1	Low	High	Low	Low
2	Very low	High	medium	Low
3	High	High	Low	Very low
4	High	High	High	High
5	High	High	High	High
6	High	High	High	High

Table 6.6 Table providing an overview of how efficient the binding of either the PEG or L - dopa was on the particle surface (a). The confirmation that the PEG molecules were still bound to the AuNS at the end of the experiment (b). (c) Confirms the presence of L - dopa in the particle solution and (d) confirms the yield of L - dopa molecules detected cross linked with the PEG in the presence of EDC/Sulfo – NHS to form a stable amide bond.

Experiment 1

Experiment 1 displays a medium strength signal for both Au and Ag, suggesting a 50:50 organic material binding compared to sample 2 and 6. Sample 1 shows a stronger signal for the C-O/C-N grouping, suggesting more attachment for PEG only. There is a relatively strong peak on the COO group which correlates to the L - dopa signal. And 50:50 signal on the NH_2 to NH signal suggesting only 50% of the L - dopa molecules were activated and potentially coupled with the PEG.

Experiment 2

Experiment 2 demonstrated a very high peak in both Au and Ag, which suggests very limited organic binding. The sample doesn't show a particularly strong signal to either the C-O/C-N or the C-H groupings, suggesting limited presence of both PEG and L - dopa. Looking at 'N' value (Figure 6.14, c) there's is a very low signal at NH_2 (unreacted L - dopa) and medium

signal at NH (reacted signal). It could be argued that this was not a failure, but a low yield result. Analysing Figure 6.14 a, further for experiment 2 - the broad peak that covers both detection peaks of C-O/C-N and C-H suggests an equal amount of PEG to L - dopa. The same conclusion can be drawn from analysing Figure 6.14, b, as the peak does not favour one side over the other, again suggesting a 50:50 ratio of PEG : L - dopa molecule. However, analysing Figure 6.14, c, there was a clear peak detected at the N-H region confirming the activation of the PEG – L - dopa amide bonding, but very little, if any of these amide bonds were found detected on the AuNS surface (Figure 6.14 Au 4f and Ag 3d). The modifications to the protocol for sample 2 effectively worked, in the sense that the PEG molecules coupled to the L - dopa molecules on pretty much a 1:1 basis, unfortunately however, a limited volume was detected bound to the AuNS.

Experiment 3

Experiment 3 demonstrated small peaks in both the Au and Ag organic material binding analysis (Figure 6.14, Au 4f and Ag 3d), suggesting a good volume of surface bound elements. A strong peak was confirmed in the C-O/C-N region suggesting high affinity PEG to Au binding (Figure 6.14, a). Figure 6.14 b demonstrates a strong peak in the COO region confirming the presence of L - dopa, however Figure 6.14 c displays a strong peak detected for NH_2 than NH, thus confirming that even though L - dopa is present in the sample, the majority was inactivated by approximately 75%.

Experiment 4

Experiment 4 also demonstrated small peaks in the Au but a stronger peak in the Ag region when analysing the organic material binding data (Figure 6.14, Au 4f and Ag 3d), suggesting a semi - good volume of surface bound elements. Strong signals were observed detecting PEG and L - dopa (Figure 6.14 a, b) along with a strong signal for activated L - dopa seen in Figure 6.14, c (N-H), and minimal detection of NH_2, confirms all the PEG molecules

cross linked with the L - dopa molecules. The only puzzling aspect to this experiment was the increase in Ag peak.

Experiment 5

Experiment 5, again, demonstrated small peaks in Au and Ag confirming good organic compound covering (Figure 6.14, Au 4f and Ag 3d). The peak detected residing in between the C-O/C-N and C-H regions in Figure 6.13 a, and in between the C-O-C/C-OH and COO regions in 6.14 b, suggests the presence of both PEG and L - dopa. Experiment 5 obtained the lowest peak for NH_2, (alongside experiment 6) and the highest peak displayed for the NH region, suggesting a very high yield of PEG coupled L - dopa detected on the surface of the AuNSs. Interestingly, the results of experiment 5 were similar to those of experiment 2 except the difference in amide bonds forming and the inability of the PEG/L - dopa to bind to the AuNSs in experiment 2. The EDC used in both these experiments was dissolved in MES at pH 7, however, the particles in experiment 2, after COOH activation were re suspended in the more acidic MES (pH 4.7) that clearly inhibited the amide bond formation and the potential negative impact from the detected potassium ions.

Experiment 6

Strong peaks were detected confirming both PEG and L - dopa alongside a strong peak in NH detection and minimal peak detected in the NH_2 region, thus suggesting a high yield of amide bond formations (Figure 6.14, a, b, c). Experiment 6 also demonstrates the lowest Au/Ag peak (Figure 6.14, Au 4f and Ag 3d), so would conclude from the XPS data that experiment 6 is potentially the optimal protocol variation to achieve the highest yield of amide bonds with 100% binding coverage, when compared to the other experiments.

The original suggestion for optimal COOH activation was sought to occur when EDC is dissolved in acidic MES buffer at pH 4.7-6.0[110]. However, these experiments proved that that most efficient COOH activation occurred when the EDC was dissolved in MES buffer at a

neutral pH (pH 7), (experiment 5) or in H_2O (experiment 6). Previous literature also found that to aid the coupling by sulfo – NHS the environment needed to be neutral (pH 7-8)[110], to which this study concurred (experiment 4-6). However, the TEM images (Figure 6.12 f) of the AuNS after completing the protocol for experiment 6 demonstrated that the star morphology was not optimal compared to the AuNSs from experiment 4 and 5 (Figure 6.12 d, e), therefore, taking all XPS and TEM images into account, the protocol designed and followed for experiment 5 provided the optimal conditions to successfully bind L - dopa to PEG via EDC/NHS coupling.

6.4 Conclusion

In conclusion, each of the methods chosen in attempt to functionalise the AuNSs with L - dopa were validated to indicate whether they were successful or not to systematically optimise the synthesis route. Using L - dopa to directly reduce the Au to form NPs or to directly immobilize onto the AuNS surface would have allowed for a desirable 'one pot' synthesis method to be utilised. However, the most beneficial functionalisation was the EDC/NHS coupling of L - dopa to PEG molecules. This method provides the possibility of post functionalisation of the particles, whereas the other methods would not have. As these L - dopa AuNSs are to deliver the peptide drug to the neurons, the minimal amount of L - dopa required to shuttle the AuNS across the BBB can be studied so that the nano stars can be functionalised with the minimal L - dopa requirement whilst further post functionalisation of immobilising the neuroprotective drugs onto the remaining surface area of the AuNS. The EDC/NHS coupling route only utilises one of the active groups on the L - dopa molecule (amine), while leaving the carboxyl group and the catechol group free for BBB crossing. Further examination in to exactly how L - dopa binds to and crosses the BBB using BBB cell culture models is important for future cell work especially if the results confirm L - dopa can cross by either one or both of the carboxyl or catechol groups.

7 Conclusions and future work

This thesis sought to develop a novel multifunctional drug therapeutic for the treatment of Parkinson's disease by utilising recent advances in nanotechnology. Direct comparison was made between the efficacy and potency of two different gold nano structures with different geometries: nanostars and nanospheres, which were synthesised as potential drug delivery vehicles for H3/H6 neuroprotectants. Although a great deal of work has been conducted on spherical gold nanomaterials in medicine, much less is known about how AuNS interact with neurons and endothelial cells inside the brain. An advantage of AuNS is that they are plasmonic and so can be detected in the Near Infrared Region (NIR2) of the light spectrum that allows a visualisation of how the particles can distribute inside the brain.

In Chapter 4 high quality and optically tunable gold nanostars (AuNS) and nanospheres (AuNP) with the following target properties: to cross the BBB and interact with neurons, were developed by optimising synthesis conditions that produced highly controlled particles with tailorable sizes and shapes. AuNS and AuNP were synthesised with a diameter of 50 nm diameter as this has been shown to be optimal for shuttling neuroprotective drugs inside the brain[59, 60]. The AuNS and AuNP were synthesised to incorporate the same gold mass as well as the same size in diameter, however, the morphological uniformity of the AuNPs was not as controllable as the AuNSs.

The 50 nm AuNS and NPs were fabricated with H3 and H6 neuroprotectants. Some of these nanostructures were then further functionalised with PEG to enhance the stabilization and half - life of the peptides in circulation. It was found that the H6 peptide in the presence of PEG altered the surface chemistry of the AuNPs that subsequently altered the aggregation state of the AuNPs but this was not observed with the AuNSs. The H6 peptide proved difficult to functionalise onto the AuNPs possibly because it's structural format is more linear than the coiled structure of the H3 peptide. The AuNSs were successfully functionalised with both the H3 and H6 peptides and demonstrated high particle stability in water, cell culture media and

Bovine Serum Albumin (BSA), suggesting they were suitable for subsequent testing in cell culture (Chapter 5).

The neurotrophic effects of the new peptide – targeted nano structures were evaluated in chapter 5. First the quantity of Au that would be administered with each drug dose was measured. Au is FDA approved for medicinal use, however, it is not biodegradable and could cause toxicity, so exposure should be kept to a minimum for subsequent, future translation in man. H6 and H3 in the presence of PEG altered the surface chemistry of the AuNPs which resulted in a 5 – fold increase in Au : H3/H6 peptide ratio when compared to the H3/H6 PEGylated functionalised AuNSs. Without the addition of PEG, the Au content measured for the H3/H6 AuNSs at all concentrations (2, 5, 10, 20 and 40 µg/mL) was equal and marginally elevated in the H3/H6 AuNPs.

One of the hypotheses was that the nanostars would demonstrate improved efficacy compared to nanospheres because the spike like features could penetrate through the plasma membrane and deliver the peptide into the neuronal cytoplasm.

The findings presented in chapter 5 suggest that the nanostars have advantages over spherical shaped NPs due to the significant difference in the neuronal interaction observed. There was a ca. 30% increase in peptide targeted AuNSs internalised by the neurons, and a ca. 10% increase in AuNS that were membrane bound/associated when compared to their spherical counterparts. Whereas there was ca. 40% more AuNPs found in the extracellular matrix compared to the AuNSs. This suggests that the H3/H6 AuNSs demonstrated an improved efficacy compared to AuNPs because the spike like features are able to penetrate through the plasma membrane and deliver the peptide directly into the neuronal cytoplasm. This also advocates that the spikes on the nanostars were more effective in the tight intercalated neuronal network because the spikes branching through these structures, enabled more surface contact with the neurons than the AuNPs. The AuNS morphology and heightened neuronal interaction could contribute to the AuNS + H3/H6 increased ability to produce neurites when administered in doses as low as 10 µg/mL and their great efficacy to protect neurons against drug induced (hydrogen peroxide (H_2O_2) oxidative stress and toxin *(*6-hydroxydopamine *(*6-OHDA) induced cytotoxicity. Taken together, the results put forward, are that the AuNS + H3 + PEG are the best performing nanostructure. This nanostructure is a promising candidate as a novel neurotherapeutic that can effectively interact with neurons,

exerting limited toxicity, whilst alleviating features seen in Parkinson's disease pathology; such as repairing damaged neurons through stimulating neurite outgrowth and prevent cell death whilst protecting neurons from damage and toxicity.

One of the main obstacles faced in designing a new neuro - therapeutic, is their ability to cross the blood - brain barrier (BBB) and protect neurons with minimal side effects. However, AuNS have potential as a neuroprotective platform as previous work has shown they have an enhanced ability to cross the BBB. The Porter group has shown that AuNS can cross the plasma membrane of brain endothelial cells in high amounts (ca. 20% efficiency of BBB transport *in vitro* studies) and that Au nano flower morphologies can be functionalised with L - dopa, that allowed passage across the BBB *via* the large amino acid (LAT - 1) transporter, with an efficiency of up to 40%, which is a markedly higher increase rate of BBB crossing seen compared to other literature using BBB – targeting methods.

Utilising this successful method, chapter 6 sought to functionalise the AuNS for BBB targeting and crossing using the L - dopa which transports across the BBB *via* the LAT 1 transporter. Four different methods were trailed to functionalise the AuNSs with L - dopa. The aim of the synthesis was to build on the results of Chapter 5 to produce a star - shaped nano particle that could cross the BBB, and in future work, could be subsequently functionalised with PEG and the neuroprotective (H3/H6) peptides to interact with the dopaminergic neurons to offer neuroprotection along with fluorescent dyes that will allow for bioimaging studies to monitor the distribution of the new novel therapeutics.

The first attempt at synthesis was unsuccessful. Using L - dopa as a reducing agent to directly immobilise on to the AuNS surface, did not produce the desired AuNS morphology, contrary to the findings of Ong Zhan et al. in previous work by the group[59]. However, there is a major disadvantage to this approach as it would be difficult to control the amount of L - dopa used to reduce the Au and thus attached to the surface of the nanostructures. L - dopa is toxic above a threshold dose and could have toxic effects in the brain[60]. The amount of L - dopa on the surface of the nanostructure and dose given to the cells must be carefully limited and controlled if these structures are moved forward into the clinic.

The second functionalisation protocol examined, was the concept of producing L - dopa reduced nano seeds, to grow into AuNS *via* seed mediated growth methods. This method, like the first, is not ideal as the control of L - dopa is again limited and the L - dopa

molecules would not be immobilised onto the star surface, which (assumedly) would be required for site targeting. Removing the citrate ions from this method to replace them with L - dopa caused a change in the surface tension that allowed elevated levels of particle aggregation.

The next route trialled was to directly bind the L - dopa to the AuNS surface *via* direct binding of the catechol group to the Au ions. However, this method did not produce positive results due to the inability to control the fast reduction kinetics observed when the catechol underwent rapid oxidative conversion to bind to the Au.

The final (and successful) method of functionalising the AuNS with L - dopa was *via* EDC/NHS coupling (Figure 7.1).

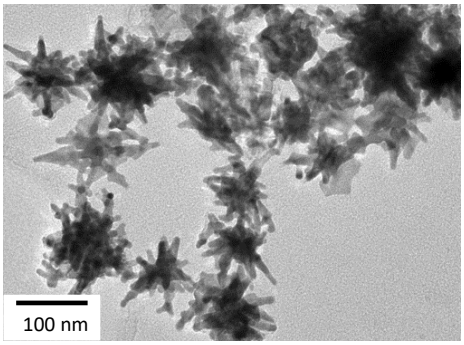


Figure 7.1 TEM image of the successful L - dopa functionalised AuNS *via* EDC/HHS coupling. The particles produced were ca. 50 nm. The AuNSs demonstrated a very high yield of PEG – L - dopa binding to the NS surface. This will enable further functionalisation with the H3/H6 peptides.

This is the most promising functionalisation route as the particles can also undergo post modification. With this method the L - dopa molecules will bind directly to the PEG molecules, that were previously functionalised to the surface of the AuNSs *via* the Au – thiol binding. The EDC activates the Carboxyl group on the L - dopa, and the Sulfo - NHS enhances the coupling of the amine group on the L - dopa to the PEG molecules, and leaves the carboxyl group and the catechol group free for LAT – 1 targeting and binding. However, previous work has not proven exactly how the L - dopa targets and binds to the LAT 1, and whether it is *via* one or more of the L - dopa groups. This should be examined in future studies. The post modification to this method would then allow the minimal amount of PEG to be immobilised

onto the AuNS; that correlates with the minimal amount of L - dopa required to cross the BBB, thus reducing toxicity to the BBB and neurons. The AuNS can subsequent be further fabricated with either of the H3 or H6 peptides to produce a brain delivery, neuroprotective nano neurotherapeutic technology.

To further extend this research, studies into how this new nano neurotherapeutic interacts and crosses the BBB *in vitro* and *in vivo* should be investigated, to determine the exact amount of L - dopa required to cross the BBB. Cellular and then *in vivo* studies evaluating the toxicity of the L - dopa - AuNS would also be advantageous. *In vivo* bio - distribution studies in healthy and PD animals should be conducted to characterise the bio - distribution of the particles inside the brain, to confirm they cross the BBB *in vivo* and to also determine their distribution after they have crossed into the brain parenchyma. The next step would be to test the best performing brain targeting H3/H6 nanostructures in PD animal models of the disease to study their neuroprotective properties. Before translation into animal models, further research is needed to confirm the minimal amount of L - dopa required to shuttle nano particles across the BBB and examine off target toxicity of L - dopa, so no unnecessary detrimental effects are established.

Another interesting avenue of further research would be to test the particles as imaging agents both *in vivo* and *in vitro,* e.g. by attaching fluorescent dyes onto their surface. This property could be used to study the distribution of the H3/H6 nanostructures inside the body and the brain. It could also be used in other types of engineering, for example to study the anatomy of the brain in healthy and diseased tissues, including PD and brain cancers to help to more precisely guide the delivery of drugs to the diseased cells (e.g. using surgically guided methods). The AuNS could also be conjugated with different peptides or antibodies and used as imaging probes (e.g. using SNOM methods) for intracellular tracking and imaging of organelles.

The successfully designed H3/H6 AuNS - peptide platform has the potential to act as both a versatile neuro - protectant and also as a technology to improve the efficiency for neuronal targeting for these and other small molecule drugs that cannot cross the BBB unaided, for treatment of a broad spectrum of neurodegenerative disorders and other brain diseases such as brain cancers. In combination with neurotrophic peptides, nanostars hold promise as a novel theranostic platform with multiple functions, such as neuroprotection,

delivery of high drug loads across the BBB, and bio imaging capability, which may lead to the urgent change required in the treatment of neurological diseases.

8 Appendix

8.1 Effect of peptide targeted nano stars on hippocampal neurons against Aβ-induced neurotoxicity *in vitro*.

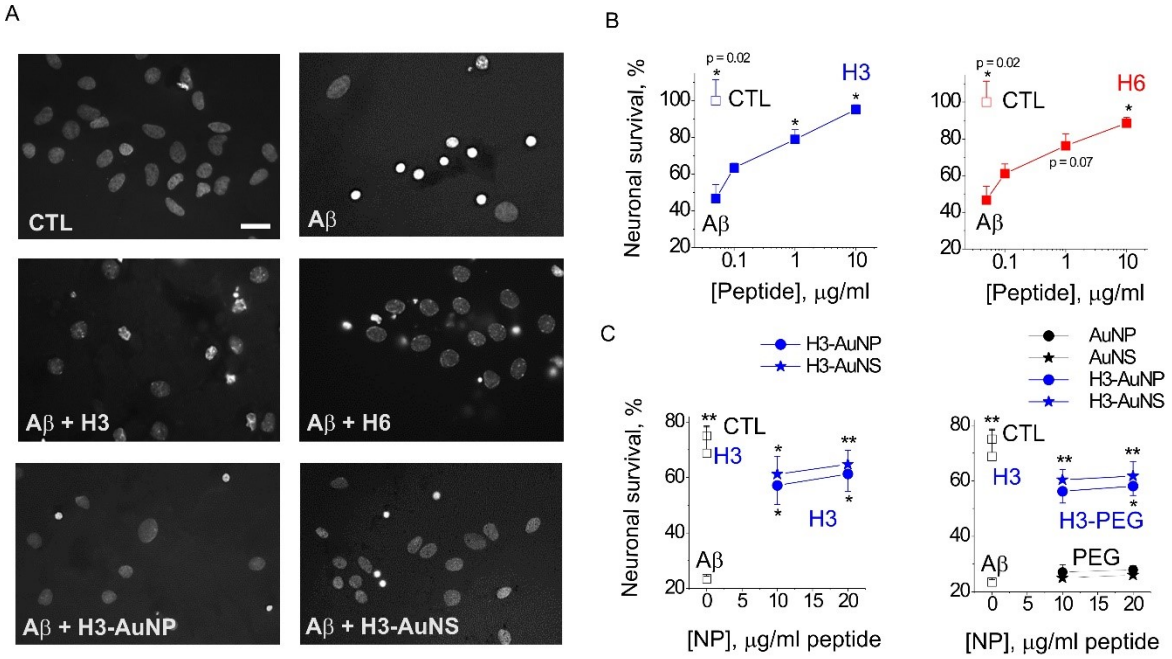


Figure 8.1 S100A4 mimetic peptides and peptide-conjugated AuNP/NS protect hippocampal neurons against Aβ - induced neurotoxicity *in vitro*. (A) Representative images of Hoechst - stained hippocampal neurons left untreated (CTL) or challenged with oligomeric $A\beta_{1-42}$ (Aβ) in the absence or presence of H3/H6 peptides, H3 - AuNP (nanospheres), or H3 - AuNS (nanostars, all 10 μg/ml). Scale bar, 10 μm. (B, C) H3 and H6 peptides (B) and (+/- PEG) - H3 - functionalized AuNP/NS (C) protect cultured hippocampal neurons against Aβ - induced death. CTL, untreated cells; Aβ (8 μM) – neurotoxin only - treated cells. H3 - PEG, H3 and PEG-functionalized AuNP/NS. PEG, PEG - only conjugated AuNP/NS. One - way ANOVA vs Aβ, three to four independent experiments, *$p < 0.05$; **$p < 0.01$.

Previous data also suggests that the S100A4 protein and its peptide derivatives (H3/H6) interact with and exert neuroprotection *via* ErbB family receptors and prevent the Aβ - induced disruption of neuronal membrane structure. Thus, they may launch intracellular pro - survival pathways and/or compete with the deleterious interactions of the Aβ with ErbBs

and membrane bilayer. The neuronal survival effects of the peptide targeted nano structures against Aβ - induced neurotoxicity were evaluated.

The results obtained in collaboration with Dr Stanislava Pankratova, (Laboratory of Neural Plasticity, Department of Neuroscience, Faculty of Health and Medical Science and Comparative Paediatrics and Nutrition, Department of Veterinary and Animal Sciences, Faculty of Health and Medical Sciences, University of Copenhagen, Copenhagen, Denmark) evaluated the neuroprotective effect of H3, H6, and H3 +/- PEG - AuNP/NS in hippocampal neurons subjected to oligomeric Aβ. The $A\beta_{1-42}$ treatment strongly (ca. 2.5 - fold) reduced neuronal viability after 48 h (Fig. 8.1 A - C), and this decrease was counteracted by both H3 and H6-peptide in a dose - dependent manner (Fig. 8.1 B). H3 nano - formulations, both +/- PEG, robustly increased survival of Aβ-challenged neurons (Fig. 8.1 C) with no significant differences in the neuroprotective effect between nano - compound geometries. PEG - only conjugated AuNP/NS did not affect the death rate of Aβ - treated neurons (Fig. 8.1 C, right, PEG). Thus, both unconjugated S100 - derived peptides and the +/- PEG H3 nano - compounds were efficient in the neuronal model of AD, suggesting these peptide targeted nano structures can also provide novel therapeutic effects for other neurodegenerative disorders such as Alzheimer's disease.

8.2 Toxicity study

To confirm The S100 peptide - based AuNS are neuroprotective in vitro, this work collaborated with Darya Kiryushko, (Centre for Neuroinflammation and Neurodegeneration, Imperial College London, Hammersmith Hospital Campus, Burlington Danes Building, 160 Du Cane Road, W12 0NN London, UK) carrying out a comprehensive toxicity study.

8.3 Inductively coupled plasma – optical emission spectrometry (ICP) analysis

ICP analysis was used to determine gold content within multiple experiments within this study. The detection and quantification was compared against the standards shown in Figure 8.2

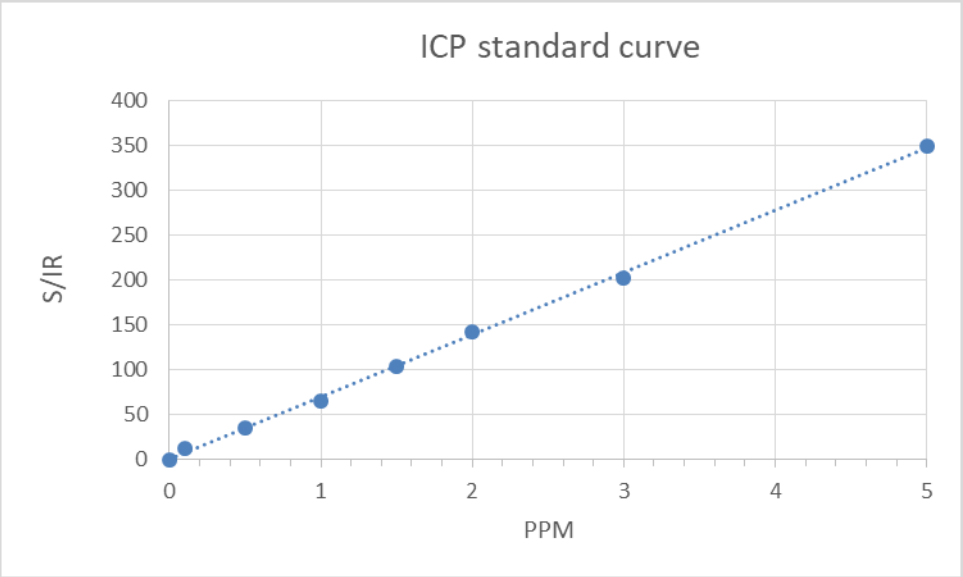


Figure 8.2. ICP standards used to quantify the gold content in the gold samples analysed in this study

8.4 X-ray Photoelectron Spectroscopy (XPS) confirmation of PEG – L - dopa EDC/NHS coupling

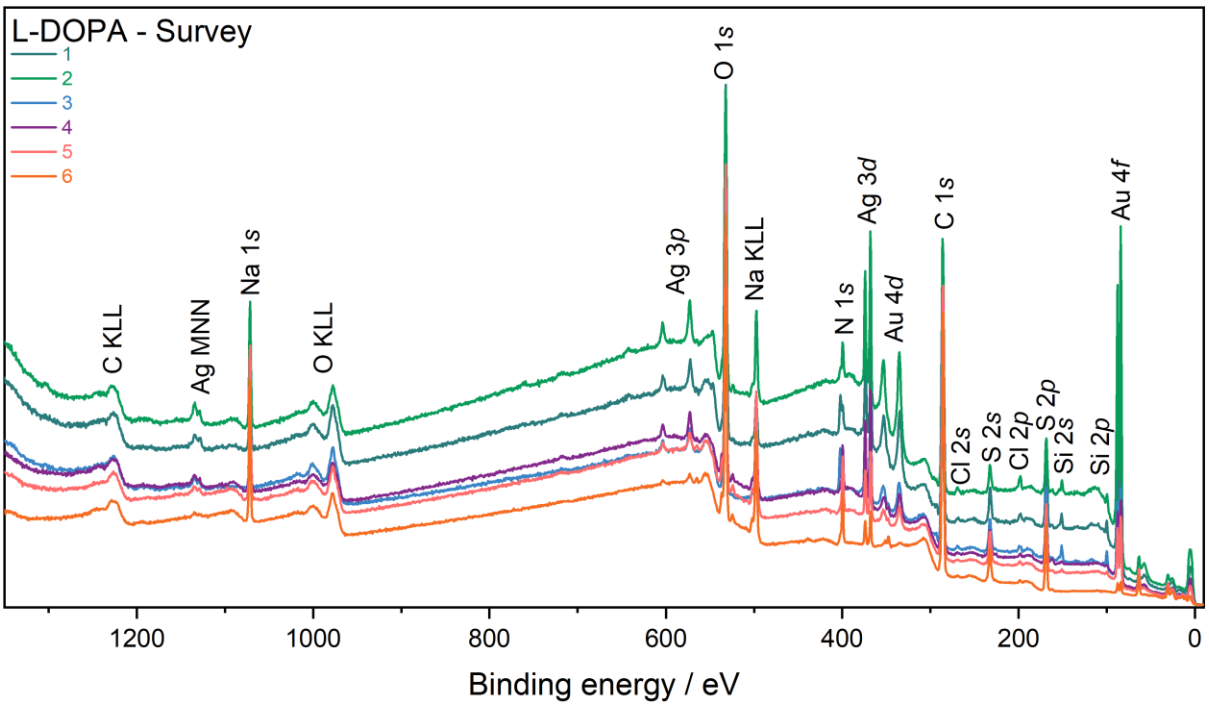


Figure 8.3 Full XPS spectra of the elemental peaks for all 6 EDC/NHS coupling L - dopa to PEG experiments under different conditions.

9 References

1. Gustavsson, A., Svensson, M., Jacobi, F., Allgulander, C., Alonso, J., Beghi, E., Dodel, R., Ekman, M., Faravelli, C., Fratiglioni, L., Gannon, B., Hilton Jones, D., Jennum, P., Jordanova, A., Jönsson, L., Karampampa, K., Knapp, M., Kobelt, G., Kurth, T., Lieb, R., Linde, M., Ljungcrantz, C., Maercker, A., Melin, B., Moscarelli, M., Musayev, A., Norwood, F., Preisig,M., Pugliatti, M., Rehm, J., Salvador-Carulla, L., Schlehofer, B., Simon, R., Steinhausen, H., Stovner, L., Vallat, J., Van den Bergh, P., van Os, J., Vos, P., Xu, W., Wittchen, H., Jönsson, B., Olesen, J. Cost of disorders of the brain in Europe 2010. European Neuropsychopharmacology. **2011**, 21 (10) 718-779
2. Olesen, J, Leonardi, M., The burden of brain diseases in Europe. Eur. J. Neurol. 10. **2003** 471–477
3. A. Duro-Castano, D. Moreira Leite, J. Forth, Y. Deng, D. Matias, C. Noble Jesus, and G. Battaglia, 'Designing Peptide Nanoparticles for Efficient Brain Delivery', *Adv Drug Deliv Rev,* 160 **2020**, 52-77.
4. V. Soroka, D. Kiryushko, V. Novitskaya, L. C. Ronn, F. M. Poulsen, A. Holm, E. Bock, and V. Berezin, 'Induction of Neuronal Differentiation by a Peptide Corresponding to the Homophilic Binding Site of the Second Ig Module of the Neural Cell Adhesion Molecule', *J Biol Chem,* **2002**, 277 24676-83
5. G. Theodorou, Q. Jiang, L. Malms, X. Xie, R. C. Coombes, E. O. Aboagye, A. E. Porter, M. P. Ryan, and F. Xie, 'Fluorescence Enhancement from Single Gold Nanostars: Towards Ultra-Bright Emission in the First and Second near-Infrared Biological Windows', *Nanoscale,* **2018**, 10 15854-64
6. Dmtriteva, O., Pankratova, S., Owczarek, S., Sonn, K., Soroka, V., Ridley, C., Marsolais, A., Lopez-Hoyos, M., Ambartsumian, N., Lukanidin, E., Bock, E., Berezin, V., Kiryushko, D. The Metastasis – promoting S100A4 protein confers neuroprotection in brain injury. *Nature Communications*. **2012** 3 article 1197
7. Kiryushko, D., Novitskaya, V., Soroka, V., Klingelhofer, J., Lukanidin, E., Berezin, V., Bock, E. Molecular mechanisms of Ca(2+) signaling in neurons induced by the S100A4 protein. *Journal of Molecular Cell Biology* **2006** 26 (9) 3625-38.
8. Moldovan, M., Pinchenko, V., Dmytriyeva, O., Pankratova, S., Fugleholm, K., Klingelhofer, J., Bock, E., Berezin, V., Krarup, C., Kiryushko, D. Peptide mimetic of the S100A4 protein modulates peripheral nerve regeneration and attenuates the progression of neuropathy in myelin protein P_0 null mice. *Molecular Medicine*. **2013** 19 43-53
9. Bogaerts, V., Theuns, J. and Van Broeckhoven, C. Genetic findings in Parkinson's disease and translation into treatment: a leading role for mitochondria?. *Genes, Brain and Behavior*, **2008** 7 (2), 129 – 151
10. Fahn, S. and Sulzer, D., Neurodegeneration and Neuroprotection in Parkinson Disease. *NeuroRX*, **2004** 1 (1), 139 - 154
11. Whitton, P.S., Inflammation as a causative factor in the aetiology of Parkinson's disease. *British Journal of Pharmacology*, **2009** 150 (8), 963 - 976

12. Blonder, L. and Slevin, J., Emotional Dysfunction in Parkinson's Disease. *Behavioural Neurology*, **2011** 24 (3), 201 - 217.
13. Yacoubian, T. and Standaert, D., (2009). Targets for Neuroprotection in Parkinson's Disease. *Biochimica et Biophysica Acta (BBA) - Molecular Basis of Disease*, **1792** (7), 676 - 687
14. Tansey, M., McCoy, M., Frank-Cannon, T., Neuroinflammatory mechanisms in Parkinson's disease: Potential environmental triggers, pathways, and targets for early therapeutic intervention. *Experimental Neurology*. **2007** 208 (1), 1 – 25
15. Dauer, W., Kholodilov, N., Vila, M., Trillat, A., Goodchild, R., Larsen, K., Staal, R., Tieu, K., Schmitz, Y., Yuan, C., Rocha, M., Jackson-Lewis, V., Hersch, S., Sulzer, D., Przedborski, S., Burke, R., Hen, R. Resistance of α-synuclein null mice to the parkinsonian neurotoxin MPTP. PNAS **2002** 99 (22), 14524 - 14529
16. Przedborski, S. Pathogenesis of nigral cell death in Parkinson's disease. *Parkinsonism and Related Disorders*. **2005** 11 (1), 3 - 7
17. Steidinger, T., Standaert, D., Yacoubian, T. A neuroprotective role for angiogenin in models of Parkinson's disease. *Journal of Neurochemistry*. **2010** 116 334-341
18. O'Callaghan, J., Sriram, K., Miller, D. Defining "Neuroinflammation". *New York Academy of Sciences*, **2008** 1139 318 - 330
19. Palacino, J., Sagi, D., Goldberg, M., Krauss, S., Motz, C., Wacker, M., Klose, J., Shen, J. Mitochondrial Dysfunction and Oxidative Damage in parkin-deficient Mice. *The Journal of Biological Chemistry*. **2004** 279 (18), 18614 – 18622
20. Ischiropoulos, H and Beckman, J. Oxidative stress and nitration in neurodegeneration: Cause, effect, or association?. *The Journal of Clinical Investigation*. **2003** 111 (2), 163 - 169
21. Ghadge, G., Lee, J., Bindokas, V., Jordan, J., Ma, L., Miller, R., Roos, P. Mutant Superoxide dismutase-1-Linked Familial Amyotrophic Lateral Sclerosis: Molecular Mechanisms of Neuronal Death and Protection. *The Journal of Neuroscience* **1997** 17 (22), 8756 – 8766.
22. Hauser, D and Hastings, T, Mitochondrial dysfunction and oxidative stress in Parkinson's disease and monogenic parkinsonism *Neurobiol Dis* **2012** 51 35 **–** 43
23. Greggio, E., & Cookson, M. R. Leucine-rich repeat kinase 2 mutations and Parkinson's disease: three questions. *ASN neuro*, **2009** 1 13-24
24. Mullin S, Schapira A. The genetics of Parkinson's disease. Br Med Bull. **2015** 114 (1) 39 - 52
25. Birsa, N., Norkett, R., Wauer, T., Mevissen, T., Wu, H., Foltynie, T., Bhatia, K., Hirst, W., Kimanser, D., Plun-Favreau, H., and Kittler, J. Lysine 27 ubiquitination of the Mitochondrial Transport Protein Miro is Dependent on Serine 65 of the Parkin Ubiquitin Ligase. *The Journal of Biological Chemistry* **2014** 289 (21) 14569-14582
26. Dorszewska, J., Prendecki, M., Lianeri, M., & Kozubski, W. Molecular Effects of L - Dopa Therapy in Parkinson's Disease. *Current genomics*, **2014** 15 (1), 11–17.
27. DeMaagd G, Philip A. Parkinson's Disease and Its Management: Part 1: Disease Entity, Risk Factors, Pathophysiology, Clinical Presentation, and Diagnosis. P T. **2015** 8 504 - 532.
28. Munhoz RP, Teive HA, Troiano AR, Hauck PR, Herdoiza Leiva MH, Graff H, Werneck LC. Parkinson's disease and thyroid dysfunction. Parkinsonism Relat Disord. **2004** 6 381 - 383

29. Teo, K.C., Ho, SL. Monoamine oxidase-B (MAO-B) inhibitors: implications for disease-modification in Parkinson's disease. *Translational Neurodegeneration* **2013** 2, 19 1-10
30. Riederer, P and Laux, G. MAO-inhibitors in Parkinson's Disease. Experimental Neurobiology. **2011** 1 1-17
31. Schapira, A., Present and future drug treatment for Parkinson's disease. Journal of Neurology, Neurosurgery and Psychiatry. **2005** 76 1472-1478.
32. Schapira, A., Mitochondrial dysfunction in Parkinson's disease. Cell Death and Differentiation. **2007** 14 1261-1266
33. Schapira, A., Gegg, M. (2011) Mitochondrial Contribution to Parkinson's Disease Pathogenesis. Parkinson's disease. **2011** 7 1-47
34. Duchen, M. Mitochondria in health and disease: perspectives on a new mitochondrial biology. *Molecular Aspects of Medicine* **2004** 25 365-451
35. Calabresi, P., Di Filippo, M., Ghiglieri, V., Tambasco, N., Picconi, B. Levodopa-induced dyskinesias in patients with Parkinson's disease: filling the bench-to-bedside gap. *Lancet Neurology*. **2010** 9 1107 - 1117
36. Hickey P, Stacy M. Available and emerging treatments for Parkinson's disease: a review. *Drug Des Devel Ther*. **2011** 5 241-254
37. Downward, E. Parkinson's disease.net **2017**
38. Donato, R., Cannon, B., Sorci, G., Riuzzi, F., Hsu, K., Weber, D., Geczy, C. Functions of S100 Proteins. *Current Molecular Medicine*. **2013** 13 (1) 24–57.
39. Grum-Schwensen,B., Klingelhöfer,J., Beck, M., Bonefeld, C., Hamerlik, P., Guldberg, P., Grigorian, M., Lukanidin, E., Ambartsumian. N. S100A4-neutralizing antibody suppresses spontaneous tumor progression, pre-metastatic niche formation and alters T-cell polarization balance. *BMC cancer* **2015**
40. Boye, K and Mælandsmo, G. S100A4 and Metastasis A Small Actor Playing Many Roles. *American Journal of Pathology* **2010** 176 (2) 528–535
41. M. Kubánková, I. López-Duarte, D. Kiryushko, and M. K. Kuimova, 'Molecular Rotors Report on Changes in Live Cell Plasma Membrane Microviscosity Upon Interaction with Beta-Amyloid Aggregates', *Soft Matter,* **2018** 14, 9466-74.
42. M. Kubánková, P. A. Summers, I. López-Duarte, D. Kiryushko, and M. K. Kuimova, 'Microscopic Viscosity of Neuronal Plasma Membranes Measured Using Fluorescent Molecular Rotors: Effects of Oxidative Stress and Neuroprotection', *ACS Appl Mater Interfaces,* **2019** 11, 36307-15.
43. S. Pankratova, J. Klingelhofer, O. Dmytriyeva, S. Owczarek, A. Renziehausen, N. Syed, A. E. Porter, D. T. Dexter, and D. Kiryushko, 'The S100a4 Protein Signals through the Erbb4 Receptor to Promote Neuronal Survival', *Theranostics,* **2018** 8, 3977-90.
44. V. Soroka, D. Kiryushko, V. Novitskaya, L. C. Ronn, F. M. Poulsen, A. Holm, E. Bock, and V. Berezin, 'Induction of Neuronal Differentiation by a Peptide Corresponding to the Homophilic Binding Site of the Second Ig Module of the Neural Cell Adhesion Molecule', *J Biol Chem,* **2002** 277, 24676-83.
45. P. Valente, D. Kiryushko, S. Sacchetti, P. Machado, C. M. Cobley, V. Mangini, A. E. Porter, J. P. Spatz, R. A. Fleck, F. Benfenati, and R. Fiammengo, 'Conopeptide-Functionalized Nanoparticles Selectively Antagonize Extrasynaptic N-Methyl-D-Aspartate Receptors and Protect Hippocampal Neurons from Excitotoxicity in Vitro', *ACS Nano,* **2020** 14, 6866-77.
46. F. Aberg, and E. N. Kozlova, 'Metastasis-Associated Mts1 (S100a4) Protein in the Developing and Adult Central Nervous System', *J Comp Neurol,* **2000** 424, 269-82.

47. V. Novitskaya, M. Grigorian, M. Kriajevska, S. Tarabykina, I. Bronstein, V. Berezin, E. Bock, and E. Lukanidin, 'Oligomeric Forms of the Metastasis-Related Mts1 (S100a4) Protein Stimulate Neuronal Differentiation in Cultures of Rat Hippocampal Neurons', *J Biol Chem,* **2000** 275, 41278-86.
48. Helfman, D., Kim, E., Lukanidin, E. *et al.* The metastasis associated protein S100A4: role in tumour progression and metastasis. *Br J Cancer* **2005** 92**,** 1955–1958
49. Fei, F., Qu, J., Li, C. *et al.* Role of metastasis-induced protein S100A4 in human non-tumor pathophysiologies. *Cell Biosci* **2017** 7, 64
50. Winge, D.R., Energy: Electron Transport & Oxidative Phosphorylation. Molecular Cellular Biology. **2012** 32 (14) 2647–2652
51. Sheikhloo, Z., Salouti, M., Katiraee, F. Biological Synthesis of Gold Nanoparticles by Fungus *Epicoccumnigrum. Journal of Cluster Science* **2011** *22* (4) 661–665
52. Kedia, A and Kumar, P (2013) Controlled reshaping and plasmon tuning mechanism of gold nanostars. *Journal of Materials Chemistry C*, **2013**, 1, 4540–4549
53. Yeh, Y., Creran, B., Rotello, V. Gold nanoparticles: preparation, properties, and applications in bionanotechnology. *Nanoscale* **2012** 4 1871-1880
54. Shilo, M., Sharon, A., Baranes, K., Motiei, M., Lellouche, J., Popovtzer, R. The effect of nanoparticle size on the probability to cross the blood - brain barrier: an in-vitro endothelial cell model Journal of Nanobiotechnology **2015** 1-7
55. Song, J., Jang, H., Kin, B. Biological synthesis of gold nanoparticles using *Magnolia kobus* and *Diopyros kaki* leaf extracts. *Process Biochemistry* **2009** 44 (10) 1133-1138
56. Huanga, X and El-Sayeda, M. Gold nanoparticles: Optical properties and implementations in cancer diagnosis and photothermal therapy *Journal of Advanced Research* **2010** 1 13-28
57. Li, N., Zhao, P., Astruc, D. Anisotropic Gold Nanoparticles: Synthesis, Properties,
58. Applications, and Toxicity. *Angewandte Chemie International Edition*, **2014** 53, 1756 – 1789
59. Dykman, L and Khlebtsov, N. Gold Nanoparticles in Biology and Medicine: Recent Advances and Prospects. *Acta Naturae* **2011** 3 (2) 34-55
60. Ong, Y., Chen, Z., Nabavi, S., Regoutz, A., Payne, D., Elson, D., Dexter, D., Dunlop, I., Porter, A Multibranched Gold Nanoparticles with Intrinsic LAT-1 Targeting Capabilities for Selective Photothermal Therapy of Breast Cancer *ACS Applied materials and interfaces* **2017**, 9, 39259-39270
61. Gonzalez-Carter, D., Ong, Z., McGilvery, C., Dunlop, I., Dexter, D., Porter, A. 'L - Dopa Functionalized, Multi-Branched Gold Nanoparticles as Brain-Targeted Nano-Vehicles', *Nanomedicine,* **2019** 15, 1-11.
62. Turkevich, J., Stevenson, P., Hillier, J. A study of the nucleation and growth processes in the synthesis of colloidal gold. *Discussions of the Faraday Society*, **1951**, 11 55-75.
63. Yuan, H., Khoury, C. G., Hwang, H., Wilson, C.M., Grant, G. A., Vo-Dinh, T. Gold nanostars: surfactant-free synthesis, 3D modelling, and two-photon photoluminescence imaging. *Nanotechnology.* **2012**, 23 (7) 1-9
64. Pi, J., Stella, M., Fernando, N., Lam, A., Regoutz, A., Ratcliff, L. 'Predicting Core Level Photoelectron Spectra of Amino Acids Using Density Functional Theory', *The Journal of Physical Chemistry Letters,* **2020**, 11 2256-62.

65. Regoutz, A., Wolinska, M., Fernando, N., Ratcliff, L. 'A Combined Density Functional Theory and X-Ray Photoelectron Spectroscopy Study of the Aromatic Amino Acids', *Electronic Structure,* **2020** 2, 1075 - 1088
66. Kimling, J., Maier, M. Turkevich Method for Gold Nanoparticle Synthesis Revisited, *J. Phys. Chem. B* **2006**, 110*,* 15700 - 15707.
67. Sizochenko, N., Mikolajczyk, A., Syzochenko, M., Puzyn, T., Leszczynski, J. Zeta potentials (ζ) of metal oxide nanoparticles: A meta-analysis of experimental data and a predictive neural networks modelling *Nano Impact* **2021**, 22, 2400 - 2407
68. Lopes Rodrigues, R., Xie, F., Porter, A., Ryan, M. 'Geometry-Induced Protein Reorientation on the Spikes of Plasmonic Gold Nanostars', *Nanoscale Advances,* 2 **2020**, 1144-51.
69. Turecek, P., Bossard, M., Schoetens, F., Ivens, I. 'Pegylation of Biopharmaceuticals: A Review of Chemistry and Nonclinical Safety Information of Approved Drugs', *J Pharm Sci,* 105 **2016**, 460-75.
70. Alaqad, K and Saleh, T. Gold and Silver Nanoparticles: Synthesis Methods, Characterization Routes and Applications towards Drugs. *Journal of environmental and analytical toxicology*. **2016** 4 (4) 1-10
71. Adams, F., La Rosa, F., Kumar, S., Edwards-Prasad, J., Kentroti, S., Vernadakis, A., Freed, C., Prasad, K. 'Characterization and Transplantation of Two Neuronal Cell Lines with Dopaminergic Properties', *Neurochem Res,* **1996** 21, 619-27.
72. Anantharam, V., Kitazawa, M., Wagner, J., Kaul, S., Kanthasamy, A. 'Caspase-3-Dependent Proteolytic Cleavage of Protein Kinase Cdelta Is Essential for Oxidative Stress-Mediated Dopaminergic Cell Death after Exposure to Methylcyclopentadienyl Manganese Tricarbonyl', *J Neurosci,* **2002** 22, 1738-51.
73. Blesa, J., Phani, S., Jackson-Lewis, V., Przedborski, S. 'Classic and New Animal Models of Parkinson's Disease', *J Biomed Biotechnol,* **2012**.
74. Bramlett, H and Dietrich, W. 'Pathophysiology of Cerebral Ischemia and Brain Trauma: Similarities and Differences', *J Cereb Blood Flow Metab,* **2004** 24**,** 133-50
75. Cantu, D., Fulton, R., Drechsel, D., Patel, M. 'Mitochondrial Aconitase Knockdown Attenuates Paraquat-Induced Dopaminergic Cell Death Via Decreased Cellular Metabolism and Release of Iron and H(2)O(2)', *J Neurochem,* **2011**, 118 79-92
76. Carlsson, T., Schindler, F., Hollerhage, M., Depboylu, C., Arias-Carrion, O., Schnurrbusch, S., Rosler, T., Wozny, W., Schwall, G., Groebe, K., Oertel, W., Brundin, P., Schrattenholz, A., Hoglinger, G. 'Systemic Administration of Neuregulin-1beta1 Protects Dopaminergic Neurons in a Mouse Model of Parkinson's Disease', *J Neurochem,* **2011**, 117 1066-74.
77. Cheng, Y,. Loh, Y., Birch, N. 'Neuroserpin Attenuates H2o2-Induced Oxidative Stress in Hippocampal Neurons Via Akt and Bcl-2 Signaling Pathways', *J Mol Neurosci,* **2017**, 61 123-31.
78. Choi, D., Kim, Y,. Kim, G., Joh, T., Beal, M., Kim, Y. 'Role of Matrix Metalloproteinase 3-Mediated Alpha-Synuclein Cleavage in Dopaminergic Cell Death', *J Biol Chem,* **2011,** 286 14168-77.
79. Depboylu, C., Rosler, T., de Andrade, A., Oertel, W., Hoglinger, G. 'Systemically Administered Neuregulin-1beta1 Rescues Nigral Dopaminergic Neurons Via the Erbb4 Receptor Tyrosine Kinase in Mptp Mouse Models of Parkinson's Disease', *J Neurochem,* **2015**, 133 590-7.

80. Dranka, B., Zielonka, J., Kanthasamy, A., Kalyanaraman, B. 'Alterations in Bioenergetic Function Induced by Parkinson's Disease Mimetic Compounds: Lack of Correlation with Superoxide Generation', *J Neurochem,* **2012**, 122 941-51.
81. Gerecke, K., Wyss, J., Carroll, S. 'Neuregulin-1beta Induces Neurite Extension and Arborization in Cultured Hippocampal Neurons', *Mol Cell Neurosci,* **2004**, 27 379-93.
82. Ghashghaei, H., Weber, J., Pevny, L., Schmid, R., Schwab, M., Lloyd, K., Eisenstat, D., Lai, C., Anton, E. 'The Role of Neuregulin-Erbb4 Interactions on the Proliferation and Organization of Cells in the Subventricular Zone', *Proc Natl Acad Sci U S A,* **2006**, 103 1930-5.
83. Guo, W., Wang, J., Li, R., Peng, Y. 'Neuroprotective Effects of Neuregulin-1 in Rat Models of Focal Cerebral Ischemia', *Brain Res,* 1087 **2006**, 180-5
84. Qian, X., Shen, Q., Goderie, S., He, W., Capela, A., Davis, A., Temple, S. Timing of CNS Cell Generation: A Programmed Sequence of Neuron and Glial Cell Production from Isolated Murine Cortical Stem Cells. *Neuron* **2000**, 28 (1) 69-80
85. Iwakura, Y., Nawa, H. 'Erbb1-4-Dependent Egf/Neuregulin Signals and Their Cross Talk in the Central Nervous System: Pathological Implications in Schizophrenia and Parkinson's Disease', *Front Cell Neurosci*. **2013**.
86. Jo, H., Kim, D., Shin, M., Cho, S., Park, J., Lee, C., Yeo, J., Choi, Y., Yeo, H., Sohn, E., Son, O., Cho, S., Kim, D., Yu, Y., Lee, K., Park, J., Eum, W., Choi, S. 'Tat-Hsp22 Inhibits Oxidative Stress-Induced Hippocampal Neuronal Cell Death by Regulation of the Mitochondrial Pathway', *Mol Brain,* 10 **2017**, 1
87. Kobori, N., Clifton, G., Dash, P. 'Altered Expression of Novel Genes in the Cerebral Cortex Following Experimental Brain Injury', *Brain Res Mol Brain Res,* 104 **2002**, 148-58.
88. Kozlova, E and Lukanidin, E. 'Mts1 Protein Expression in the Central Nervous System after Injury', *Glia,* 37 **2002**, 337-48.
89. Mei, L and Xiong, W. 'Neuregulin 1 in Neural Development, Synaptic Plasticity and Schizophrenia', *Nat Rev Neurosci,* 9 **2008**, 437-52.
90. Min, S., An, J., Lee, J., Seol, G., Im, J., Kim, H., Baik, T., Woo, R. 'Neuregulin-1 Prevents Amyloid Beta-Induced Impairment of Long-Term Potentiation in Hippocampal Slices Via Erbb4', *Neurosci Lett,* 505 **2011**, 6-9.
91. Offenburger, S., Jongsma, E., Gartner, S. 'Mutations in Caenorhabditis Elegans Neuroligin-Like Glit-1, the Apoptosis Pathway and the Calcium Chaperone Crt-1 Increase Dopaminergic Neurodegeneration after 6-Ohda Treatment', *PLoS Genet,* 14 **2018**,
92. Prasad, K., Clarkson, E., La Rosa, F., Edwards-Prasad, J., Freed, C. 'Efficacy of Grafted Immortalized Dopamine Neurons in an Animal Model of Parkinsonism: A Review', *Mol Genet Metab,* 65 **1998**, 1-9
93. Ryu, J., Yu, H,. Cho, H,. Kim, H., Baik, T., Lee, S., Woo, R. 'Neuregulin-1 Exerts Protective Effects against Neurotoxicities Induced by C-Terminal Fragments of App Via Erbb4 Receptor', *J Pharmacol Sci,* 119 **2012**, 73-81.
94. Salinas, K., Kereselidze, Z., DeLuna, F., Peralta, X., Santamaria, F. 'Transient Extracellular Application of Gold Nanostars Increases Hippocampal Neuronal Activity', *Journal of nanobiotechnology,* 12 **2014**, 31-31.
95. Sies, H. 'Hydrogen Peroxide as a Central Redox Signaling Molecule in Physiological Oxidative Stress: Oxidative Eustress', *Redox Biol,* 11 **2017**, 613-19.

96. Xu, Q., Kanthasamy, A., Jin, H., Reddy, M. 'Hepcidin Plays a Key Role in 6-Ohda Induced Iron Overload and Apoptotic Cell Death in a Cell Culture Model of Parkinson's Disease', *Parkinsons Dis,* **2016**
97. Zhang, L., Fletcher-Turner, A., Marchionni, M., Apparsundaram, S., Lundgren, K., Yurek, D., Seroogy, K. 'Neurotrophic and Neuroprotective Effects of the Neuregulin Glial Growth Factor-2 on Dopaminergic Neurons in Rat Primary Midbrain Cultures', *J Neurochem,* **2004**, 91 1358-68
98. Piyushkumar, S., Anjali, A., Dash, A., Shah, D., Kumari, N., Patel, M. A Combined Approach of Gold Nanoparticles with Cannabinoids for the Treatment of Cancer -A Review. **2020** 12. 393-405.
99. Bahar, Y., Khan, A., Muhammad, R., Mohammad, R. Gold, Silver, and Palladium Nanoparticles: A Chemical Tool for Biomedical Applications Frontiers in Chemistry **2020** 8 2296-2646
100. Vincent, X., Serge, M., Frank, F. Advances in optoplasmonic sensors – combining optical nano/microcavities and photonic crystals with plasmonic nanostructures and nanoparticles" *Nanophotonics*, **2018**, 7 (1) 1-38
101. Baron, R., Zayats, M., Willner, I. Dopamine-, L - Dopa-, Adrenaline-, and Noradrenaline-Induced Growth of Au Nanoparticles: Assays for the Detection of Neurotransmitters and of Tyrosinase Activity. *Analytical Chemistry,* **2005**. 77 (6) 1566-1571.
102. Ho, A., Chang, H., Su, W. DOPA-Mediated Reduction Allows the Facile Synthesis of Fluorescent Gold Nanoclusters for Use as Sensing Probes for Ferric Ions. *Analytical Chemistry***, 2012.** 84 (7) 3246-3253.
103. Park, S.Y. Simple and rapid detection of L - Dopa decarboxylase activity using gold nanoparticles. Analyst, **2013**. 138 (11) 3146-3149.
104. Wiley, DT., Webster, P., Gale, A., Davis, ME. Transcytosis and brain uptake of transferrin-containing nanoparticles by tuning avidity to transferrin receptor. Proc Natl Acad Sci USA **2013** 110 (21) 8662-8667.
105. Son, Y., Kim, K., Hong, C., Nam, Y. Morphological Evolution of Gold Nanoparticles into Nanodendrites Using Catechol-Grafted Polymer Templates. *ACS Omega* **2018** 3 6683 - 6691
106. Dalsin, J., Hu, B. H., Lee, B. P. Messersmith, P. B. Musseladhesive protein mimetic polymers for the preparation of nonfoulingsurfaces. J. Am. Chem. Soc. **2003**, 125, 4253−4258.
107. Lee, H.; Dellatore, S. M., Miller, W. M., Messersmith, P. B. Mussel-inspired surface chemistry for multifunctional coatings.Science **2007**, 318, 426−430.
108. Lee, Y., Park, T. G. Facile fabrication of branched goldnanoparticles by reductive hydroxyphenol derivatives.Langmuir **2011**, 27, 2965−2971.
109. Kim, I., Son, H. Y., Yang, M. Y., Nam, Y. S. Bioinspired designof an immobilization interface for highly stable, recyclable nanosized catalysts.ACS Appl. Mater. Interfaces **2015**, 7, 14415−14422.
110. Son, H. Y., Ryu, J. H., Lee, H., Nam, Y. S. Bioinspiredtemplating synthesis of metal−polymer hybrid nanostructures within3D electrospun nanofibers. ACS Appl. Mater. Interfaces **2013**, 5, 6381−6390.
111. Thermo scientific instructions NHS and Sulfo - NHS

112. Clark, AJ. Increased brain uptake of targeted nanoparticles by adding an acid-cleavable linkage between transferrin and the nanoparticle core. *Proc Natl Acad Sci* **2015**, 112 (40) 12486–12491
113. Gromnicova, R., Davies, H., Sreekanthreddy, P., Romero, IA., Lund, T., Roitt, IM. Glucose coated gold nanoparticles transfer across human brain endothelium and enter astrocytes in vitro. PloS one, **2013** 8, 81043.
114. Boado, RJ., Li, JY., Nagaya, M., Zhang, C. Pardridge WM. Selective expression of the large neutral amino acid transporter at the blood–brain barrier. *Proc Natl Acad Sci,* **1999** 96, 12079-84.
115. Li L, Di X, Zhang S, Kan Q, Liu H, Ly T, Wang Y, Fu Q, Sun J, He J. Large amino acid transporter 1 mediated glutamate modified docetaxel-loaded liposomes for glioma targeting. Colloids and Surfaces B: Biointerfaces.
116. Yin T, Xie W, Sun J, Yang L, and Liu J. Penetratin Peptide-Functionalized Gold Nanostars: Enhanced BBB Permeability and NIR Photothermal Treatment of Alzheimer's Disease Using Ultralow Irradiance. *ACS Appl. Mater. Interfaces*, **2016**, 8 (30), 19291–19302.
117. Nance EA, Woodworth GF, Sailor KA, Shih T-Y, Xu Q, Swaminathan G, et al. A dense poly (ethylene glycol) coating improves penetration of large polymeric nanoparticles within brain tissue. Science translational medicine **2012** 4 (149)
118. Daneman, R and Prat, A. The Blood – Brain Barrier. *Cold Spring Harbour Perspectives in Biology.* **2015** 1 1-24
119. Williams, D.; Carter, C. *Transmission electron microscopy: a textbook for materials science*. Springer: New York, **2009**.
120. Bell, D. C.; Erdman, N. *Low Voltage Electron Microscopy*; Bell, D. C., Erdman, N., Eds.; John Wiley & Sons, Ltd: Chichester, UK, **2012**.
121. Singh P, Pandit S, Mokkapati VRSS, Garg A, Ravikumar V, Mijakovic I. Gold Nanoparticles in Diagnostics and Therapeutics for Human Cancer. *Int J Mol Sci*. **2018**; 19 (7)
122. Teleanu DM, Chircov C, Grumezescu AM, Volceanov A, Teleanu RI. Impact of Nanoparticles on Brain Health: An Up to Date Overview. *J Clin Med*. **2018**; 7 (12)
123. Carradori D., Balducci C., Re F., Brambilla D., Le Droumaguet B., Flores O., Gaudin A., Mura S., Forloni G., Ordoñez-Gutierrez L., et al. Antibody-functionalized polymer nanoparticle leading to memory recovery in alzheimer's disease-like transgenic mouse model. Nanomed. *Nanotechnol. Biol. Med*. **2018**; 14, 609–618
124. Loureiro J.A., Gomes B., Fricker G., Coelho M.A.N., Rocha S., Pereira M.C. Cellular uptake of plga nanoparticles targeted with anti-amyloid and anti-transferrin receptor antibodies for alzheimer's disease treatment. *Coll. Surf. B Biointerfaces*. **2016**; 145, 8–13.
125. Zheng X., Zhang C., Guo Q., Wan X., Shao X., Liu Q., Zhang Q. Dual-functional nanoparticles for precise drug delivery to alzheimer's disease lesions: Targeting mechanisms, pharmacodynamics and safety. Int. J. Pharm. **2017**; 525: 237–248.
126. Sridhar V., Gaud R., Bajaj A., Wairkar S. Pharmacokinetics and pharmacodynamics of intranasally administered selegiline nanoparticles with improved brain delivery in parkinson's disease. Nanomed. *Nanotechnol. Biol. Med*. **2018**; 14: 2609–2618.
127. Raj R., Wairkar S., Sridhar V., Gaud R. Pramipexole dihydrochloride loaded chitosan nanoparticles for nose to brain delivery: Development, characterization and in vivo anti-parkinson activity. *Int. J. Biol. Macromol.* **2018**; 109, 27–35.

128. Motyl J., Przykaza Ł., Boguszewski P.M., Kosson P., Strosznajder J.B. Pramipexole and fingolimod exert neuroprotection in a mouse model of parkinson's disease by activation of sphingosine kinase 1 and akt kinase. *Neuropharmacology*. **2018**; 135, 139–150.
129. Hegazy M.A., Maklad H.M., Samy D.M., Abdelmonsif D.A., El Sabaa B.M., Elnozahy F.Y. Cerium oxide nanoparticles could ameliorate behavioral and neurochemical impairments in 6-hydroxydopamine induced parkinson's disease in rats. *Neurochem. Int.* **2017** 108, 361–371.
130. Saraiva C., Paiva J., Santos T., Ferreira L., Bernardino L. Microrna-124 loaded nanoparticles enhance brain repair in parkinson's disease. J. Control. Release. **2016** 235, 291–305.
131. Hobson D.W., Guy R.C. Nanotoxicology. In: Wexler P., editor. Encyclopedia of Toxicology. *3rd ed. Academic Press; Oxford,* UK: **2014**. 434–436.
132. Viswanath B., Kim S. Influence of nanotoxicity on human health and environment: The alternative strategies. Rev. Environ. Contam. *Toxicol.* **2017** 242, 61–104
133. Ai J., Biazar E., Jafarpour M., Montazeri M., Majdi A., Aminifard S., Zafari M., Akbari H.R., Rad H.G. Nanotoxicology and nanoparticle safety in biomedical designs. *Int. J. Nanomed.* **2011** 6, 1117–1127
134. Aillon K.L., Xie Y., El-Gendy N., Berkland C.J., Forrest M.L. Effects of nanomaterial physicochemical properties on in vivo toxicity. *Adv. Drug Deliv.* Rev. **2009** 61, 457–466.
135. Zhang X.-Q., Xu X., Bertrand N., Pridgen E., Swami A., Farokhzad O.C. Interactions of nanomaterials and biological systems: Implications to personalized nanomedicine. *Adv. Drug Deliv.* Rev. **2012** 64, 1363–1384.
136. Gatoo M.A., Naseem S., Arfat M.Y., Dar A.M., Qasim K., Zubair S. Physicochemical properties of nanomaterials: Implication in associated toxic manifestations. BioMed Res. Int. **2014**
137. Khan I., Saeed K., Khan I. Nanoparticles: Properties, applications and toxicities. *J. Chem*. **2017**
138. Singh A.K. Chapter 1—Introduction to nanoparticles and nanotoxicology. In: Singh A.K., editor. Engineered Nanoparticles. Academic Press; Boston, MA, USA: **2016**. 1–18.
139. Caudle W.M. Occupational metal exposure and parkinsonism. Neurotoxicity of Metals. *Springer; New York, NY, USA:* **2017**. 143–158
140. Li J., Martin F.L. Chapter 4—Current perspective on nanomaterial-induced adverse effects: Neurotoxicity as a case example. *Neurotoxicity of Nanomaterials and Nanomedicine.* **2017**. 75–98.
141. Gao H., Jiang X. Introduction and overview. In: Jiang X., Gao H., editors. Neurotoxicity of Nanomaterials and Nanomedicine. Academic Press; Cambridge, MA, USA: **2017**.
142. Lovisolo D., Dionisi M., Ruffinatti F.A., Distasi C. Nanoparticles and potential neurotoxicity: Focus on molecular mechanisms. *AIMS Mol. Sci.* **2017** 5, 1–13.
143. Jiang X., Gao H. Preface. In: Jiang X., Gao H., editors. Neurotoxicity of Nanomaterials and Nanomedicine. Academic Press; Cambridge, MA, USA: **2017**.